Seasonal forecasting of wind energy resource and production in France and associated risk

Bastien Alonzo

université PARIS-SACLAY

NNT : 2018SACLX062

Thèse de doctorat

Seasonal Forecasting of Wind Energy Resource and Production in France, and Associated Risk

Thèse de doctorat de l'Université Paris-Saclay
préparée à l'École Polytechnique

École doctorale n°579 Sciences mécaniques et énergétiques, matériaux et géosciences (SMEMAG)
Spécialité de doctorat: mécanique des matériaux

Thèse présentée et soutenue à Palaiseau, le 16 Novembre 2018, par

Bastien Alonzo

Composition du Jury :

Emmanuel Gobet Professeur, CMAP (UMR 7641)	Président
Michel Déqué Ingénieur IPEF, Météo-France CNRM (UMR 3589)	Rapporteur
Pierre Pinson Professeur, Denmark Technical University	Rapporteur
Laurent Dubus Ingénieur, EDF	Examinateur
Vincent Lefieux Ingénieur, RTE	Examinateur
Philippe Drobinski Directeur de recherche, LMD (UMR 8539)	Directeur de thèse
Riwal Plougonven Professeur, LMD (UMR 8539)	Co-Directeur de thèse
Peter Tankov Professeur, ENSAE-CREST (UMR 9194)	Co-Directeur de thèse

Remerciements

J'ai effectué ma thèse au Laboratoire de Météorologie Dynamique de l'école Polytechnique (LMD) et au Laboratoire de Probabilité et Modèles aléatoires de l'université Paris Diderot (LPMA). Je tiens remercier tous ceux que j'ai cotoyés pendant ces trois années de recherche.

Je souhaite bien sur remercier l'Agence Nationale de la Recherche qui, via le projet FOREWER (ANR-14-CE05- 0028), a financé ce travail, et m'a permis de le développer sereinement, dans un contexte de partenariat de recherche académique et industrielle. Par la même occasion, je remercie tous les acteurs de ce projet de recherche.

Je tiens à remercier l'ensemble des membres du Jury, et particulièrement Michel Déqué et Pierre Pinson pour avoir accepté d'être Rapporteurs de mon manuscrit.

Je remercie aussi l'équipe de l'école doctorale SMEMAG, et particulièrement Xavier Quidelleur et Thi Kim Ngan Ho; ainsi que l'équipe de l'école doctorale de Polytechnique, et particulièrement Audrey Lemaréchal et Emmanuel Fullenwarth. Je remercie aussi toute l'équipe administrative du LMD pour leur gentillesse et leur aide pendant ces trois ans.

J'aimerais remercier mon directeur de thèse Philippe Drobinski pour sa confiance, son énergie, sa pédagogie, et sa disponibilité pendant ces trois années de thèses. Je le remercie particulièrement pour son despotisme tyrannique, car sans cette terreur, je ne serais jamais allé aussi loin.

Je voudrais également remercier mes co-directeurs, Riwal Plougonven, notamment pour le nombre indénombrable de données extraites des serveurs du Centre Européen, et Peter Tankov, particulièrement pour sa patience et sa pédagogie. Plus généralement, je voudrais les remercier pour leur bienveillance, leurs conseils, leur aide, et leur disponibilité tout au long de la thèse.

Je remercie aussi mes collègues de travail pour leur apport d'idées, les discussions constructives, les remises en question, les relectures...

Plus particulièrement, je remercie Bénédicte Jourdier et Hans-Kristian Ringkjob pour leur implication dans mes premiers travaux de recherche.

Je remercie aussi Mathilde Mougeot et Aurélie Fischer pour leurs explications et expertise sur les modèles statistiques de downscaling.

Également, je remercie Aurore Dupré pour tout le travail commun que nous avons effectué ces derniers temps. Je lui souhaite de finir sa thèse comme elle l'a commencée, brillamment.

Je remercie les stagiaires et étudiants pour leur travail précieux : Medhi, Côme, Rebecca, Lishan, et Naveen. Parce que ce sont les ruisseaux, les rivières qui se jet-

tent dans les fleuves se déversant dans l'océan des sciences.

Je remercie évidemment tous mes collègues de non-travail. Ceux qui ont partagé les moments de pauses, cafés, déjeunés, et pôts en tout genre. Les personnes citées plus haut pourront bien sur se reconnaître ici.

Je remercie plus particulièrement Nicolas Da-Silva, pour le long chemin parcouru ensemble au sein de ce laboratoire, du master au doctorat. Cinq années de voisinage j'ai compté, nostalgie. Cinq années à partager le même bureau et le même directeur. Cinq années de travail, de soutien mutuel, d'entraide, de victoires et de défaites footbalistiques. Merci.

Je remercie aussi Trung Nguyen-Quang, pour son indéfectible humour et sa bonne humeur. Surtout, tellement de curiosité, de courage.

Je remercie aussi Laurent pour être un super défenseur et goal, mais surtout pour sa bienveillance, son attention, son aide, ses conseils, notamment pendant l'écriture du manuscrit et avant la soutenance.

Par ailleurs, je remercie tous les doctorants et postdoctorants du laboratoire. Ce fut une expérience si enrichissante de partager l'ensemble de vos cultures, si diverses. Merci pour ce tour du monde statique. Merci aussi à l'équipe de foot du LMD du tournoi inter-labo printanier. Merci à : Xudong, Thibault, Olivier, Léo, Artemis, Rodrigo, Fausto, Felipe, Aurore, Stavros, Nico, Sun, Adrien, Eivind, Ayat, Aurélien, Trung, Rémy, Fuxing, Camill, Julio, Marco, Ariel, Sara, Daeyoung, Drew, Eric, Alexis...

Enfin parce que la thèse ne quitte jamais la tête (et la tête ne quitte jamais les épaules), je tiens à remercier mes parents, mon frère, Aurélie, Joaquin, Pauline et mes amis pour ce qu'ils sont : ma famille.

À mes parents qui m'ont soutenu dans mes projets depuis le début, qui m'ont fait confiance, merci pour tout.

À mon frère, Aurélie et Joaquin qui forment une merveilleuse petite famille, pour ce magnifique petit neveu que vous m'avez fait.

À Pauline, ma Merveille, pour cette aventure de tous les jours, pour ce que j'apprends de toi tous les jours, pour tous les jours passés, les présents, et les futurs.

À mes amis qui croient encore que j'étudie les tortues. Peu leur importe, car ils savent au fond que, pour nous, le vent souffle comme les Alyzés, toujours dans la même direction, jamais opposée.

Prévision saisonnière de la ressource et de la production éoliennes en France, et du risque associé

Résumé en Français:

L'augmentation de la part des énergies renouvelables intermittentes dans le mix énergétique génère des problématiques liées à la prévisibilité de la production d'électricité. Notamment, à l'échelle saisonnière, les gestionnaires du réseau de transport d'électricité sont contraints de projeter la disponibilité des moyens de production ainsi que de prévoir la demande, afin de garantir l'approvisionnement pour le prochain hiver ou été. Néanmoins, les projections actuelles sont principalement basées sur des données historiques (climatologie) de températures (consommation), vents de surface (production éolienne), ou encore de rayonnement solaire (production photovoltaïque).

Si la prévisions de l'énergie éolienne aux échelles de temps courtes allant de la minute à quelques jours ainsi que la tendance des vents aux échelles climatiques ont été largement étudiées, la prévision de la production éolienne à l'échelle de temps intermédiaire allant d'une quinzaine de jours à la saison n'a reçu que peu d'attention. La prévisibilité du temps aux moyennes latitudes à ces horizons intermédiaires est en effet encore une question ouverte. Cependant, plusieurs études récentes ont montré que les modèles numériques de prévisions du temps étaient capables d'apporter de l'information sur la variabilité de la circulation atmosphérique de grande échelle, à l'échelle saisonnière. Par exemple, *Scaife et al., 2014* montre que la corrélation entre l'Oscillation Nord Atlantique (NAO) observée et prédite par les modèles de prévision saisonnière atteint 0.6. La NAO est un indicateur de l'état du gradient de pression entre la dépression islandaise et l'anticyclone des Açores qui module le rail des dépressions impactant fortement le temps en Europe du Nord. Cet indicateur, parmi d'autres, a donc une forte influence en Europe , notamment sur les précipitations, les températures, et les vents de surface.

L'idée développée dans ce travail est de construire la relation entre de tels indicateurs de la circulation atmosphérique à grande échelle et le vent de surface en France. Cela permet donc de prendre en compte la variabilité interannuelle du vent de surface, ce dont n'est pas capable par définition la climatologie. Cette thèse consiste en 4 travaux distincts. Les deux premières études ont pour objet la prévision de la ressource et la production éoliennes à l'échelle saisonnière. Deux modèles sont développés en utilisant une approche de modèle parfait, basée sur la réanalyse ERA-Interim du Centre Européen (European Center of Medium-range Weather Forecast, ECMWF). Le premier modèle paramétrique fait l'hypothèse que le vent suit la distribution de Weibull. L'autre non-paramétrique s'inscrit dans le contexte de la prévision probabiliste. La troisième étude se place dans le même contexte de modèle parfait, et a pour objectif de mesurer et reconstruire, non pas le vent local, mais le risque saisonnier au niveau national de déséquilibre entre la production éolienne et la consommation en France. Enfin, la quatrième étude analyse et améliore, à l'aide de modèles statistiques, la représentation du vent provenant du modèle numérique de prévision du temps d'ECMWF à un site spécifique d'observation, donnant ainsi une perspective de sortie du contexte de modèle parfait utilisé dans les études précédentes.

Le premier modèle, paramétrique, est basé sur la prévision de la distribution saisonnière du vent de surface, à différents points de grille en France, estimée par une distribution théorique de Weibull. Le lien est construit entre différents paramètres de la distribution et les indicateurs de grande échelle à l'aide d'une régression polynomiale. La reconstruction de la distribution saisonnière du vent de surface montre que l'information contenue dans la circulation atmosphérique de grande échelle permet en partie d'expliquer la variabilité saisonnière du vent de surface. Ce modèle est donc plus performant que la climatologie, notamment au nord de la France, en hiver et en automne. Une des limites les plus importantes de ce modèle est son caractère paramétrique. De plus, l'évaluation de la

moyenne d'ensemble des prévisions saisonnières d'ECMWF montre que l'information sur les indicateurs de grande échelle est perdue au bout d'un mois environ.

Le deuxième modèle, non paramétrique, est basé sur l'estimation de la densité de probabilité du vent de surface journalier conditionnel à l'état de l'atmosphère, représenté par un seul index résumant l'ensemble des indicateurs de grande échelle. Le modèle est dit "probabiliste", car il a pour but de donner la densité de probabilité du vent à chaque pas de temps de prévision. Les outils spécifiques d'évaluation de modèles probabilistes sont utilisés pour évaluer la calibration et la précision du modèle. L'évaluation du modèle et de la climatologie montre que le modèle est mieux calibré que la climatologie, mais aussi plus précis. Encore une fois, cela est le cas plus spécifiquement au nord de la France, en hiver et en automne. L'application du modèle probabiliste aux ensembles de prévisions saisonnières d'ECMWF après post-traitement des ensembles, permet d'obtenir des prévisions de la distribution du vent de surface calibrées, et plus précises que la climatologie à l'échelle saisonnière, dans un nombre significatif de cas.

La même idée est utilisée dans le but de reconstruire la probabilité jointe de la consommation et de la production nationale française, permettant ainsi de mesurer le risque de déséquilibre entre l'offre et la demande. Un modèle supplémentaire est proposé afin de mesurer les risques de situation extrêmes de déséquilibre. Les modèles proposés semblent reconstruire les mesures de risques définies de manière précise. L'analyse de l'état des indicateurs de grande échelle lors de l'apparition d'un risque permet d'expliquer les causes météorologiques de cette apparition.

L'une des perspectives de ce travail serait de sortir de l'approche de modèle parfait afin de raffiner la représentation du vent de surface aux sites spécifiques de production éolienne. C'est dans ce contexte que plusieurs techniques de downscaling sont étudiées dans le but de reconstruire le vent de surface à un site d'observation spécifique, à partir des données provenant du modèle numérique de prévision du centre Européen.

Ce travail apporte un éclairage important sur la possibilité de prédire le vent de surface et la production d'énergie éolienne en France à l'échelle saisonnière, à l'aide d'indicateurs de la circulation atmosphérique de grande échelle. Les modèles proposés montrent de meilleures performances que la climatologie qui est actuellement utilisée notamment pour d'estimer le risque de déséquilibre entre l'offre et la demande d'électricité à l'échelle saisonnière.

Contents

Chapter 1

Introduction

Contents

1.1 Renewable energy growth

In the recent years, the energy transition has been on the forefront of political and societal issues, mainly due to the increasing awareness of the need to maintain climate change within acceptable bounds. This has led many countries to encourage the use of renewable energy. Since 2008, the European Union (EU) targets 20% of renewable energy contribution to the total energy mix by 2020, and 27% by 2030. Owing to a well-established technology and the ever stronger push towards replacing fossil fuels with clean renewable power, wind energy has seen a dramatic growth in the recent years. As an illustration of this sharp increase, the newly installed wind capacity in the world in 2016 has been 55GW, corresponding to an increase of 12.6% in the total installed capacity (Global Wind Energy Council (GWEC, 2016)). In 10 years, the total worldwide installed capacity has almost been multiplied by 7, going from 74GW installed in 2006 to almost 500GW in 2016 (Figure 1.1). In the EU, the total installed wind power capacity has grown from 13 GW in 2000 to 142 GW in 2015 (EWEA, 2016). The actual share in the final consumption met by wind energy in the EU was 11.4% in 2015 (EWEA, 2016). The number of wind farms increases each year and feeds the electrical network with a larger amount of energy. In 2016, France has seen its highest capacity growth rate ever recorded. This sharp increase of connected wind power has for instance allowed the network to receive 8.6 GWh from wind power plants, on November 20th at night, corresponding to 17.9% of the energy produced at this time (RTE, 2016a).

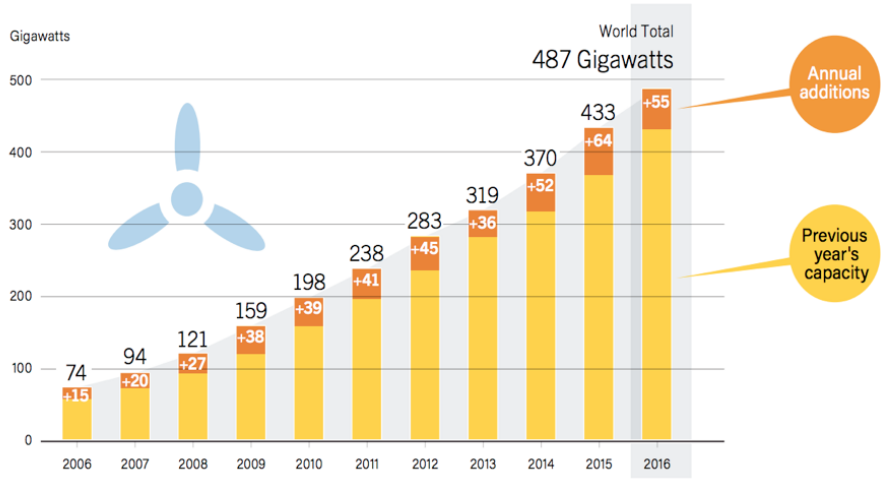

Figure 1.1: Wind energy growth - Cumulated installed capacity from 2006 to 2016 - Figure taken from report of REN21 2017 (REN21, 2017)

The increase of wind and PV power raises the issue of their natural varability. For producers, the management of price fluctuations, the optimisation of operation costs, and of the wind turbines' maintenance are typical concerns. For transmission system operators (TSOs), the exact balance between electricity supply and

demand at every time step is becoming more and more challenging as the number of wind farms and PV power plants connected to the electrical network increases. Naturally variable renewable energy penetration is thus a challenging issue, because the predictability of this type of energy is related to very complex processes of the atmospheric circulation. The atmospheric circulation displays variability at very different spatial and temporal scales, and its chaotic nature might limit or slow down the penetration of such energy production means.

1.2 Variability and its implications

1.2.1 Atmospheric variability

The Earth is often described as a thermodynamic system in equilibrium. Motions in the atmosphere are mainly initiated by solar radiation heating the atmosphere. The amount of energy from the sun is much larger in equatorial regions than in polar regions. Thermal gradient generates heat fluxes crossing latitudes by means of three cells constrained by the Coriolis force, namely the Hadley cell (in tropical regions), the Ferrel cell (at midlatitude) and the polar cell (in polar regions). This circulation is known as the global atmospheric circulation (Figure 1.2).

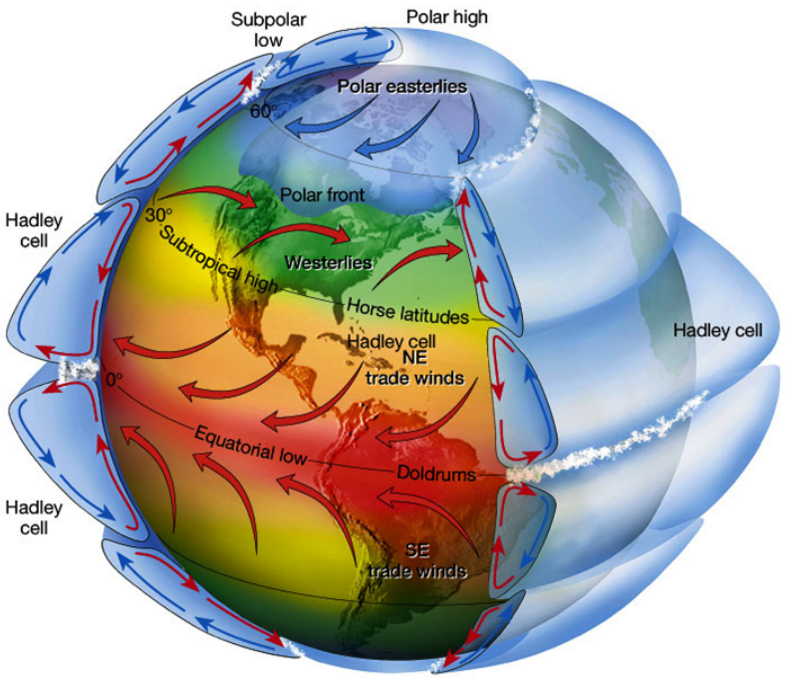

Figure 1.2: Schematic of the global atmospheric circulation. The motions in the vertical cross section represent the circulation averaged in time and along parallels.

The atmosphere is a complex system and the atmospheric circulation involves motions on a wide range of space and time scales, interacting to produce variability

on scales from seconds to decades. Figure 1.3 shows the typical spatial scales of the atmospheric circulation and the corresponding time scale as well as examples of phenomena associated with them.

In the vertical, the atmosphere can be divided into 4 layers depending on the sign of the vertical pressure gradient. The layer in which we live, which touches the surface and has temperature decreasing with height is the troposphere. It typically extends to 10km altitude at midlatitudes. It is heated from below, by the absorption of solar radiation at the surface. More precisely, the lowest part of the troposphere is the boundary layer (typically 1km thick). It is in contact with the surface and directly influenced by exchanges of heat, momentum. The rest of the troposphere is called the free troposphere.

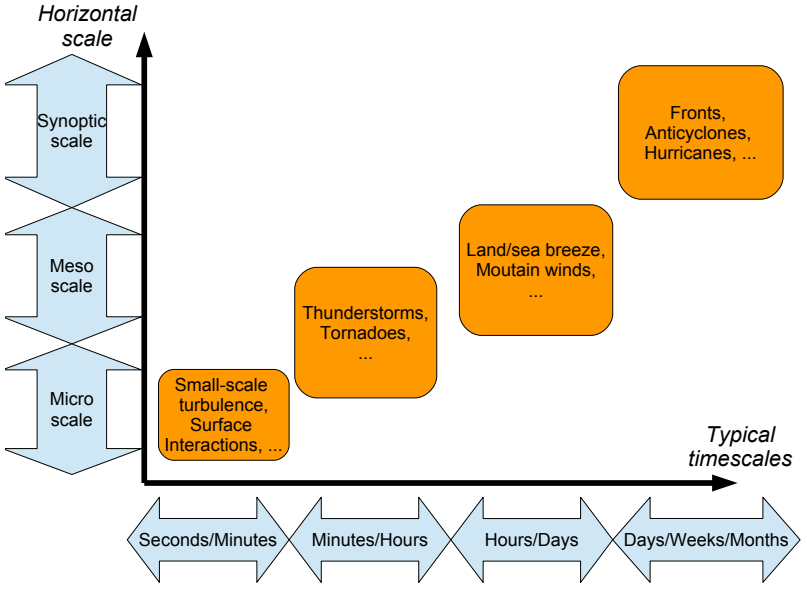

Figure 1.3: Spatio-temporal timescales driving the variability of the atmospheric circulation

In the free troposphere (typically above 1km) and in mid or high latitudes, the flow is quasi two-dimensional, the synoptic scale (about a thousand km) is predominant, and the wind is mainly geostrophic, i.e. equilibrium between the Coriolis and the pressure forces. At those altitudes, the circulation patterns extend to a very large spatial scale. The geostrophic balance results in wind parallel to the isobars, explaining cyclonic (around low pressure) and anticyclonic (around high pressure) circulations.

In the lowest layer of the atmosphere, called the boundary layer (Figure 1.4) (typically extended to 1km in vertical), the flow is three dimensional and vertical mixing is usually strong. Turbulent eddies with dimensions at most comparable to the boundary layer height are predominant, so that the wind displays rapid variations from seconds to minutes. Those fluctuations are strongly linked to the interaction

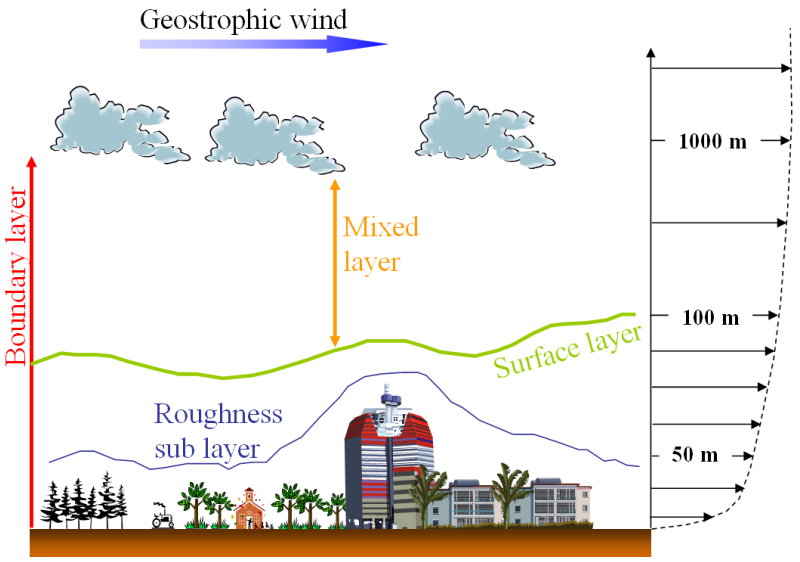

Figure 1.4: Vertical profile of wind speed in the boundary layer

of the flow with the surface. Within the boundary layer, meteorologists distinguish the surface layer (typically up to 100m) where surface friction induces high vertical shear of the flow and thus generates turbulence. The vertical profile of the wind in these parts of the atmosphere is logarithmic, and depends on the surface roughness and friction velocity which describes the turbulence of the flow.

While the previous paragraphs emphasize the contrast between the synoptic scale in the free troposphere and the short, turbulent scales of the boundary layer, there are also motions influenced by the surface at intermediate scales (from few km to a few hundreds). Larger scale flow also interacts with surface orography which drives the dynamics of the near surface wind speed by deflecting, accelerating the flow, or even giving birth to wakes and orographic waves breaking. The flow impinging on a hill may pass over or may split around, depending on the flow mean velocity, and the height of the obstacle (Smith, 1989). If a valley is formed by two reliefs the flow channelled in between can be accelerated and give birth to sustained strong winds, as it is the case in the south of France for the Mistral and Tramontane winds. In coastal areas, local thermal differences between land and sea can generate sea breeze systems often driven by the diurnal cycle, which generates temperature gradients between a rapidly heating land surface and slowly heating ocean (Simpson, 1994).

In flat areas, surface wind speed is induced by and varies with the large-scale flow. Systems such as fronts and cyclones can produce sustained strong winds. These systems are associated with jet streams induced by strong latitudinal thermic gradients (Figure 1.5). At midlatitude, the jet stream forms a barrier between polar cold air and warmer midlatitude air mass. It displays a seasonal variability and is usually stronger in winter, when thermal gradients are more important. It also displays spatial variability, with areas of stronger winds. These areas are usually

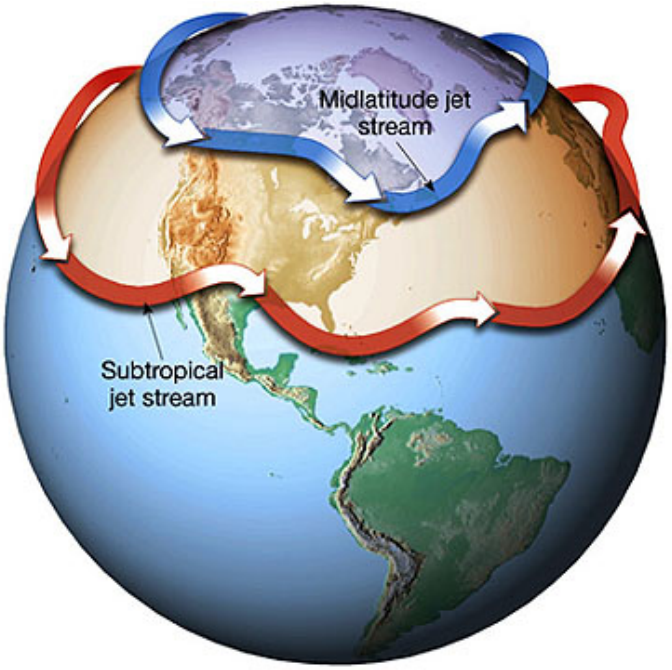

Figure 1.5: Schematic configuration of the polar and subtropical jet streams

related with the formation of precipitation systems such as lows, fronts and storms (Hall et al., 2015).

The jet stream state can be associated with weather regimes, which is a quite intuitive notion as they correspond to long periods of similar weather type. They can be defined by the probability of occurrence, the persistence, or the quasi-stationary character of large scale atmospheric circulation patterns ((Michelangeli et al., 1995)). For instance, (Plaut and Simonnet, 2001), amongst others, discuss two of the usual European weather regimes, namely the Atlantic Ridge regime (AR) which induces westerlies over Western Europe and the Blocking regime (BL) which results in North-easterlies and is often associated with a cold spell over central and western Europe. Weather regimes come from the classification of large scale atmospheric circulation patterns obtained through dimension reduction techniques.

A typical example of such a pattern is the North Atlantic Oscillation (NAO) quantified by an index which measures the time-varying pressure difference between the Islandic low and the Azores high pressure system. The strong pressure difference between these locations forms the storm track which brings high precipitation systems and strong westerlies in Northern Europe (Trigo et al., 2002). When the NAO index is positive, the pressure gradient strengthens, so that the storm track is enhanced. Conversely, negative NAO index values correspond to a weaker pressure gradient. As a consequence, the interannual variability of the European weather is partly explained through the NAO index (Lau, 1988; Rogers, 1997; Trigo et al., 2002; Scaife et al., 2014). A more famous large scale pattern is the so called El Nino

Southern Oscillation (ENSO) which comes from the displacement of the Walker cell in the pacific region. The displacement of this cell has strong impacts on the oceanic circulation in the pacific tropical region (Rasmusson and Carpenter, 1982). This oscillation has been shown to influence the atmospheric circulation at the global scale (Cassou, 2008), but mainly in tropical regions (Luo et al., 2005).

1.2.2 Implication for energy management

Assessing wind energy production from surface wind speed is not straightforward and demands a lot of considerations. First, measurements are usually available at 10m which is a level of reference in meteorology. Wind turbines harvest wind at heights ranging from 50m to 140m (Hernández et al., 2017), so that vertical extrapolation of the surface wind speed at the hub height is often necessary to evaluate the power production. The vertical extrapolation of wind speed is based on surface boundary layer theory and depends on many parameters so that it always induces uncertainties (Kubik et al., 2011). Second, assessing the resource for prospection purposes also should be based on a long time series of observations typically of the range of 30 years, which corresponds to the climatological scale. Indeed, climatology consists in a long time series that gathers the interannual variability modes of the variable of interest. Unfortunately, continuous and homogeneous observations are usually not available on such long time periods, so that numerical modelling and downscaling is needed to obtain a modelled long time series representative of a site or a region. The wind speed obtained is very often fitted with the theoretical Weibull distribution which has over the years become a standard in the wind energy industry. This distribution is based on two parameters only and is thus easy to fit, which is one of the main reasons of its widespread use. It shows good results in many regions, but its use has been challenged as it is not always the best theoretical distribution to represent observations, especially in mountainous regions (Drobinski et al., 2015; Jourdier and Drobinski, 2017; Earl et al., 2013). Finally, to obtain wind energy production, the power curve of a given turbine is applied to the wind speed distribution, which results in uncertainties. Indeed, in practice, the real power obtained from a turbine differs from the one expected from the manufacturer's power curve, for instance due to the variations of the air density or the varying intensity of turbulence.

If the assessment of the resource in advance for prospection purposes constitutes a domain in itself, the management of installed wind energy is also a large domain of interest. Indeed, energy transition from conventional production means as coal, gas, oil, and nuclear to mainly wind and solar energy constitutes a real change of paradigm. Wind and solar power production is naturally variable and hard to predict whereas conventional plants are much easier to control. The variability of the resource at different timescales raises many issues related to the economic viability of producers, the management of the supply and demand balance, but also to turbines maintenance planning, turbines safety, network safety etc. (Table 1.1).

Notation	Timescale	Applications
Very short-term	less than 30min	Market clearing Network safety Turbine safety
Short-term	30min to 1-day ahead	Balancing supply and demand Intra-day and Day-ahead spot market Operating wind farm Ramp detection for turbines safety
Medium-term	Several days	Operating wind farm Maintenance Scheduling Optimizing costs
Long-term	Month - Season	Network management Maintenance Scheduling
Very long-term	Years - Climate	Prospection Evaluation of investments

Table 1.1: Important timescales to manage wind energy intermittency and corresponding applications

1.3 Strategies for forecasting wind energy

1.3.1 State of the art

Several forecasting problems in the wind energy sector can be related to different scales of the atmospheric variability (Table 1.1). Different strategies for accurately forecasting wind speed and power have been developed depending on these different spatio-temporal scales. These strategies can usually be classified into 2 categories :

- Statistical methods based on time series analysis. These methods are often based on fitting relations or learning algorithms that are able to reproduce from past observations and/or explanatory variables, the variable of interest at a given horizon. Many models exist from the simplest linear regression, or autoregressive model, to much more complex models such as artificial neural networks (ANN).

- Physical methods based on numerical models that solve the physical equations driving the atmospheric motions. Wind speed and components from numerical models allows to compute wind energy production from the power curve given by wind turbine suppliers.

At very short timescales (below 30 minutes), for the safety of the electricity network, energy is exchanged on the balancing market so that 'real time' forecasts are needed (Table 1.1 & 1.2). Turbulence in the near surface boundary layer is then of great importance when trying to forecast very short-term wind power. Persistence is a classical benchmark method for very short-term forecasts as the autocorrelation of

the wind can be strong at very short-term horizons. Several statistical methods have been studied and can, in some cases, over-perform the persistence (See for instance (Dowell and Pinson, 2016; Potter and Negnevitsky, 2006; Carpinone et al., 2015)). Nowcasting is a method based on high resolution Numerical Weather Prediction (NWP) models with real-time assimilation and time extrapolation of observations. It was historically used to follow heavy precipitation events in real-time. Some tools have been developed to apply this method to wind energy forecasts. It is however expensive in terms of computing resources so that statistical methods are usually preferred in the wind energy sector due to operational constraints.

At short timescales, wind energy producers must sell energy on the day-ahead and intra-day energy market, on which energy is sold at maximum a day ahead but can also be sold from 30 minutes to several hours ahead (Table 1.1 & 1.2). Short-term forecasts of wind speed and power are thus vital for wind energy producers to operate their wind farms and sell their production in an optimal way.

Table 1.2: Energy Markets : timescales and use

	Long-term Market	**Spot Market**		**Balancing Market**
Horizon	Months to years	Day-ahead	Intra-day (30min to hours)	Real-time (less than 30min)
Use	Managing price fluctuation	Electricity exchange on the market		Balancing supply and demand

Many studies focus on the short-term prediction of wind speed. Most of them use purely statistical methods fed with past observations as in Sfetsos (2002) who compare Artificial Neural Networks (ANN) methods with Autoregressive Integrated Moving Average (ARIMA) models from 1 hour to 1 day or Gomes and Castro (2012) who also develop ANN and Autoregressive Moving Average (ARMA) models but only at 1 hour horizon or Barbounis et al. (2006) who uses ANN to forecast wind speed at 3 days horizons with hourly resolution. NWP forecasts are also found useful at this timescale. NWP predictions can be used as such (Wagenbrenner et al., 2016; Sperandio et al., 2013) or can be post-processed using statistical models (Horvath et al., 2011; Giorgi et al., 2011).

At the turbine and farm level, forecasts of sudden changes (also called ramps) of the wind speed have long been a point of concern, not only for marketing purpose, but also for turbine safety. Ramp detection is also a large field of research and can be addressed by purely statistical methods (Wytock and Kolter, 2013; Cui et al., 2015) or NWP forecasts (Bossavy et al., 2013).

At medium-term timescales (several days to maximum 10 days), forecasting methods have also been investigated in depth. Benchmarks have been provided within the ANEMOS project (Kariniotakis and Mayer, 2004; Marti et al., 2006) as well as within the International Energy Agency (IEA) task 36 (Möhrlen et al., 2018). Several methods, mainly based on NWP ensemble forecast outputs, have been pro-

posed and analysed (Taylor and Buizza, 2002; Roulston et al., 2003; Taylor et al., 2009; Wan et al., 2014; Alessandrini et al., 2015; Taillardat et al., 2016). At these timescales, NWP prediction model outputs are much more widely used because of their ability to accurately forecast relatively large-scale systems for time horizons of half a day to weeks. Moreover, studies have dealt with the assessment of probabilistic forecasts (Pinson et al., 2007; Mohrlen and Bessa, 2018) and the way to use them in risk assessment and decision making frameworks (Pinson et al., 2009b).

On much longer timescales and with very different motivations, the impact of climate change on wind speeds has also been addressed (Sailor et al., 2008; Najac et al., 2009; Pryor and Barthelmie, 2010) in order to assess trends of wind energy production for prospection purposes (Table 1.1).

1.3.2 Toward seasonal prediction

Whereas both relatively short and very long timescales have been thoroughly studied, the intermediate timescale going from a fortnight to the seasonal horizon is a research topic for which not so many studies exist. This timescale is of interest for anticipating maintenance operations, and to a lesser extent for market risk management. In particular, seasonal forecasting is becoming very important for Transmission System Operators (TSOs) as the proportion of intermittent resources in the energy mix increases.

Figure 1.6 shows for a scenario of wind energy penetration (Burtin and Silva, 2015) (60% of renewables, and 280GW of onshore wind power installed in Europe) the daily wind power production computed from 30 climatic years (i.e reanalyzed years from ERA-Interim reanalysis ((Dee et al., 2011), for which the atmosphere state is estimated numerically from observations). It displays a strong seasonal variability as the average capacity factor is 30% in winter and 15% in summer. However, the spread of the production amongst these 30 years is the most problematic for network management. Indeed, from year to year, the average daily onshore wind power in winter can vary from less than 50GW to more than 150GW.

TSOs are responsible for balancing supply and demand of energy and they are required to make seasonal projections, e.g., to guarantee the security of energy supply during the coming winter, which becomes more difficult with the increased variability of energy production. The risk of not being able to satisfy the energy demand may be quantified in terms of the notion of Loss of load expectation (LOLE). Quoting from (NationalGrid, 2016), the LOLE is a "measure of the risk across the whole winter of demand exceeding supply under normal operation. It gives an indication of the amount of time across the whole winter that the System Operator may need to call on a range of emergency balancing tools to increase supply or reduce demand." For instance, a cold winter characterised by weaker winds than normal may in some cases lead to a lack of energy if not enough other production means have been made available upstream to meet the energy demands.

Figure 1.7 displays a sensitivity analysis performed before the winter of 2016/2017

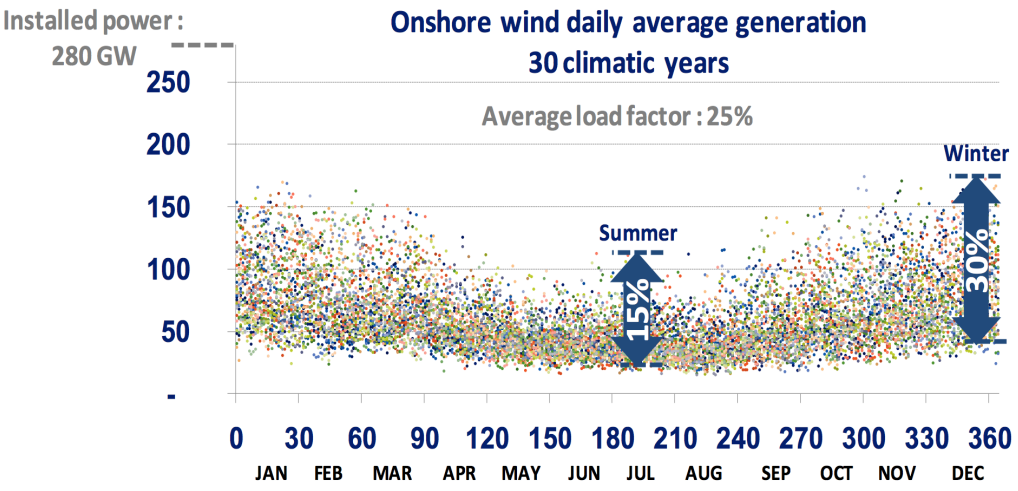

Figure 1.6: Variability and dispersion of the capacity factor at the seasonal and interannual scale - EDF scenario of 60% REN in the European energy mix (Burtin and Silva, 2015)

by the European Network of Transmission System Operators for Electricity (ENTSOE), here for France and for the second week of January 2017 specifically. It uses 14 climatic years to compute likely consumption and wind energy production. Information about the availability of other means of production for this winter, like nuclear plants in France, also plays a significant role in this sensitivity analysis. It shows that for low temperature and low wind energy capacity factor risks of deficit exist with the current European energy mix even after importing electricity from other countries (ENTSOE, 2016). It is thus essential to produce informative forecasts of surface wind speed at this timescale. Here, meteorological information comes only from a limited climatology (14 years). Note that we present here the risk of lower than expected production which is of high concern for TSOs, but the inverse risk of higher production than consumption is also hazardous as it may result in sharp drops of electricity prices.

In France, RTE (Réseau de Transport d'électricité) uses essentially the climatological surface wind speed to estimate the production at the seasonal scale. Indeed, at such long-term timescales, predictability of the weather is an open question, and it is particularly the case for surface variables which are influenced by many small scale phenomena.

Nevertheless, some studies show good results in forecasting the monthly mean wind speed at several observation sites by using Artificial Neural Network models (ANN) (Bilgili et al., 2007; More and Deo, 2003; Azad et al., 2014), giving an accurate trend of the wind speed a season ahead, but a limited information on the wind variability at higher frequency. Other authors forecasted daily mean wind speed at the seasonal scale using ANN (Azad et al., 2014; Wang et al., 2015; Guo et al., 2012)

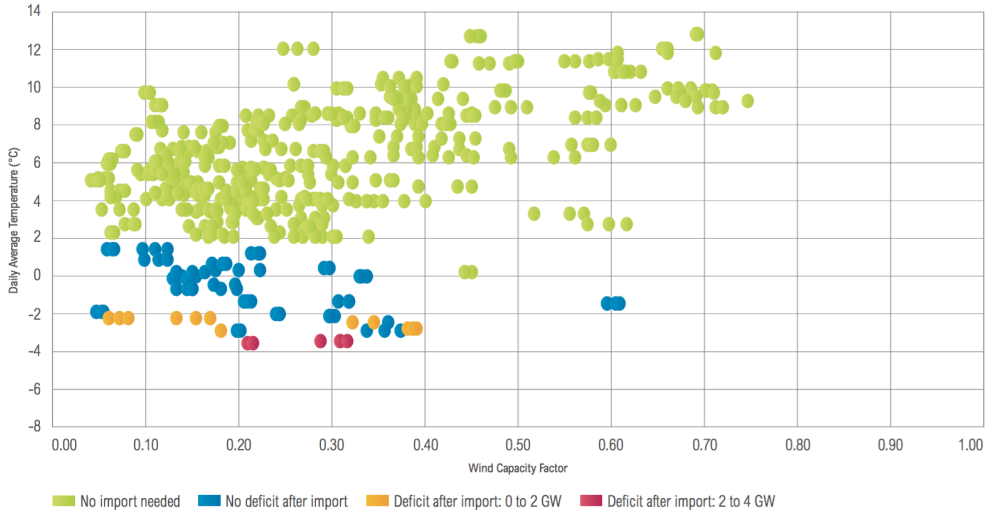

Figure 1.7: Sensitivity analysis in France over 14 climatic years - Each point corresponds to a day. This figure is taken from the ENTSOE winter outlook report 2016/2017 (ENTSOE, 2016)

allowing to gather more information on the wind variability inside a given season , and also allowing to evaluate the energy production. Azad et al. (2014) interestingly decompose the wind speed signal at different scales (namely the yearly, monthly, and daily trends). Wang et al. (2015) uses the same idea of scale decomposition by combining a trend component with a seasonal component together modulated by higher frequency variations of the wind speed signal. As ANN behaves like a black box fed with data, the results are difficult to explain physically. Moreover, each method focuses on different observation sites, thus making comparisons difficult. In addition, these studies provide 'point forecasts', which give one value for the wind energy production at the seasonal horizon, but do not consider the uncertainty on the forecast (as a rule, forecast uncertainty is difficult to quantify with neural networks since the underlying probabilistic model is not easy to define). At such timescales, the idea of point forecast is very questionable due to the dominant chaotic nature of the atmospheric system at the timescale exceeding typically 10 days (Kalnay, 2003).

At this long-term horizon, the concept of probabilistic forecast therefore gains sense, not only because of the uncertain nature of the forecast, but also because the decision making process is based on probabilities. Decision processes may be of several nature. At the seasonal scale, on the producers' side, turbines maintenance scheduling on days when production is expected to be lower than normal is a good example of a decision making process. On the side of TSOs, the amount of emergency production means needed to overpass a given risk of imbalance between supply and demand can be cited.

Even though there are few works on seasonal forecasts for surface wind speeds,

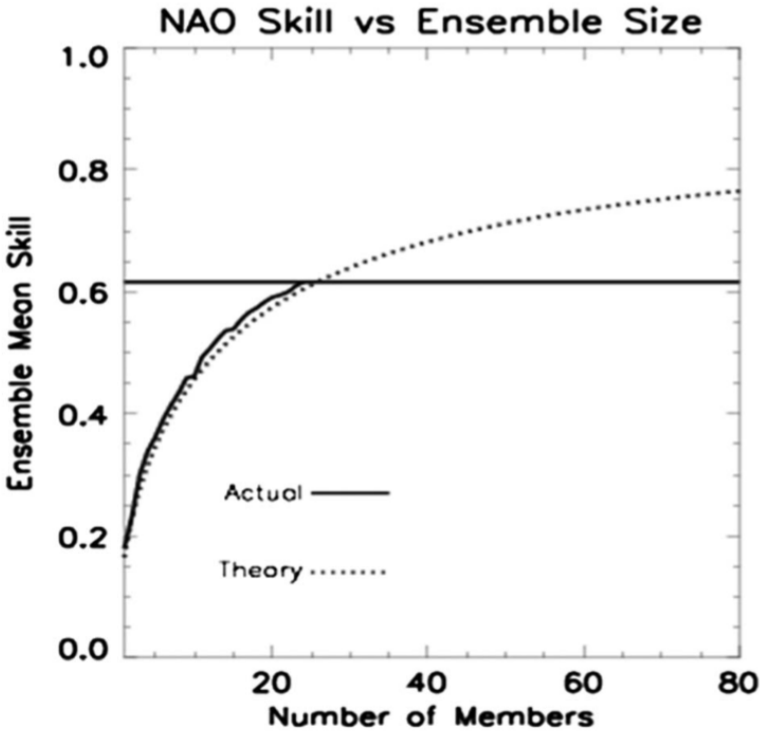

Figure 1.8: Correlation between observed and mean ensemble forecasted NAO seasonal index at one month lead time in winter 1993 to 2012 as a function of the ensemble size - Figure taken from (Scaife et al., 2014)

seasonal forecasting of other meteorological quantities is a popular research topic with continuous improvement. For example, there have been many works on seasonal forecasts of recurrent oscillating patterns in the atmosphere, such as the El Nino which has strong impacts on the weather variability mainly in the pacific region, but also at the global scale (Owen and Palmer, 1987; Cassou, 2008). Its impacts on weather predictability have been highlighted especially in the tropics (Luo et al., 2005). Other recurrent oscillating patterns in the Northern hemisphere are related to European atmospheric circulation variability (Casanueva et al., 2014; Folland et al., 2008). Predictability of such oscillations has shown good skill (Dunstone et al., 2016; Smith et al., 2016) so that they may inform on the atmospheric circulation variability at the scale of the month and eventually the season (Davies et al., 1997; Rodwell et al., 1999; Johansson, 2006; Weisheimer et al., 2017). Particularly, the North Atlantic Oscillation (NAO) has strong impact on temperature, precipitation, wind speed in Europe as it is related to the storm track which is very active in winter (Lau, 1988; Rogers, 1997; Trigo et al., 2002; Scaife et al., 2014). Skill of ensemble forecasts systems in predicting NAO has been demonstrated by Scaife et al. (2014), as shown in Figure 1.8 which highlights that depending on the forecast ensemble

size the correlation between observed and forecasted NAO seasonal index can be as much as 0.6 and theoretically may reach almost 0.8.

More recently, NWP seasonal ensemble forecasting systems have been shown to carry valuable information even at seasonal timescales and for surface variables linked to wind, solar, hydro power, and electricity demand (Dubus, 2012; Krakauer and Cohan, 2017; Torralba et al., 2017; Clark et al., 2017; Vitart and Robertson, 2018). Dubus (2012) shows that using European Center of Medium-range Forecast (ECMWF) monthly forecasts of surface temperature in France allow to be more accurate than forecast references (comparable to climatology) very often up to week 2, and sometimes to week 3 or 4. It is also shown that river discharge essential for the operation and planning of hydroelecricity can be linked to large-scale atmospheric circulation via an analog method which results on average in better skill scores than climatology. Krakauer and Cohan (2017) investigate the monthly based correlation between wind, solar energy and typical large scale atmospheric patterns, at the global scale. They show that the interannual variability of wind and solar energy resource can be related to these large-scale atmospheric patterns. Clark et al. (2017) show that, at the scale of Europe, the correlation between monthly mean 10m wind speed and temperature with the forecasted monthly index of NAO is significant. This suggests that useful forecasts could be obtained through this relationship. The NWP model forecasts assessed are shown to give more valuable signal in the West of France and over the North Sea compared to other regions. Torralba et al. (2017) assess the ECMWF seasonal ensemble forecasts skill for forecasting the seasonal mean of the surface wind speed in winter, at a global scale. The study shows that, after bias-correction and calibration of the ensemble, reliable forecasts of the seasonal mean of the surface wind speed are available in different regions of the world. Forecast skill is demonstrated especially in the tropics, but also at mid-latitude, in the North Atlantic region where the installed capacity is important.

1.4 Objectives of the work

The general problem raised in this work is to know whether seasonal ensemble forecasts from NWP models allow to go further than the current climatological approach to forecast the wind energy resource, production, and potential risk of imbalance between production and consumption at the seasonal scale.

As explained, at the seasonal scale, the main accurate information we can expect from NWP forecasts is the representation of the large-scale flow. Especially, they should have skill in forecasting large-scale atmospheric recurrent patterns such as the NAO which strongly influence the European climate, and in particular the surface wind speed.

In this context, we define three main objectives for the thesis :

- The first aim is to relate the surface wind speed in France to the large scale circulation of the atmosphere. This relation will serve to estimate part of

the variability of the surface wind speed from information on the large scale atmospheric state. More particularly, we want to show that a major part of the interannual variability of the surface wind speed in France is explained by the large scale flow.

- Second, the thesis aimed at showing that the information on the large scale atmospheric circulation contained in seasonal ensemble forecasts provides useful information on the surface wind speed, on monthly to seasonal timescales.

- The third objective is to show that the approach described above can be used directly for assessing the risk of imbalance between consumption and production at the seasonal horizon. This implies to define risk indicators that quantify the potential imbalance between production and consumption, and to develop a methodology to estimate the risk from seasonal forecasts.

Finally, while the central aim of the thesis has focused on seasonal forecasting, a complementary objective has been to intiate a comparison between modeled winds and observed winds. A first aim has been to test, for one location, how accurate the modeled winds are, and a second aim has been to explore how much information could be gained by post-processing the model output (downscaling).

1.5 Outline

Chapters 2 and 3 adress the first and second objectives. They describe two methodologies to model the relationship between large scale circulation patterns and local surface winds and to obtain, from seasonal forecasts information, the likely surface winds at locations in France.

In the second chapter we model the local surface wind speed distribution in the parametric setting, by assuming that it follows the two-parameter Weibull law. We show that the models are more accurate than the climatology in some regions and seasons. The study also highlights that the hypothesis of theoretical Weibull distribution leads to errors in the representation of the wind speed distribution. Computing the capacity factor from the obtained distributions shows that the wind power output is overestimated by all methods including parametric and non-parametric climatology. However, it is also shown that no valuable signal of the large-scale circulation variability remains in the forecasted ensemble mean after at most one month.

In the third chapter, we use a non-parametric method to reconstruct and forecast the daily wind speed distribution from a fortnight to 3-month horizon in France using again the information coming from the large-scale circulation of the atmosphere. The conditional probability density function of the wind speed knowing a single index which summarises the information on the large scale circulation of the atmosphere is estimated by kernel density estimation. The model is shown to be well calibrated

as well as more accurate than the seasonal climatology in reconstructing wind speed distribution. While applying the method to seasonal forecast ensemble, we show that post-processing allows to recalibrate and sharpen the ensemble so that even at the seasonal scale, the method can be more accurate than climatology for specific regions and seasons.

In the fourth chapter, we adress the third objective and turn to modelling the risk of imbalance between consumption and wind energy production at the seasonal scale, in winter and fall. Two types of risk measures are defined : one measures the probability of deviation of consumption and production from their climatological means, and the other measures the risk of encountering extreme situations of imbalance. Using again the valuable information on the large-scale circulation, we build the seasonal joint distribution of the national consumption and the national wind energy production to compute the first risk measure. It is shown that we accurately reconstruct the variability of the risks of imbalance. Significant deviation from the climatological state are well highlighted by the model, especially in winter, when the model retrieves 75% to 80% of the deviations. In fall, significant deviations from climatology are less frequent, and the model performs worse. The second risk measure is estimated by quantile regression. Reconstructed quantiles are shown to be reliable, and the model highlights risky extreme events that could be very persistent.

The fifth chapter is dedicated to the downscaling of wind speed at a given observation site. Indeed, this kind of downscaling models would allow to go beyond the perfect model approach adopted in the manuscript. We evaluate several statistical downscaling methods based on explanatory variables from Numerical Weather Prediction (NWP) model. The study shows that statistical downscaling methods significantly reduce biases and increase correlations between the observed and reconstructed time series. Such methods could be applied to obtain more realistic spatial representation of the French wind energy production for instance.

1.6 Description of the Data

1.6.1 ERA-Interim Reanalysis

Throughout the manuscript, we use the ERA-Interim (ERA-I) reanalysis dataset from the European Center of Medium Range Weather Forecasts (ECMWF) (Dee et al., 2011) to describe the atmospheric variables, both the surface winds and temperature and the large-scale circulation. To understand what a reanalysis dataset is, let us first define an analysis for the atmospheric state at a given time. An analysis is the best estimate of the atmospheric state (winds, temperature, pressure, ...) given information from both observations and the previous forecasts from a NWP model. The analysis is obtained in the same format as the model output, and the mathematical methods to merge optimally the information from observations and model output are called data assimilation. To obtain a description of the atmosphere

over a long period, which is homogeneous over the whole period, it is necessary that the model and the data assimilation methods used remain the same. Hence, operational centers regularly conduct dedicated efforts to build a dataset of analyses that are consistent in time (ie frozen model and data assimilation scheme), and such a dataset is designated as a *reanalysis*.

Databases containing only observations do not allow for such spatial and temporal homogeneity. Therefore, ERA-I is here considered as a reference following the 'perfect model' approach (Elia et al., 2002) common in meteorological studies. This approach can be seen as the use of reanalysis data as a substitute observations which we try to predict. Such approach has the advantage of isolating the errors related to statistical modeling only. As a consequence, it gives an upper limit of the achievable forecast skill. This approach is limited by the realism of the atmospheric modeled fields: whereas the large-scale circulation is very well described in the reanalysis, some errors are expected for surface winds, which vary on shorter scales than mid-tropospheric pressure. Nonetheless, previous comparisons to observations (Jourdier, 2015) justify the use of the reanalyzed surface winds as a good description of the variability of surface winds in France. We focus on France and its vicinity not only because the reanalyzed winds had been assessed there, but also because France has a significant wind energy potential and interestingly includes regions with different wind regimes. In Northern France the wind energy potential stems from the storm tracks, whereas local orographic effects and channeling play a major role in strong wind events of Southern France (Drobinski et al., 2015).

The large-scale circulation is well represented by the 500-hPa geopotential height (Z500). Z500 is defined as the height of the constant pressure level of 500hPa. From a map of Z500, troughs and ridges, highs and lows, which are typical markers of air mass distribution and motions (thus of the large-scale circulation of the atmosphere), can be easily identified. Clustering techniques allow to highlight large-scale atmospheric circulation regimes which explain a large part of the climate variability over Europe (Michelangeli et al., 1995).

We retrieve all the information on the atmosphere (large-scale state, surface winds, surface temperature) from ERA-I, with a grid resolution of 0.75° [1] and over a time period spanning from January 1, 1979 to December 31, 2015[2] (Table 1.3). The daily time series[3] of 500-hPa geopotential height (Z500) is retrieved over a large domain that spans the North Atlantic Ocean and Europe (20°N to 80°N and 90°W to 40°E), (Figure 1.9, a). The daily surface wind speed is retrieved over a smaller domain which covers France and parts of neighbouring countries (40.5°N to 52.5°N and -6.75°W to 10.5°E) (Figure 1.9, b). Surface wind speed is averaged to daily frequency in order to remove the intra-day variability of the wind. Indeed, the large-scale circulation of the atmosphere cannot explain intra-day variability such

[1]The French domain has 408 grid points and the large domain has over 13000 points

[2]ECMWF data are available at http://apps.ecmwf.int/datasets/

[3]ERA-Interim provides 6-hourly outputs of Z500 and surface wind speed, from which we compute the daily averages used in this study.

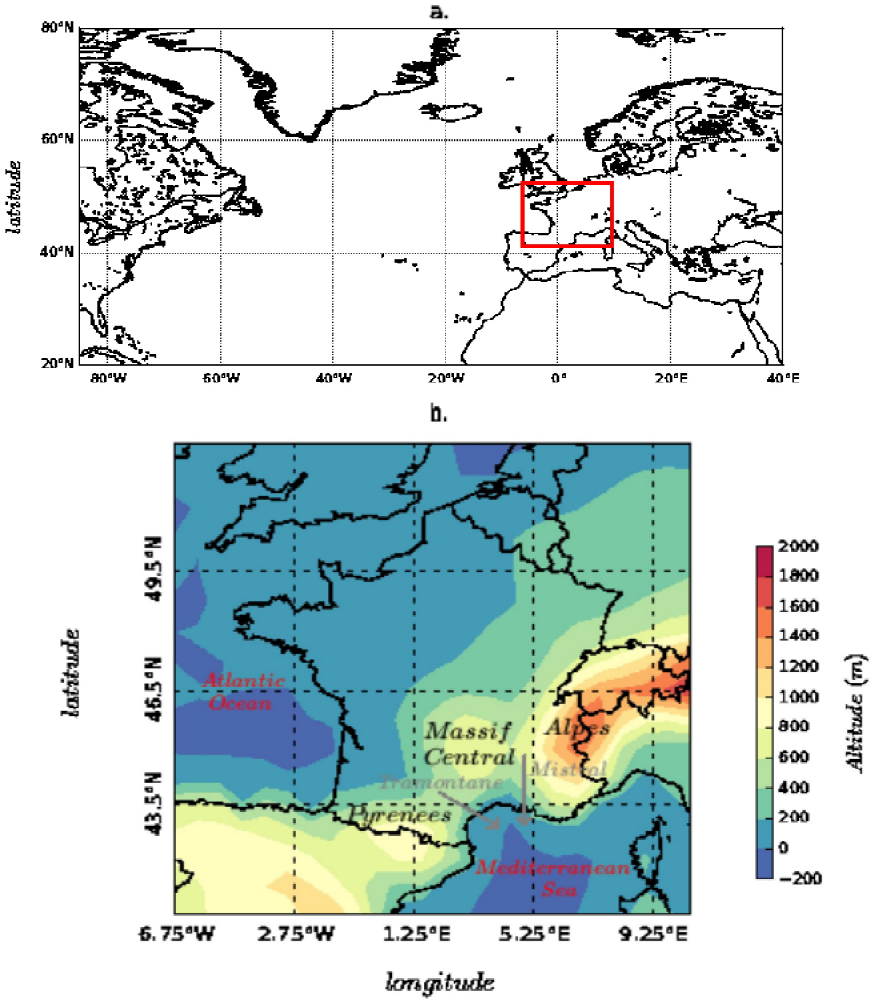

Figure 1.9: (a) North Atlantic/European domain from where the Z500 is retrieved. The red box corresponds to the domain in panel b. (b) Domain covering France and part of its neighbouring countries. The colors represents the altitude above the sea level.

as the diurnal cycle. Finally, the daily surface temperature (at 2m) is retrieved from ERA-I over the French domain (Figure 1.9, b). The average temperature over France (defined by its country borders, inland) is computed in order to compute the French national daily peak consumption in Chapter 4.

1.6.2 ECMWF seasonal ensemble forecasts

The ECMWF seasonal ensemble forecasts system 4 is a coupled ocean-atmosphere numerical weather prediction model (NWP). The atmospheric model is based on the Integrated Forecast System (IFS Cy36r4). It has 91 vertical levels and a horizontal

resolution of approximately 0.75°. The ocean model is NEMO (Nucleus for European Modelling of the Ocean) with 42 vertical levels, and 1° horizontal resolution. The ECMWF seasonal forecast ensemble consists of 51 members and provides a forecast 7 months into the future.

A forecast ensemble consists in a certain number of forecasts for the same period, with members typically differing by slight differences in their initial states, or in the model parameters. One member is called the control member and its initial state (known as the analysis) is given by the aggregation of the last forecast and the assimilation of all observations available. All other members start from a slightly perturbed initial state. Due to the chaotic character of the atmospheric circulation, the members spread, sampling a range of different possible states of the atmosphere which grows with the forecast horizon.

We retrieve the 500hPa geopotential height from ECMWF seasonal ensemble forecasts between January 2012 and December 2015 (Table 1.3). This range of dates results from a compromise: on one hand we wish to have a long period in order to have more statistically robust results. On the other hand, we need to restrict to a period over which changes to the modeling system (model and data assimilation scheme) do not introduce major discontinuities. A major change of the assimilation system and forecast model limits the use of seasonal forecasts before November 2011. A seasonal forecast is started from the first day of each month, and contains predictions for the 7 following months with a time step of 6 hours. Consequently, 48 forecast sets are used in the manuscript.

Variable	Domain	Time period	Frequency	Treatment
ERAI Z-500	North Atlantic and Europe, 0.75° resolution	Jan 1, 1979 to Dec 31, 2015	6-hourly	Daily averaging
ERAI Surface wind speed	France, 0.75° resolution	Jan 1, 1979 to Dec 31, 2015	6-hourly	Daily averaging
ERAI temperature at 2m	France, 0.75° resolution	Jan 1, 1979 to Dec 31, 2015	6-hourly	Daily averaging & National averaging
Z-500 ECMWF forecast ensemble	North Atlantic and Europe, 0.75° resolution	Jan 2012 to Dec 2015	monthly	select forecast horizons of 3 months
Surface wind speed ECMWF forecast ensemble	France, 0.75° resolution	Jan 2012 to Dec 2015	monthly	select forecast horizons of 3 months

Table 1.3: Summary of data used for the manuscript. Every ECMWF forecast ensemble contains 51 members and includes forecasts with lead times from 6 hours to 7 months, with a time step of 6 hours.

The number of forecasts available may limit of the generalization of the results obtained, especially when looking at forecasting skill for specific periods of the year. The choice to use the recent ECMWF seasonal ensemble forecasts is made because

the forecast system of ERA-I reanalysis and of the ECMWF seasonal forecasts do not differ too much. The ECMWF seasonal ensemble forecasts has also the advantage to consist of a large number of members, which gives a good framework for probabilistic forecasting. Other dedicated databases of seasonal ensemble re-forecasts (i.e seasonal forecasts of past years with recent forecast systems) could be used to evaluate the potential generalization of our results. Nevertheless, seasonal ensemble re-forecasts generally have fewer members, and may not fit to our 'perfect model' approach which considers ERA-I surface wind speed as a reference.

We retrieve the forecasted Z500 field over the large domain (Figure 1.9a.), to be used in our forecasting procedure, and the forecasted surface wind speed over the French domain (Figure 1.1b), to be used for comparison purposes. We average the data at daily frequency, and keep only forecasts for the time horizon of up to 3 months. The description of data sets used along the manuscript is summarized in Table 1.3.

1.6.3 Principal component analysis

To obtain a more compact representation of the large-scale situation we perform a Principal Component Analysis (PCA) on Z500 of ERA-I over the 37 years period. The PCA method is widely used in climate science in order to decompose a spatio-temporal field into an orthogonal basis that maximizes the variance. It is the eigendecomposition of the Z500 spatio-temporal field which results in eigenvectors called the Empirical Orthogonal Functions (EOFs) which represent the typical oscillation patterns spanning the North Atlantic domain. Each EOF is associated with its eigenvalue giving the amount of variance explained by the EOF, and one scalar time series (the corresponding Principal Component (PC)) which describes how each pattern evolves in time.

In other words, denoting by $Z_t(x)$ the $Z500$ signal of day t at the spatial location x, the PCA provides a representation

$$Z_t(x) = \sum_{i=1}^{n} X_t^{(i)} f_i(x) + \mathcal{E}_t(x),$$

where $X_t^{(i)}$ are the PCs, $f_i(x)$ are the EOFs and $\mathcal{E}$ is the component which is not explained by the first n PCs.

The first EOFs explain most of the variance of the dataset (Table 1.4). A posteriori, they can be explained physically, to a certain extent, because they are the signature of the atmosphere dynamics. They are indeed closely related to the large scale atmospheric patterns found by Michelangeli et al. (1995) andPlaut and Simonnet (2001) (see section 1.2.1). As a matter of fact, they correspond to the preferential states of the atmosphere, under the assumption that these patterns are quasi-stationnary, meaning that on the long term their time derivative vanishes. This assumption amounts to saying that these patterns evolve in a stable climate.

Pattern	PC	Variance explained (%)	Cumulative variance explained (%)
Seasonal cycle	1	54.1	54.1
NAO	2	8.1	62.2
SCA	3	5.6	67.8
EA	4	5.2	72.9
EU2	5	3.9	76.8

Table 1.4: *Variance Explained:* Five first Principal Components of the Z500 and the percentage of variance explained by each of them.

Figure 1.10 shows the five first EOFs and their associated PCs. The first PC corresponds to the seasonal cycle (Fig 1.10. a,b), explaining as much as 54.1% of the variance in the dataset: in winter the meridional pressure gradient strengthens, leading to stronger winds and more intense synoptic systems. The following four PCs have a clear physical interpretation (Vrac et al., 2013; Cassou et al., 2004), they all be related to teleconnection patterns, respectively the North Atlantic Oscillation (NAO) (Fig 1.10. c,d), the Scandinavian pattern (SCA) (Fig 1.10. e,f), the Eastern Atlantic Pattern (EA) (Fig 1.10. g,h) and the 2nd European pattern (EU2) (Fig 1.10. i,j). These five first PCs explain 76.8% of the variance in the entire dataset (Table 1.4). Even if next PCs can not be clearly identified with classical atmospheric patterns, they should nevertheless contain information on large-scale variability, and will be also used in the following.

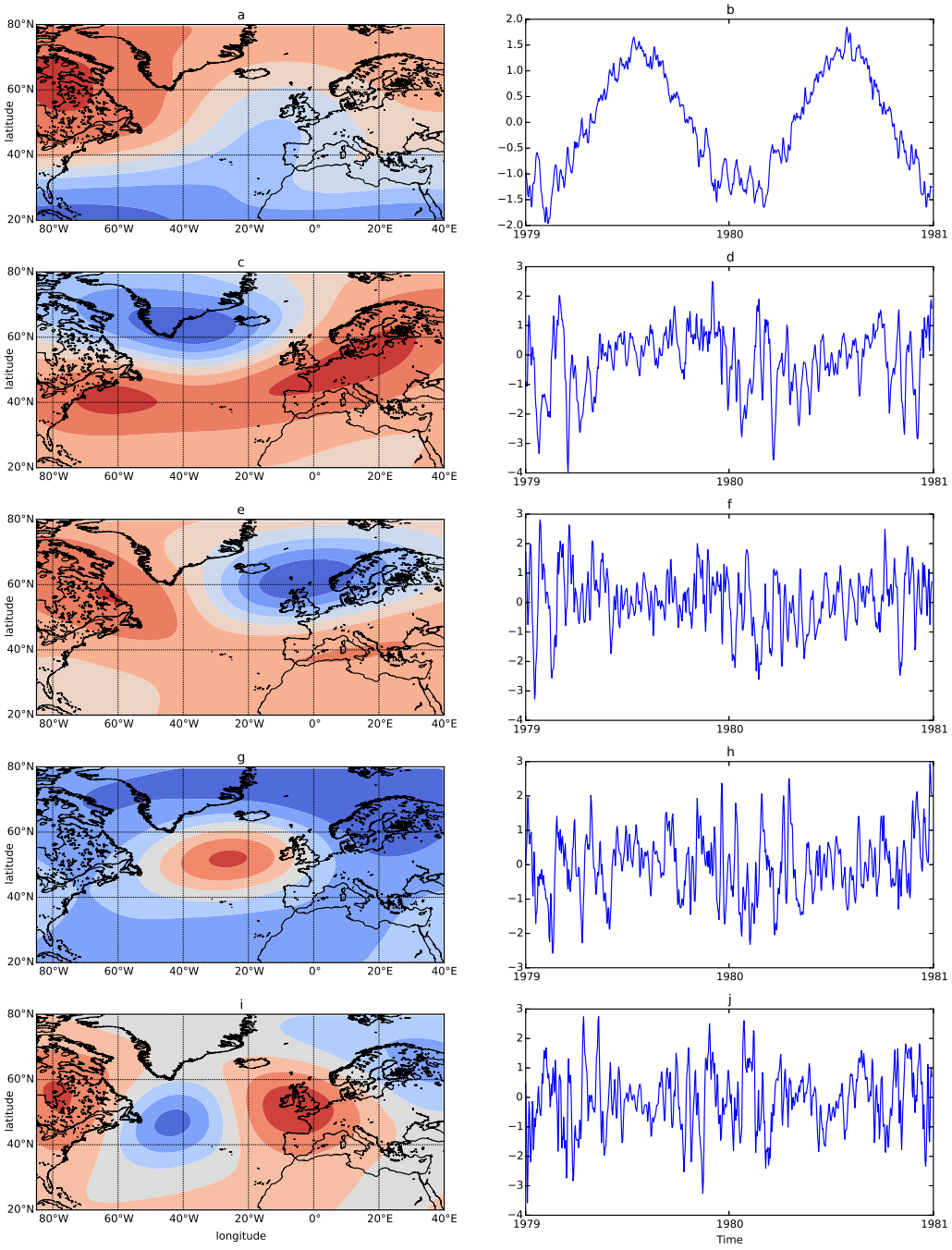

Figure 1.10: Five firsts EOFs (left side) and five first PCs (right side) of the PCA performed on the calibration and validation period and on the North Atlantic/Europe domain of ERA-Interim Z500 dataset. - a,b Seasonal pattern - c,d North Atlantic Oscillation pattern - e,f Scandinavian pattern - g,h Eastern Atlantic pattern - i,j European 2^{nd} pattern ; EOF and PC respectively

Chapter 2

Modelling the Variability of the Wind Energy Resource on Monthly and Seasonal Timescales

Contents

2.1 Introduction

Variables tied to surface phenomena such as surface wind speed are not accurately described by NWP models at the seasonal timescale. Numerical models nevertheless have recently been shown to be able to forecast with a good accuracy the large-scale circulation of the atmosphere at timescales of a month and possibly a season. The idea developed in this chapter, but also all through the manuscript is that surface wind speed is closely related to the large scale circulation of the atmosphere at such timescales. Therefore, this information can be used to predict the surface wind speed at monthly to seasonal scale.

The following chapter adresses mainly the first objective by proposing a method to build the relationship between the large scale atmopheric circulation represented by the Principal Components (PCs, See section 1.6.3) of the Z500 and the local surface wind speed distribution in France. This relationship will serve to estimate part of the variability of the surface wind speed from information on the large scale atmospheric state. More particularly, we want to show that a major part of the interannual variability of the surface wind speed in France is explained by the large scale flow. The comparison with the climatological approach supports our hypothesis that the proposed method fits to better modelling of the surface wind speed than the current approach. In a second step, the assessment of the NWP forecasts of the large scale circulation patterns aims at giving a first insight on the information given by such forecast and thus to partly answer the second objective of the thesis. To this purpose, we use reanalysis data from the European Center of Medium-range Weather Forecasts (ECMWF), called ERA-Interim (ERA-I), in a perfect model approach similar to Elia et al. (2002), as well as the ECMWF seasonal ensemble forecasts as described in section 1.6.2.

In this chapter, we link the large-scale circulation of the atmosphere with the parameters of the Weibull distribution in order to model the monthly and seasonal distribution of the surface wind speed at different locations in France. Building the monthly or seasonal distribution of the surface wind speed allows to retrieve the corresponding wind energy capacity factor through theorical power curve adapted for surface wind speed. Three distinct methods are used to model the monthly and seasonal Weibull distribution of the surface wind speed. The first method aims at better modeling the tail of the distribution which is important in terms of capacity factor and wind power assessment. In the second method, we fit directly the seasonal (monthly) shape and scale parameters to the seasonal (monthly) mean of the PCs of the Z500. The third method aims at taking into account the spread of the distribution and is based on the regression between two percentiles and the PCs of the Z500.

Assessing the proximity of the modelled monthly and seasonal Weibull distributions with the empirical Cumulative Distribution Function (CDF) using an adapted statistical test allows to assess the ability of the model to accurately reconstruct the seasonal distribution of the wind speed. Climatological CDF skill is compared to

the model skill as it is the usual reference for this timescale. The performance of the model is shown to have spatial and seasonal variability which can be explained physically considering the explanatory variables taken into account. The model is shown to have good skill compared to the empirical climatology and even better skill compared to climatology fitted with Weibull distribution, which confirms that theorical Weibull distribution may not be the best way to address surface wind speed distribution. An attempt of forecast is performed using the ECMWF seasonal ensemble mean forecast. Unfortunately, the error of the ensemble mean forecast displays a saturation after at most one month and does not allow for accurate prediction of the seasonal distribution of surface wind speed.

In the first part of this chapter, the data and methodology used to link the large scale circulation with the surface wind speed and to reconstruct its monthly/seasonal distributions is described. Then, the performance of the proposed methods is evaluated by comparing their skill to the climatology. The performance is evaluated in terms of recontructed electricity generation as well. In the last part of the chapter, an attempt in forecasting wind speed distributions and electricity generation is discussed.

This work has been published in the journal *Renewable Energy*. The full citation can be found in the bibliography of the manuscript (Alonzo et al., 2017).

2.2 Data & Methods

2.2.1 Data

A more comprehensive description of the data is given in chapter 1 in section 1.6. In the following, the specificity of the data used for this study is described.

ERAI reanalysis Wind speed, geopotential height at 500hPa (Z500) are collected from ERA-Interim reanalysis (ERA-I, (Dee et al., 2011)) between 01/01/1979 and 12/31/2013 (35 years). Z500 spans the domain shown in figure 1.9 a, and the surface wind speeds are obtained for a domain shown in figure 1.9 b.

First, the 35 first years period is divided into 2 sub-periods :

- A 20-year calibration period, on which we train our methods, is defined from 1^{st} of January 1979 to 31^{st} of December 1998. On this calibration period, the local monthly/seasonal climatology of the wind speed is computed.
- A validation period lasting 15 years from 1^{st} of January 1999 to 31^{st} of December 2013 follows. This period is used to assess the reconstructed distributions with respect to seasonal and monthly wind speed distributions based on ERA-I surface wind speed.

Note that an attempt to use both the geopotential height at 500hPa (Z500) and the Mean Sea Level Pressure (MSLP) to represent large-scale circulation of

the atmosphere has been performed. Nevertheless, we only present the results of reconstruction using the Z500 variable as a predictor of the surface wind speed. Indeed, results found when adding MSLP to Z500 predictor were comparable and the improvement was neither systematic nor significant.

ECMWF Forecasts We retrieve twelve seasonal forecast sets of ECMWF's numerical weather prediction model (Molteni et al., 2011), from the years 2012, 2013 and 2014, each lasting three months, starting from January, April, July and October. Each forecast is composed of 51 seasonal forecast members from which we compute the ensemble mean, corresponding to the most likely scenario if we assume normality of the ensemble at each time step. This scenario is used as the only forecasted state of the atmosphere.

The period from 1979 to 2011 (33 years) of ERA-I is used as a calibration period in the forecast section, while the period of forecast is always of 3 months, allowing to predict either monthly or seasonal distribution of the surface wind speed. We apply the same methods using the 33 years of ERAI to learn the relationship between the surface wind speed and the large-scale circulation of the atmosphere, and apply this relation to the forecasted state of the atmosphere to predict wind speed distribution.

In this part of the chapter, we use ECMWF Analysis as reference for wind speed. Indeed, ECMWF analysis allows to confront the methods to data which are very close to the actual wind speed. The assimilation system and model may not differ to much from the one used for ERA-I reanalysis.

2.2.2 Methods

As explained in section 1.6.1, we follow an approach similar to the perfect model approach (Elia et al., 2002) by using the surface wind speed from ECMWF reanalysis (ERA-I) or analysis as the reference against which reconstructed wind speed distributions must be evaluated. By construction, the surface wind speed and 500-hPa geopotential height from ECMWF reanalysis or analysis are consistent between each other. This approach ensures to isolate the errors associated with the reconstruction methods only. Evaluating against surface wind speed measurements would require to quantify the various sources of errors, including representativity and instrument errors, which is out of the scope of this work and would not help in quantifying the ability of our method for monthly/seasonal forecast of wind speed.

In the following paragraphs, we describe in detail the reconstruction methodology which is summarized in Figure 2.1. Our attempt aims at reconstructing the distribution of winds on the monthly to seasonal timescales, but not at reconstructing daily time series of winds. Indeed, our reconstruction methodology is based on the principal components analysis of the Z500 predictor which informs about the large-scale state of the atmosphere. This knowledge will constrain the likely distribution of surface winds on timescales larger than the lifetime of individual synoptic

systems (fronts, storms) and thus will not allow to reconstruct such high frequency time series. Following the common practice, we use the Weibull distribution to summarize the surface wind speed distribution (T.Burton et al., 2011; Manwell et al., 2009).

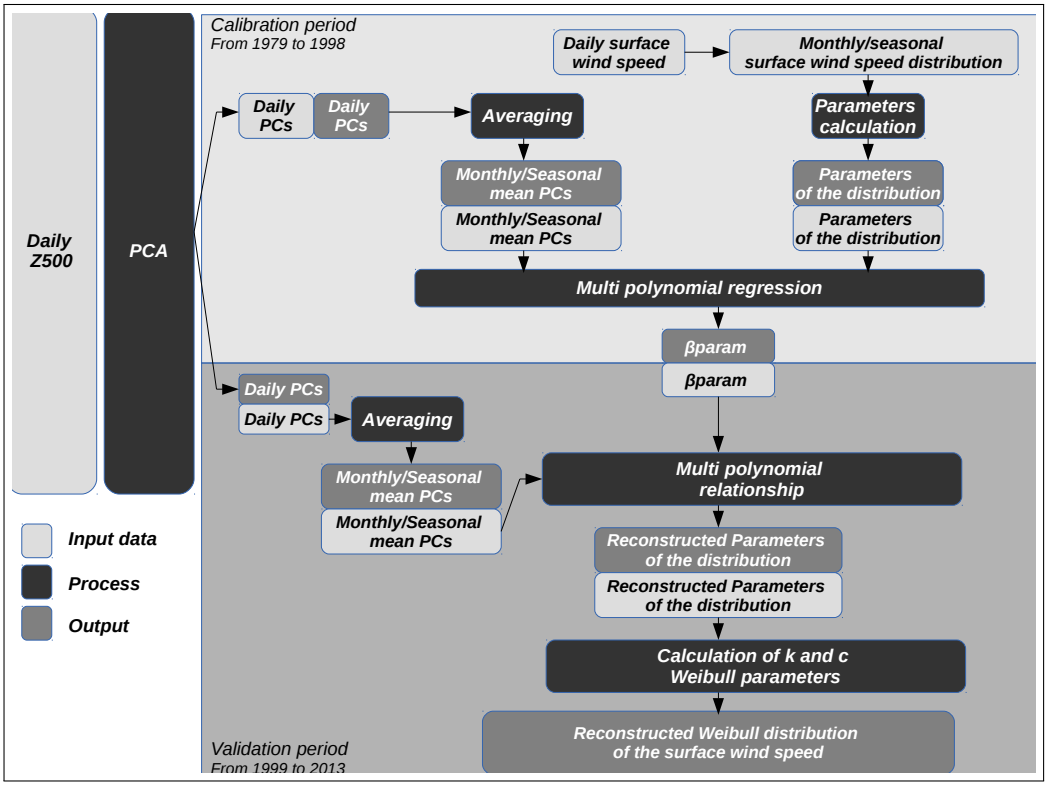

Figure 2.1: *Reconstruction Method:* Flow chart describing the reconstruction methodology

Principal component analysis To obtain a more compact representation of the large-scale situation we perform a Principal Component Analysis (PCA) on Z500 (see section 1.6.3) . The PCs resulting from this decomposition are used as explanatory variables of the surface wind speed distribution.

Weibull distribution To summarize the wind distributions, we choose the Weibull distribution as the parametric representation for montly and seasonal distribution of the surface wind speed at a given location. This theoretical distribution is widely used in the wind energy industry (Lun and Lam, 2000; Justus et al., 1976; T.Burton et al., 2011). It provides a simple way to represent the wind distribution as it is based on only two parameters: the shape parameter and the scale parameter. We must highlight the fact that other theorical distributions better capture the shape of the real wind distribution. In particular, the Rayleigh-Rice distribution can have

two modes, which is not the case for the Weibull (Drobinski et al., 2015; Jourdier and Drobinski, 2017).

The probability density function (PDF) and the cumulative distribution function (CDF) of the Weibull distribution are expressed as follows.

$$f(u;k,c) = \frac{k}{u}\left(\frac{u}{c}\right)^k e^{-(u/c)^k} \tag{2.1}$$

$$F(u;k,c) = 1 - e^{-(u/c)^k}, \tag{2.2}$$

where u is the wind speed, k and c are respectively the shape and the scale parameter.

We now define three ways to reconstruct the parameters k and c from the data. The WAsP method, referred in the following as WAsP (N.G. Mortensen and Petersen, 1998), computes these parameters from the moments $\overline{U}$ and $\overline{U^3}$, as well as the probability of exceeding the mean wind speed $1 - P(\overline{U})$ (which must be estimated from the data). The method focuses on the right-hand tail of the Weibull distribution, which is an important part of the distribution in terms of energy (Pryor et al., 2004). This is why the WAsP method is preferred amongst the wind energy industry. In this method, k and c are calculated by solving the following equations.

$$\frac{\overline{U}^3}{\overline{U^3}}\Gamma\Big(1+\frac{3}{k}\Big)^{\frac{k}{3}} = -ln(1-P(\overline{U})) \tag{2.3}$$

$$c = \sqrt[3]{\frac{\overline{U^3}}{\Gamma(1+\frac{3}{k})}} \tag{2.4}$$

In a second method, referred in the following as KCrec, we take advantage of the fact that the Weibull distribution is given by two parameters, k and c, and straightforwardly reconstruct these: they are fitted by the Maximum Likelyhood Estimator (MLE) (Cohen, 1965) on the calibration period. The MLE of the Weibull parameters is defined by the following equations.

$$\frac{\sum_{i=1}^n u_i^k \ln(u_i)}{\sum_{i=1}^n u_i^k} - \frac{1}{k} - \frac{1}{n}\sum_{i=1}^n \ln(u_i) = 0, \tag{2.5}$$

$$c = \frac{\sum_{i=1}^n u_i^k}{n}. \tag{2.6}$$

With n being the sample size.

A last method was introduced in order to take into account how spread out the wind distribution is. This method, referred in the following as Perc, uses two values, $F(u_1)$ and $F(u_2)$, of the Weibull distribution function, corresponding to wind speeds u_1 and u_2. The Weibull k and c parameters are then given explicitly by:

$$c = \frac{\ln\ln(\frac{1}{1-F(u_2)})\ln(u_1) - \ln\ln(\frac{1}{1-F(u_1)})\ln(u_2)}{\ln\ln(\frac{1}{1-F(u_2)}) - \ln\ln(\frac{1}{1-F(u_1)})}, \tag{2.7}$$

$$k = \frac{c}{u_1}\ln\ln(\frac{1}{1-F(u_1)}). \tag{2.8}$$

In order to determine the optimal values of u_1 and u_2, a synthetic test was performed. First, we generated 30 (one month) or 90 (one season) samples from the reference Weibull distribution with parameters $k = 2$ and $c = 3.5$. Next, we determined the two Weibull parameters from the simulated samples using the Perc method, using different combinations (u_1, u_2). To find the best combination, we compared the resulting distributions with the reference distribution using the Cramer-von Mises (CvM) score (see below). It was found that the best combination on a monthly scale is the 11th and 83rd percentile. On the seasonal scale, the optimal combination is the 17th and the 92nd percentile. The combination of the percentiles was not found to be very sensitive, as there was a small region around the optimum combination with very similar scores.

Cramer-Von Mises score To assess the reconstruction quality, we use the Cramer-Von-Mises score defined in Anderson (1962):

$$CvM = \frac{MN}{M+N}\int_{-\infty}^{\infty}[F_N(x) - F_M(x)]^2 dH_{M+N}(x) \tag{2.9}$$

Here, M and N are the sample sizes in each of the distributions, $F_N(x)$ and $F_M(x)$ are the CDFs of the two samples and $H_{M+N}(x)$ is the combined distribution of the two samples together. The smaller the CvM score, the better the goodness of fit between the two tested distributions. Anderson (1962) showed that Equation (2.9) is equivalent to

$$CvM = \frac{U}{NM(M+N)} - \frac{4NM-1}{6(N+M}), \tag{2.10}$$

where $U = N\sum_{i=1}^{N}(r_i - i)^2 + M\sum_{j=1}^{M}(r_j - j)^2$, r_i are the ranks of the elements of the sample of size N in the combined sample and r_j are the ranks of the sample of size M in the combined sample.

The CvM score allows to test the null hypothesis H0 :"the two samples come from the same distribution". When $M\to\infty$ and $N\to\infty$, under the null hypothesis, the CvM score follows the limiting distribution with mean $\frac{1}{6}$ and variance $\frac{1}{45}$. In this configuration, the p-value giving 95% confidence that the null hypothesis cannot be rejected is $p = 0.46136$, (Anderson, 1962).

Multi-polynomial regression We propose to link the large-scale situation and surface wind speed distribution by a multi-polynomial regression taking the monthly/seasonal

mean PCs as explanatory variables and the parameters of the Weibull distribution as dependent variables:

$$\tilde{P} = \beta_0 + \sum_{n=1}^{N} \beta_n C_n(t) + \sum_{n=1}^{N} \beta_{n,n} C_n(t)^2 + \sum_{n=1}^{N-1} \sum_{m=n+1}^{N} \beta_{n,m} C_n(t) C_m(t). \qquad (2.11)$$

Here, $\tilde{P}$ is the dependent variable (Weibull parameter k or c for a given location), C_n are the principal components and $\beta_{n,n}$ and $\beta_{n,m}$ are the regression weights found by least squares. The choice of a polynom of second order is made in order to partly model the dependence between PCs of the Z500, as for instance, Jourdier (2015) showed that the influence of NAO on the surface wind speed is strongly modulated by the state of the SCA pattern.

The number N of principal components is determined by cross validation as explained below. We perform the regression on a calibration period of 20 years between 1979 and 1998. This results in weights quantifying the relationship between the large-scale circulation and the Weibull parameters for each individual location. These weights can be combined with the known PC values on the reconstruction period of 15 years between 1999 and 2013 to reconstruct the monthly/seasonal Weibull distribution.

Optimizing the number of principal components through cross validation The first five PCs of the Z500 can be interpreted as predictors of the wind. Still, to a certain extent, the following PCs can also explain the variability of the wind at the monthly/seasonal scale. To check whether taking five PCs is really optimal, we performed a cross-validation procedure. For this purpose, we calculated the temporally and spatially averaged CvM score of 7 reconstructions of 5 years each, taking the remaining 30 years of the data set as calibration period. Figure 2.2 plots the CvM scores as a function of the number of PCs used. The minimum mean CvM is clearly apparent for all three methods for both monthly (Fig 2.2. a, b, c) and seasonal (Fig 2.2. d, e, f,) reconstruction. The minimum is found for 5 PCs for monthly distribution reconstructed by Wasp method (Fig 2.2 a), 7 PCs for monthly distribution reconstructed by KCrec method (Fig 2.2 c), and 6 PCs for the others (Fig 2.2 b,d,e,f). As the 5 first PCs are all related to well understood teleconnection patterns explaining the large-scale circulation of the atmosphere, we expect them to be accurately linked to the wind speed variability at the monthly and seasonal timescales. Results obtained by cross-validation confirm this relationship, as the optimal amount of PCs used is close to 5 (Fig 1.10)).

2.3 Evaluating the reconstruction methods

As mentionned previously, we use the wind speed from the ERA-I reanalysis as the reference wind speed. To assess the reconstruction quality, the CvM score is calcu-

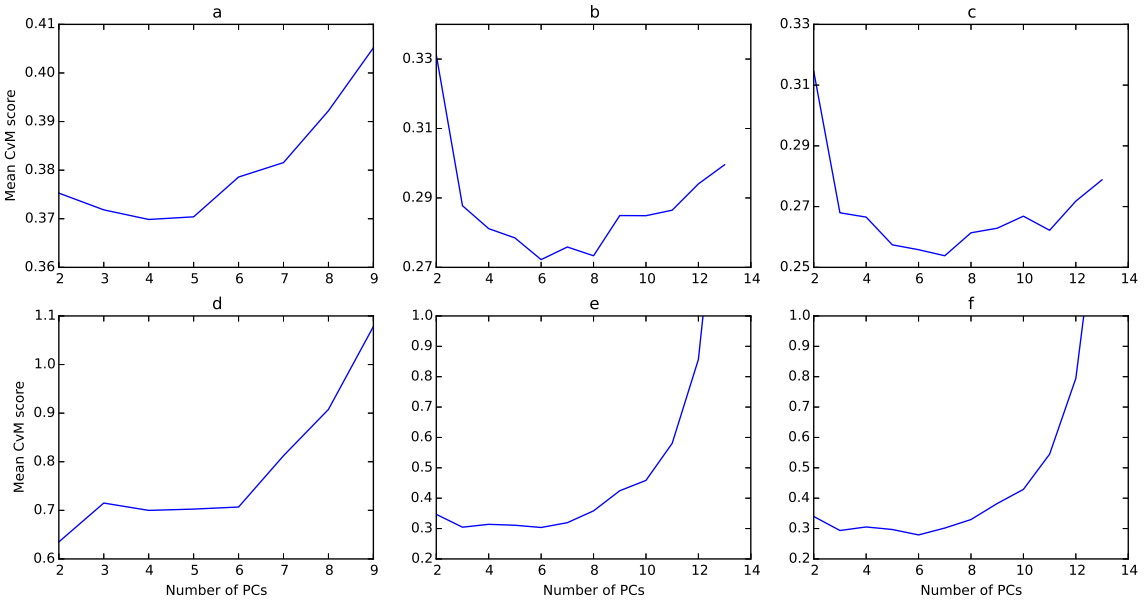

Figure 2.2: *Cross validation:* Mean CvM score obtained by cross validation as a function of the number of PCs used to reconstruct the distribution of the surface wind speed. From left to right: Wasp (a,d), Perc (b,e), and KCrec (c,f) methods; top: CvM score for monthly wind distribution reconstruction (a,b,c); bottom: CvM score for seasonal wind distribution reconstruction (d,e,f)

lated between the reconstructed CDF and the ERA-I wind CDF. The CvM scores of the reconstructed wind speed distributions are then compared to the CvM scores computed between the ERA-I wind CDF and the ERA-I climatological CDF. In simple terms, the climatological distribution is the distribution of all values of wind for each month or season in one specific location, based on all reanalysis data from this location and the specific month or season. The climatological distributions are usually used in the industry to have a first assessment of the wind energy production at a seasonal timescale. An example of ERA-I (Real), ERA-I climatological (Clim) and reconstructed (Wasp, KCrec and Perc) wind speed CDFs is shown in Figure 2.3 for the winter 2012 at a location in the North of France. In the following, the monthly and seasonal ERA-I climatological distributions (computed from the 20-year reference period) will be denoted 'climatology'.

2.3.1 Performance of methods for wind speed distribution reconstruction

The CvM score allows to test the null hypothesis (H0) that the two samples come from the same distribution. Assuming that the reconstructed distributions and the ERA-I distributions are based on samples large enough to say that the corresponding CvM scores follow the limiting distribution, we can define the p-value corresponding

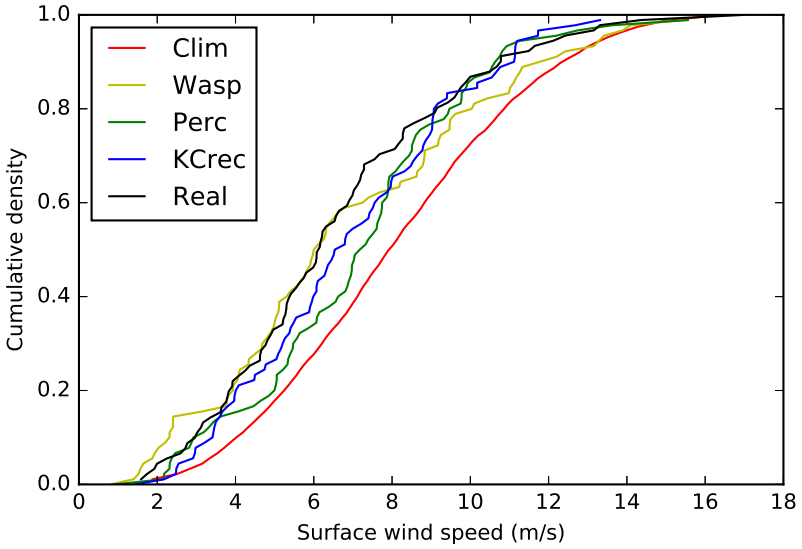

Figure 2.3: *CDFs example:* ERA-I, ERA-I climatological, and reconstructed seasonal CDFs for winter 2012 at 48.5°N 3.0°W

to 95% confidence. If the calculated CvM score is below this value, we cannot reject the null hypothesis at 95% confidence that the two compared samples come from the same distribution. We compare results of the tests for the climatology and the reconstruction methods. We can define five different cases:

- Case A: H0 cannot be rejected for the method and is rejected for the climatology
- Case B: H0 cannot be rejected for both and the CvM of the method is smaller than the CvM of the climatology
- Case C: H0 cannot be rejected for both and the CvM of the method is larger than the CvM of the climatology
- Case D: H0 is rejected for the method and cannot be rejected for the climatology
- Case E: H0 is rejected for both the method and the climatology

The hypothesis of the Weibull distribution introduces an estimation error in the reconstructed CDF. We compare results obtained for reconstructed CDF to ERA-I climatology (a) and to the parametric climatology (b) which follows a Weibull distribution fitted by MLE on the ERA-I wind speed. Results over the whole domain in all different cases are given in table 2.1 and 2.2 for monthly and seasonal reconstruction respectively.

Methods	Wasp		Perc		KCrec		Clim	Parametric Clim
CvM < p	69.1		82.1		85.2		89.3	81.7
Comparison with	a	b	a	b	a	b	-	-
Case A	5.8	11.5	6.5	11.9	6.9	13.0	-	-
Case B	17.8	24.1	25.0	34.0	27.3	37.1	-	-
Case C	45.5	33.5	50.5	36.2	51.1	35.1	-	-
Case D	26.0	24.1	13.8	11.6	11.2	9.5	-	-
Case E	4.8	6.8	4.1	6.3	3.7	5.3	-	-

Table 2.1: *CvM test results:* Percentage of time the result of the CvM test gives Cases A,B,C,D, or E on the whole domain, for the entire validation period, for monthly reconstructed distribution compared to the classical climatology (a) and to the parametric climatology (b). The p-value, p, is 0.46136 for 95% confidence level

Methods	Wasp		Perc		KCrec		Clim	Parametric Clim
CvM < p	44.3		73.3		79.8		88.6	77.3
Comparison with	a	b	a	b	a	b	-	-
Case A	3.8	8.9	5.5	11.0	6.1	13.9	-	-
Case B	10.5	13.6	22.8	31.2	23.8	34.2	-	-
Case C	30.0	21.9	45.0	31.1	49.9	31.7	-	-
Case D	48.1	41.9	20.8	15.0	14.9	11.4	-	-
Case E	7.5	13.8	5.9	11.7	5.3	8.8	-	-

Table 2.2: Same as table 2.1 but for seasonal distribution

The first lines of tables 2.1 and 2.2 show the fraction of time each method gives a reconstructed distribution not discernable from the ERA-I wind distribution at 95% confidence level (i.e H0 cannot be rejected). It shows that all methods, appart from Wasp, have a good ability to reconstruct the real wind distribution. We can also see that fitting a Weibull distribution on the climatology reduces by about 10% this percentage. Cases A and B summarize the number of time each method is doing better than the climatology (non-parametric (i.e empirical) (a) or parametric (i.e Weibull) (b)). On the contrary, Cases C and D summarize the number of times the climatology is doing better than the method. On average, on the all domain and for monthly and seasonal timescales, the non-parametric climatology (a) do better than every method more than 60% of the time (78.1% against Wasp at the seasonal scale, to 62.3% against KCrec at the monthly scale). Nevertheless, when comparing to the parametric climatology, for monthly and seasonal reconstruction, the KCrec method performs 49.1% of the time better at monthly scale, and 48.1% at the seasonal scale. This shows again the error brought by the Weibull distribution reconstruction. In all cases, methods perform better at the monthly scale than at the seasonal scale.

It is interesting to notice that the cases for which the percentage is increased at the seasonal scale are cases D and E, corresponding to the rejection of the hypothesis H0 (Tables 2.1 and 2.2). This means that the models have more difficulties to

represent the seasonal distribution of the wind speed, than the monthly distribution. The climatology seems to be less sensitive to the timescale considered.

Figure 2.4 and 2.5 show on average on the validation period the number of times each method behaves better than the classical climatology (Cases A and B). It can be seen that the Perc and KCrec methods do better than the Wasp method. Indeed, at monthly timescale, the Perc and KCrec methods can do better than the climatology in average more than 30% of the time, while the Wasp method does better than the climatology about 25% of the time on average displaying a clear difference between North and South (Figure 2.4 and Table 2.1). On a seasonal scale, the Wasp method performs clearly worse than at a monthly scale. The Perc and KCrec methods at a seasonal scale display an interesting spatial variability. Indeed, they do more than 40% of the time better than the climatology in the North of France, whereas in the South, this percentage is about 20% to 25% (Figure 2.5). When comparing to the parametric climatology, all methods display the same pattern, but all percentages are increased by more than 10% *(Not shown)*.

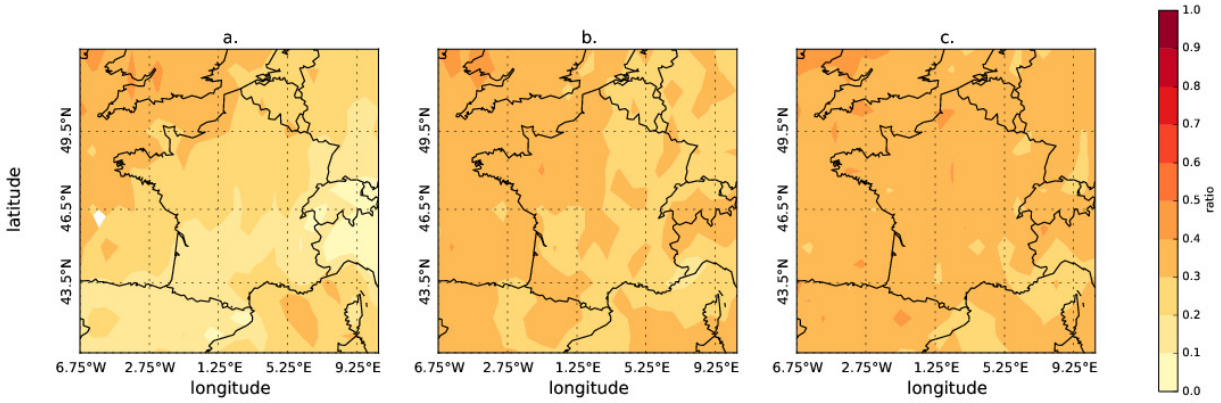

Figure 2.4: *Reconstructed CDFs vs climatology:* Fraction of times each method does better than the climatology (cases A and B) for monthly distribution reconstruction. From left to right: Wasp (a), Perc (b), KCrec (c)

Figure 2.6 shows the ratio of the number of times each method is doing better than the climatology for seasonal distributions, by taking each season separately. We can clearly see on this figure that the performance regarding the climatology of the Perc and KCrec methods, and to a certain extent the Wasp method, depends on the season and on the region. Indeed, both the Perc and the KCrec methods display a high percentage of times (up to 70% at some points) when they do better than the climatology in the North of France for the winter and autumn seasons. In the North of France, the storm track variability is highly responsible for the interannual variability of the wind speed distribution. In winter and fall, it is very active compared to spring and summer. This explains why reconstruction methods perform better than the climatology in this region, in these seasons. The comparison analysis mainly highlights the fact that, by construction, the climatology captures

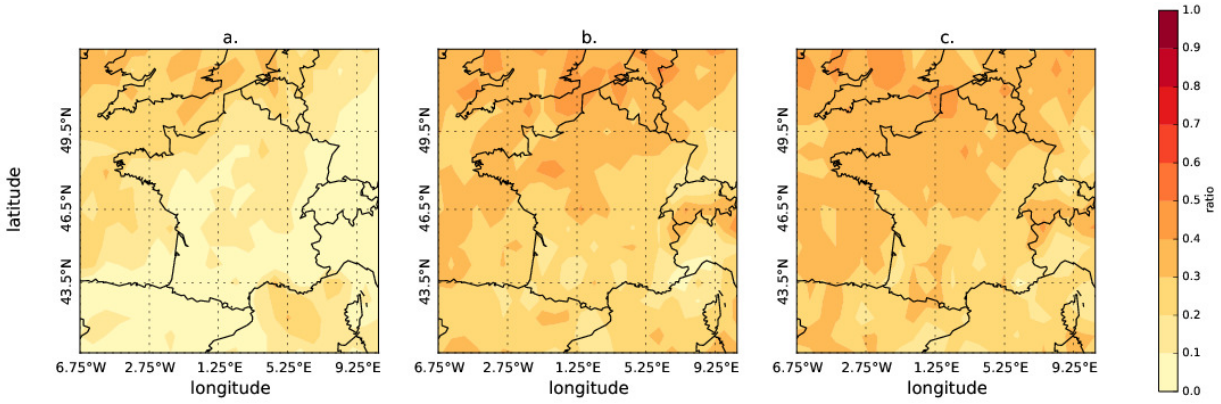

Figure 2.5: Same as Figure 2.4 but for seasonal distribution reconstruction.

only a mean state of the atmosphere over 20 year (and is not significantly affected by long-term wind trends), while the model captures the variability of the wind at timescales from intra-annual to decadal.

2.3.2 Performance of the methods for estimating the capacity factor

For wind energy purposes, it is not exactly the full wind distribution that needs to be estimated. For a given turbine, once the wind is beyond the cut-out wind speed or below the cut-in speed, the precise value does not matter. In the present section we take this into account and reevaluate each method. A preliminary step consists in designing a procedure which imitates the weighting of wind values by a power curve, in a manner which accounts for the considerable geographical variations of the wind (a single, generic power curve would not make sense).

Each wind turbine is characterized by its power curve which gives the output power as a function of the wind speed. The energy produced during a given period can be expressed as :

$$E = T \int_0^\infty P_{out}(u) dU, \tag{2.12}$$

where T is the period considered (month or season) and $P_{out}(u)$ is the output power given the wind speed u. The capacity factor (CF) is defined as the ratio between the actual energy produced during a given period and the energy that would have been produced if the wind turbine had run at its maximum power during the entire period :

$$CF = \frac{E}{P_n T}, \tag{2.13}$$

where P_n is the nominal power of the wind turbine.

In order to take into account the fact that the data used are at 10-meter height and the mean wind speed is highly varying among different locations, we use a

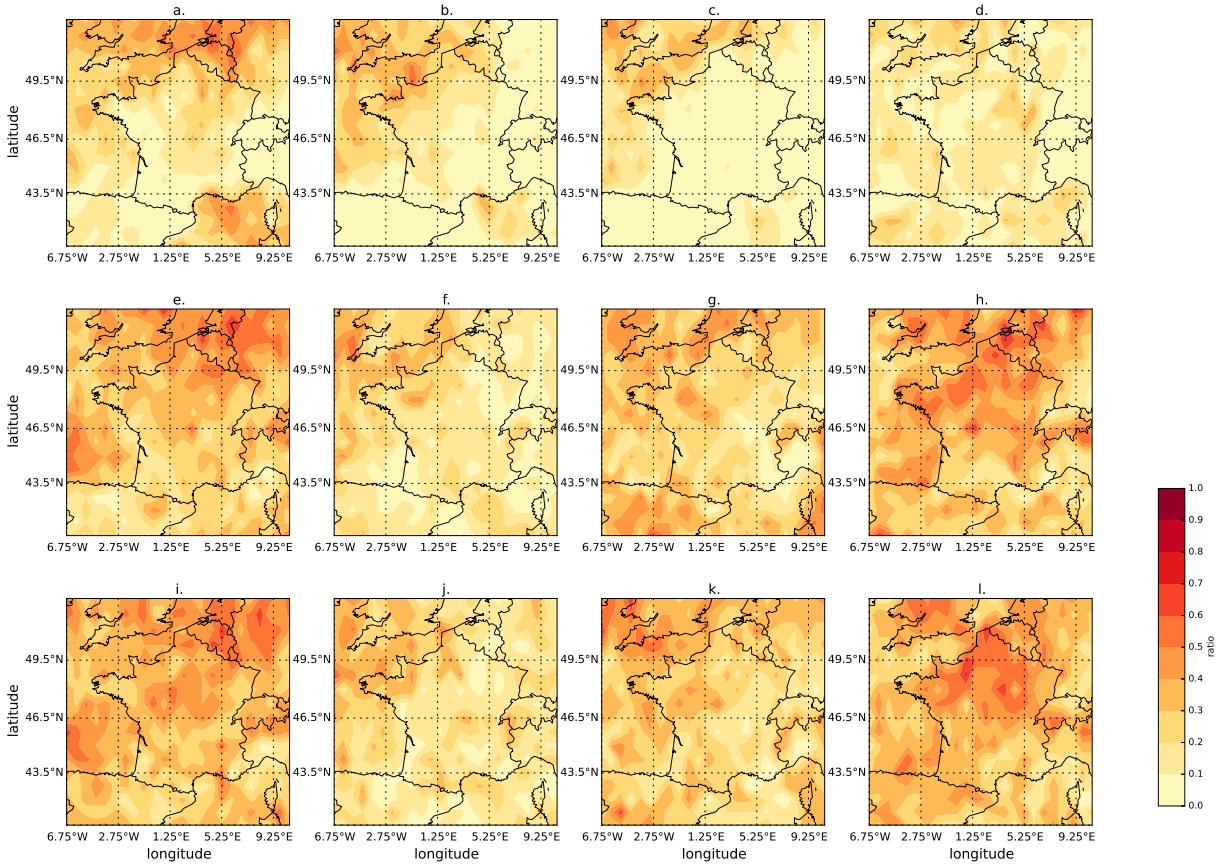

Figure 2.6: *reconstructed CDFs vs climatology, Seasonal fraction:* Fraction of time each method does better than the climatology (cases A and B) for seasonal distribution reconstruction based on Z500 for each season. From left to right: Winter, Spring, Summer and Autumn; From top to bottom: Wasp, Perc,and KCrec methods

location-adapted power curve, proposed by Jourdier and Drobinski (2017). In this curve, the wind speed is divided by a location-dependent parameter a, chosen so that the modified power curve has a capacity factor of 23% on the calibration period. This corresponds to the average capacity factor in France in 2014 (RTE, 2015). This procedure is illustrated in Figure 2.7.

To assess the accuracy of the reconstructed capacity factor, the relative error between the reconstructed capacity factor and the capacity factor from the reanalysis is computed :

$$\Delta CF = \frac{CF - CF_{real}}{CF_{real}} \tag{2.14}$$

Figures 2.8 and 2.9 show the relative error on the calculated capacity factor for monthly and seasonal reconstructions respectively. At both timescales, the Perc method overestimates it mostly onshore by about 25% on average. The KCrec

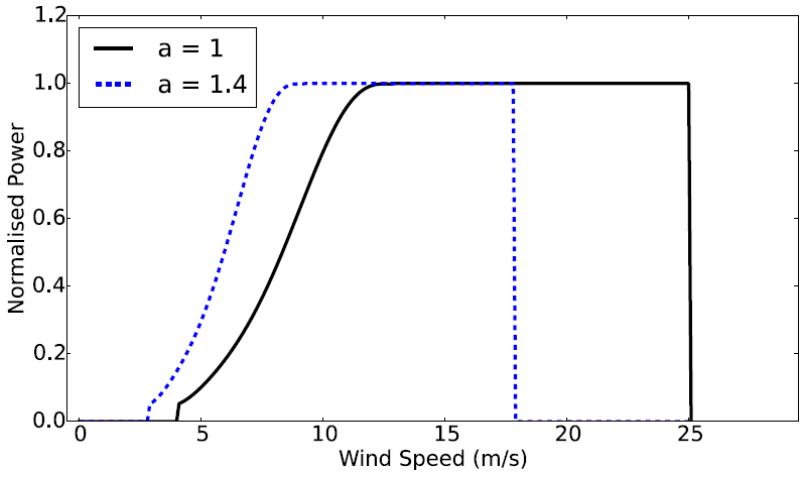

Figure 2.7: *Power curve:* Example of the location-adapted power curve. In solid black: the real power curve for wind speed at 80m height; in dashed blue: the adapted power curve. It has the same shape, but the wind speed is divided by a number a to achieve a capacity factor of 23%.

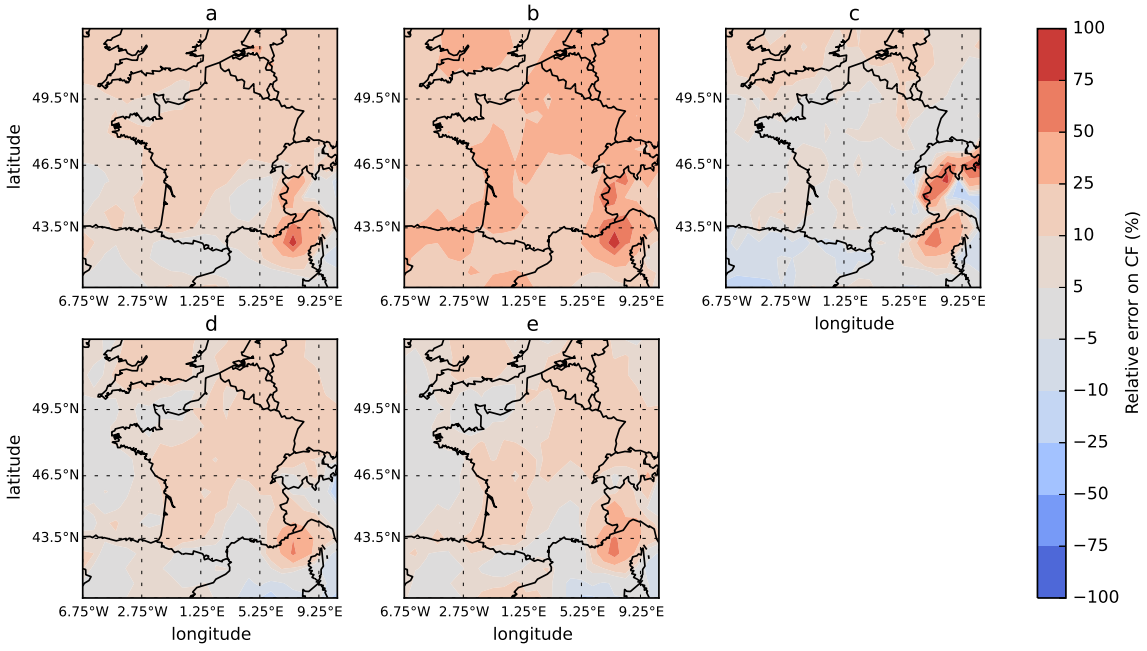

Figure 2.8: *Reconstruction of the capacity factor:* Relative error on the capacity factor (%) for monthly distributions given by: non parametric climatology (a), parametric climatology (b), Wasp (c), Perc (d), and KCrec (e)

method behaves like the Perc methods at the monthly scale, but is performing better at the seasonal scale with an overestimation of about 10% onshore. As expected, the Wasp method shows good performance in estimating the capacity factor as its

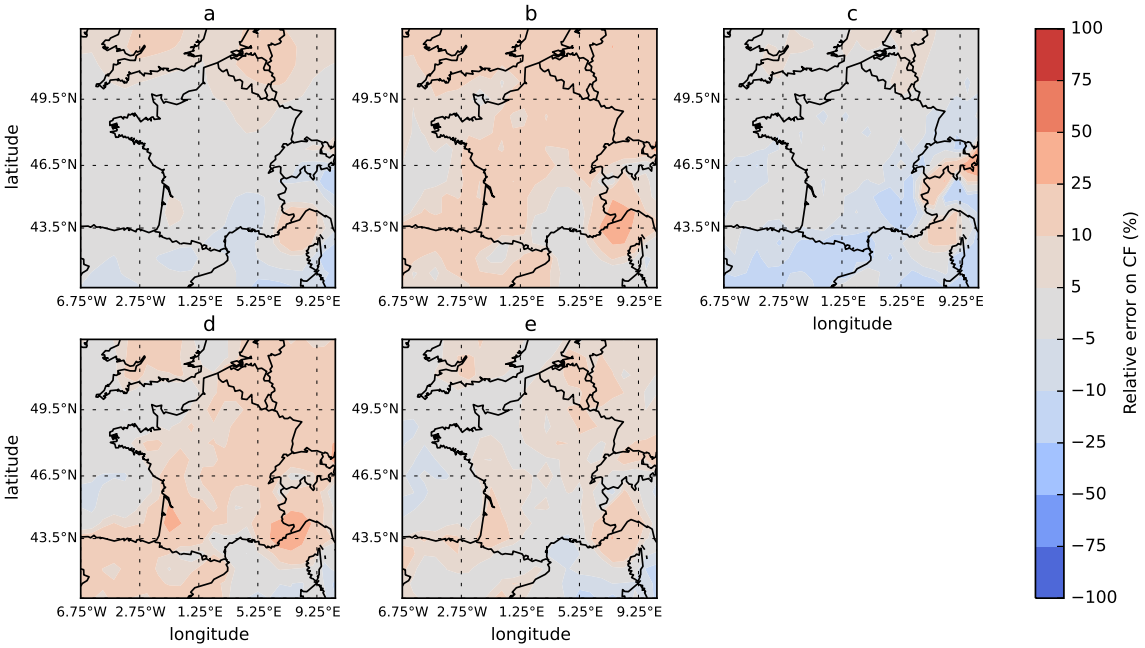

Figure 2.9: Same as Figure 2.8 but for seasonal distributions.

reconstruction focuses on the right tail of the Weibull distribution. Nevertheless, it overestimates the energy production in the Northern part of France at a monthly scale and underestimates it in the Southern part of France at a seasonal scale. The non-parametric climatology behaves very well at the seasonal scale even though it displays a slight overestimation in the North of France. At the monthly scale, on average, on the entire domain it overestimates the capacity factor by about 25%. By contrast, the parametric climatology behaves very badly at the monthly scale, overestimating the energy production by 50% in average. At a seasonal scale, this overestimation decreases but is still high, highlighting again the error induced by the Weibull distribution hypothesis.

In any case, there is a tendency of all methods to overestimate the capacity factor, mostly onshore. The climatology acts as a filter of high frequency variation of the wind, meaning that it does not describe well the tails of the distribution. As the power curve is designed so that the wind turbine works at its nominal power near the mean wind speed, this results in an overestimation of the capacity factor.

On the other hand, Drobinski et al. (2015) showed that a Weibull distribution fitted by MLE describes well the center of the distribution (near the mean wind speed), but tends to underestimate the tails of the distribution. This leads to the same consequence. This explains why the parametric climatology acts worse than the non-parametric climatology, but also why KCrec overestimates the capacity factor. This has no such effect offshore because the wind above sea is steadier so that the distribution is more peaked around the mean. Regarding the Perc method, the Weibull reconstruction is based on two percentiles defined to minimize

the CvM score. It may results in the same effect of underestimating the tails of the distribution. Future work could focus on a sensitivity analysis to the percentiles definition by minimizing the error on capacity factor.

At the seasonal scale, the real distribution is based on a larger sample which implies that the center of the distribution has a much larger weight than the tails at this scale than at the monthly scale. The effect of underestimating the tails is thus less visible.

2.4 Towards monthly and seasonal forecast of the wind speed distribution

The analysis described above has shown that the large-scale state of the atmosphere contains information on the likely distribution of surface winds, and our proposed methods allow to recover at least part of this information. A long-term perspective will be to use this to build forecasts of surface wind distributions. Below we present a preliminary attempt based on seasonal ensemble forecasts of the Z500 from ECMWF (Molteni et al., 2011), to assess the potential of this method for monthly or seasonal forecasts of the wind speed distribution.

A first step is to assess the skill in seasonal forecasts for predicting the large-scale state of the atmosphere in our region of interest. The root mean square error (RMSE) between the daily PCs of ERA-I and those of the ensemble mean seasonal forecast is shown in Figure 2.10. This figure gives an idea of the limit of predictability of such a forecast. It shows that the error increases rapidly until it levels off after 20 days indicating that there is no more valuable information on the large-scale circulation in the ensemble mean, with this specific decomposition method, under the assumption of quasi-stationarity, and under the assumption that the large-scale circulation representation in the seasonal ensemble forecasts is consistent with the one of ERA-I. As a consequence, it will not be possible to have an accurate wind distribution forecast at more than the monthly horizon using this mean state. However, it should be noted that this conclusion is stated under the assumption of stable large-scale circulation patterns. It also refers to the ensemble mean only. More information may reside in the forecast ensemble.

One technical difficulty arises: the monthly distribution of wind coming from the ECMWF analysis stands for the real distribution. As the analysis does not come from the exact same numerical model as the ERA-Interim data, a bias exists between the distributions coming from the analysis and the distributions based on ERA-Interim data. We thus apply a classical quantile/quantile correction between the 4 years based distributions of the analysis and of ERA-Interim between 2012 and 2014 at each point of the gridded domain. The quantile/quantile correction is a classical method to correct bias on each percentile of a modeled distribution (here ERA-I wind speed distribution) regarding observations (here the ECMWF analysis) (Christensen et al., 2008; Michelangeli et al., 2009). This considers that

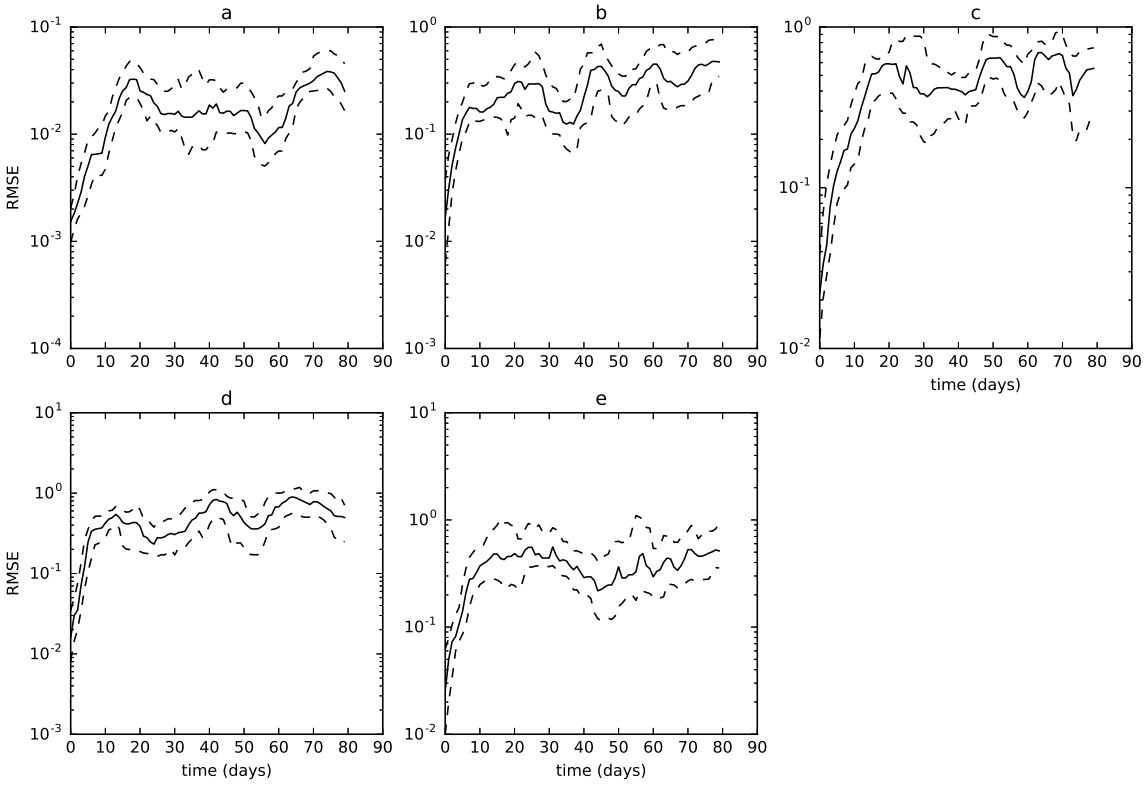

Figure 2.10: *Errors in raw seasonal forecasts:* RMSE calculated between the PCs of Era-Interim and the PCs of the seasonal forecast. The solid line represents the median of the error, dashed lines represent the 60th percentile (top) and the 40th percentile (bottom). a. Seasonal, b. NAO, c. EA, d. SCA, e. EU2

ERA-I is able to represent the distribution of the surface wind speed in the ECMWF analysis, but not the exact value of each percentile (bias on each percentile). Thus, we compute the surface wind speed distribution between 2012 and 2014, at each grid point, in ERA-I (modeled distribution) and in the ECMWF analysis (observed distribution), and build the transfer function between the two of them for each centile of the distribution. It can be expressed for one specific percentile q_τ as :

$$q_\tau^{corr} = R \times q_\tau^{mod} \tag{2.15}$$

with $R = \frac{q_\tau^{ana}}{q_\tau^{erai}}$

We apply this correction to the monthly wind distribution of the analysis to obtain our 'reference' monthly distribution. We thus make the assumption that the bias is constant over the entire period between 2012 and 2014, and in particular does not depend on the month considered. Because of the small amount of forecasts and of the uncertainties due to the bias, we will not be able to have the same deep analysis as in the reconstruction part of the study. The corrected monthly distribution of the wind speed coming from the analysis is compared to the climatology of ERA-Interim and to the forecast distributions using the CvM score.

Forecast method	Wasp	Perc	KCrec
total 1^{st} month	46.4 (*31.2*)	20.2 (*25.5*)	28.8 (*27.5*)
2012	41.0 (*35.0*)	15.1 (*20.5*)	22.9 (*23.6*)
2013	44.1 (*25.7*)	22.9 (*25.4*)	32.4 (*26.5*)
2014	54.0 (*33.0*)	22.5 (*30.4*)	31.3 (*32.3*)

Table 2.3: *Forecasts results:* Percentage of the number of times each method does better than the climatology on the whole domain for the 3 years of forecasts. First values correspond to the evaluation of the entire distribution; values in parenthesis corresponds to the evaluation of the distribution between the cut in and the cut out.

The percentage of time each method does better than the climatology, averaged over the entire domain, for the 1^{st} month of the 12 forecasts, is summarized in table 2.3. The results for the Perc and KCrec methods are comparable to the reconstruction results. On the contrary, the Wasp method shows a very high score when evaluating the entire distribution and a lesser score when evaluating the energy production, which is not consistent with the reconstruction results. When calculating the error on the capacity factor, the forecast methods always highly overestimate the wind energy production onshore (more than 100% at some points), and slightly underestimate it offshore (more than 10%). The non-parametric climatology overestimates the capacity factor by more than 10% onshore and underestimates it offshore, whereas the parametric climatology highly overestimates the energy production on the whole domain as it was the case in the evaluation part. Regarding the large uncertainty due to the limited number of forecasts, the robustness can be inferred from the consistency of the forecasts results with those obtained in the previous section. Still, work must be continued to evaluate the forecasts performance of such methods, by using larger sets of numerical seasonal climate forecasts, but also by testing methods based on non-parametric distribution estimation.

2.5 Conclusion

This chapter reveals several interesting results with respect to the two first objectives of the thesis.

As a first, a new approach for modeling the wind speed at the seasonal scale has been proposed. We suggest to model the entire monthly/seasonal distribution of the surface wind speed. Linking the surface wind speed to its synoptic predictors, we have shown that there is valuable information in the large-scale circulation variability that explains the wind speed distribution at such long timescales. The proposed methods show good performances in reconstructing the monthly and seasonal wind speed distributions. Still, on average, they do not overperform the non-parametric climatology and only slighly overperform the parametric climatology. Nonetheless, reconstruction methods performances display an interesting spatial and seasonal variability. Indeed, in the North of France in winter and fall, the proposed methods

showed better ability to model local wind speed distribution than the non-parametric climatology. This study reveals also that the parametric representation (Weibull hypothesis) of the surface wind speed distribution seems to be the major limit of the performances of the proposed methods. This suggests that non-parametric modelling could give even better results by avoiding this hypothesis.

The second objective of the thesis concerns the use of seasonal ensemble forecasts of the large scale circulation for forecasting the surface wind speed. In this study, we use the mean of the seasonal ensemble forecasts of ECMWF as the only forecasted state of the atmosphere. We show that, at the horizons exceeding a month the mean of the ensemble does not carry valuable information on the large-scale circulation variability with the given decomposition method (PCA on the Z500 on the domain of Figure 1.9a), under the hypothesis of stable patterns and of the consistency between ERA-I and ECMWF seasonal forecasts representation of the large scale circulation of the atmosphere.

Chapter 3

Probabilistic modelling and forecasting of the wind energy resource at the monthly to seasonal scale

Contents

3.1 Introduction

One of the main limitations of the previous model proposed is that theorical Weibull distribution leads to errors inherent to its parametric character (Drobinski et al., 2015; Jourdier and Drobinski, 2017; Earl et al., 2013). In this chapter, we propose a non-parametric model aimed at forecasting the distribution of the surface wind speed on a daily basis at the horizon of a fortnight to 3 months. Such model gives for each day, the Probability Density Function (PDF) of the daily mean surface wind speed.

This chapter is thus anchored in this context of probabilistic forecasting as one predictive PDF is associated with one wind speed value for each timestep. Probabilistic forecasts has seen the development of a large amount of non trivial assessment tools in recent years. A probabilistic forecast has for objective to give the narrowest intervals possible. This notion is called sharpness of the forecasts, and "the sharper, the better". However, sharpness is subject to calibration first. Calibration ensures that the model predictions are statistically consistent with the actual realizations of the variable to predict. It is a necessary feature of a probabilistic model.

Probabilistic forecasts of surface wind speed in the context of wind energy results, in part, from the need for adapted tools for decision making. Indeed, a decision can not be made from point forecasts as the future realization has probability to fall far from predicted value. Giving to decision makers a prediction associated with its probability is much more valuable. Let us consider the issue of ensuring supply and demand balance for the season to come. The risk of imbalance is drived by meteorological factors such as wind speed for wind energy production. Consider now the objective function which gives the number of hours when the network will need supplementary emergency production means (Loss Of Load Expectation) to overcome high consumption, or/and low production. This funcion depends on many parameters among which the wind energy resource (and production) which is highly variable and uncertain at the seasonal horizon. Having a good estimate of the probability density function of the surface wind speed (or wind energy production) is thus fundamental to obtain a valid decision (for instance, how much emergency production means are needed for the next season). Moreover, the more concentrated the PDF the more certain the decision.

In this particular context, this chapter addresses both the first and second objective of the thesis and focuses on the modelling and forecast of the local surface wind speed in France. In the framework of probabilistic forecasting, we investigate again how the information on the large scale circulation allows to follow the inter-annual variability of the local surface wind speed. The application of the model to the ensemble forecasts of the large scale atmospheric circulation patterns allows to deeper investigate how the information on the large scale patterns can be used to forecast local surface wind speed, including the use of post-processing methods of the ensemble. The framework of probabilistic forecasting better fits to adress the question of how long is the valuable information retained in the forecast, i.e to which

lead time can a forecast be made using the proposed approach.

Using ERA-I reanalysis in a perfect model context, we build the conditional PDF of the surface wind speed knowing a certain amount of the PCs by gaussian kernel density estimation (KDE) over 20 years of daily data. The estimation of such PDF is a challenge when considering the high dimensional space in which it lies. It nevertheless can be overcome by summarizing the information on the large scale circulation by a single index. The model we propose is non parametric. Moreover, it uses the overall daily information of the PCs and wind speed. ECMWF seasonal ensemble forecast is also used differently, as every member of the ensemble is used. A larger sample of seasonal forecasts is studied as well. The use of raw ensemble, if easier and straightforward, may not be the best way to handle ensemble forecasts. Indeed, an ensemble may not be well calibrated because of biases and/or because of a bad spread of the members. We thus use a post-processing method in order to recalibrate the ensembles and sharpen them. As in the previous chapter, climatology is used as a benchmark. It is nevertheless not assessed in the same way, as it is taken as a probabilistic forecast which must be calibrated, and as sharp as possible.

The proposed probabilistic model is first assessed over a validation period over which it is shown to be better calibrated than classical seasonal climatology. In particular, the long term trends of the surface wind speed are shown to be well followed thanks to this approach, as opposed to the climatology. The model is also much sharper than climatology, especially in winter and fall, and in the North of France, which confirms that large scale circulation patterns have higher explanatory value of the surface wind speed in this region and during cold seasons than in the South and during spring or summer. Applying the model to ECMWF raw seasonal ensemble forecasts tends on average to climatological sharpness after at most one month, and is as well calibrated as climatology. Using Ensemble Model Ouput Statistics (EMOS) post-processing method results in several cases (North of France, mainly in winter and fall) in calibrated and sharper predictions than climatology, even at the seasonal horizon. In other cases, the skill of the model is comparable to that of the climatology.

This chapter is structured as follows. Section 2 describes the method to build the probabilistic model as well as the data used in this study. Data is essentially the same as in the previous chapter. In section 3, the performance of the model is assessed on a validation period. In section 4, the probabilistic model is used to forecast the wind speed at the monthly and seasonal horizon by applying it to seasonal ensemble forecasts of large scale circulation patterns of the atmosphere.

This work is currently being reviewed in the *International Journal of Forecasting*.

3.2 Data & Methods

3.2.1 Data : ECMWF reanalysis and seasonal ensemble forecasts

As in the previous chapter, we use data from ERA-I reanalysis (Dee et al., 2011) to build and assess a probabilistic model aimed at forecasting the distribution of the daily surface wind speed, at timescales from 15 days to 3 months. Data from ERA-I is retrieved between 1^{st} January 1979 and 31^{st} December 2015 and ECMWF seasonal ensemble forecasts from 2012 to 2015 as described in section 1.6. We divide this long period of 37 years into 3 :

- A fitting period - from the 1^{st} January 1979 and 31^{st} December 1998 - in which the link between large-scale circulation and surface wind speed is created and probabilistic models are built ;
- A validation period - from the 1^{st} January 1999 and 31^{st} December 2011 - for which the large-scale circulation is known, and over which the probabilistic models are assessed, so that for each grid point the best model is chosen, resulting in a single 'optimized' combined model to be used in forecast mode ;
- A forecasting period - from the 1^{st} January 2012 and 31^{st} December 2015 - in which the optimized probabilistic model is applied to ECMWF seasonal ensemble forecasts of the Z500. In this study, 3 horizons of forecasts are assessed : 15-days, monthly, and seasonal (3 months) horizons.

A comparative study is lead between the skills of the probabilistic model built and the seasonal climatology of the wind speed. The seasonal climatology is defined as the empirical distribution function of the daily wind speed over the fitting period (20-years), built separately for each grid point and each season. Seasonal climatology is often used within the energy industry for such long term wind energy prediction (Pinson and Kariniotakis, 2009). Indeed, the persistence and autocorrelation of the wind disappear after 5 days at most, so that the seasonal pattern is the only information that remains in the absence of additional data. Note that the climatology we use in this study is only based on 20-years even if the usual way is to a climatology on at least 30-years. This has an impact on the calibration of our climatology as shown in the following but neither the sharpness nor the CRPS are significantly sensitive to this particular construction (*Not shown*).

3.2.2 Methods

Principal Component Analysis

As in the preceding chapter, we perform a PCA on the Z500, over the domain presented in figure 1.9, to highlight large scale patterns to be used as explanatory variables of the large scale atmospheric circulation (Figure 1.10). Note that in this

study, we use the daily values of the PCs of the Z500, as opposed to the preceding chapter in which we used monthly and seasonal averages.

Probabilistic Model

In the second step, we build a model for the probability distribution of the daily mean wind speed knowing the first n PCs. In other words, we want to estimate the conditional density $p(y|x_1, ..., x_n)$ of the daily surface wind speed Y given the PCs of Z500 $X^{(1)}$ to $X^{(n)}$. Estimating this conditional density directly is difficult due to the high dimension of the vector $(X^{(1)}, \ldots, X^{(n)})$. Following the idea of the single index approximation (Delacroix et al., 2003), we overcome this issue by assuming that the information about the PCs $(X^{(1)}, \ldots, X^{(n)})$ may be summarized by a single scalar index time series given by :

$$I_t = \beta_0 + \sum_{i=1}^{N} \beta_i X_t^{(i)} + \sum_{i=1}^{N} \beta_{ii} (X_t^{(i)})^2 + \sum_{i=1}^{N-1} \sum_{j>i}^{N} \beta_{ij} X_t^{(i)} X_t^{(j)}, \tag{3.1}$$

where the coefficients β_0, β_i and β_{ij} are computed by least-squares regression of the daily surface wind speed Y on the principal components $X^{(1)}, \ldots, X^{(n)}$ for each location. A test of optimization of the index parameters β_i by minimization of the continuous ranked probability score (CRPS – see below) has been performed at several locations, but did not produce a significant improvement (only of the order of 0.1% of the initial CRPS).

The conditional probability density function $p(y|I)$ is given by the standard formula :

$$p(y|i) = \frac{p(y, i)}{p(i)}, \tag{3.2}$$

where $p(y, i)$ is the joint density of the surface wind speed Y and the index I and $p(i)$ is the marginal density of the index. The surface wind speed Y and the index I being vectors on a daily basis, the model gives a different surface wind speed distribution for each day given the value of the index i_t. A Gaussian kernel density estimator (KDE) (Racine and Li, 2004) is used to estimate the joint density and the marginal density over the period of length T :

$$\widehat{p}(y|i) = \frac{\sum_{t=1}^{T} K_{h_1}(y - Y_t) K_{h_2}(i - I_t)}{\sum_{t=1}^{T} K_{h_2}(i - I_t)}, \tag{3.3}$$

where K_h is the Gaussian kernel function.

While the estimated density is not very sensitive to the choice of the kernel function, the bandwidth parameters h_1 and h_2 have a significant impact on the resulting probability density function. In our study, the bandwidth parameters have been computed by cross-validation on the fitting period (Racine and Li, 2004).

In this study, we first build several models by varying the number n of PCs from 5 to 30 with an increment of 5. These models are assessed in section 3.3 on the validation period. For each grid point the best model is chosen so that a single optimized model remains for forecasts purpose in section 3.4.

3.3 Evaluation and optimization of the model

We fit 6 probabilistic models by varying the number of PCs used to compute the index of the conditional probability function from 5 to 30 with an increment of 5. We now want to assess each of them on the validation period at each grid point of the domain to choose the best for each location which will be used in forecast mode (section 3.4).

3.3.1 Diagnostic tools

The performance of a probabilistic forecasting model is typically assessed in terms of calibration and sharpness (Carney and Cunningham, 2006; Foster and Vohra, 1998; Gneiting et al., 2007; Thorarinsdottir, 2013). While calibration refers to the statistical consistency between the model and the actual values of the variable to predict, sharpness is a property of the model only and measures the concentration of the predictive distribution.

Calibration

Consider a probabilistic forecast at time t in the form of a predictive distribution function $F_t(x)$, and corresponding to the realization x_t. Probabilistic calibration (Gneiting et al., 2007) measures the consistency between the probabilistic forecast $F_t(x)$ and the actual realization x_t by means of the probability integral transform (PIT) defined by $p_t = F_t(x_t)$. The forecast is said to be probabilistically calibrated if the PIT follows a uniform distribution. Note that applying the inverse normal transformation to the PIT leads to the Inverse Normal Transforms (INTs) that in the case of calibrated forecasts should follow a standard normal distribution.

Testing uniformity of the PIT (or normality of the INTs) with classical Kolmogorov-Smirnov (KS) or Cramer-von-Mises type tests raises the problem of autocorrelation in the PIT (INTs) sample (Hamill, 2000). In this study, we use the test developed by Knuppel (2015) which is based on the raw moments of the Standardized PIT (S-PIT) and allows for the presence of serial autocorrelations.

The S-PIT is defined by :

$$sp_t = \sqrt{12}\left(p_t - \frac{1}{2}\right) \tag{3.4}$$

Calibration can also be assessed by comparing individual quantiles of the predictive distribution to the empirical quantiles over a given period (Pinson et al., 2009a).

The quantile q_t at level τ is defined by the solution of $\tau = F_t(X < q_t)$. Consider the estimated quantile $\hat{q}_t$ and the actual event x_t. Over a period of length T, count the proportion $\hat{p}_\tau$ of 'hits' (e.g. dates when x_t is indeed smaller than $\hat{q}_t$). Then, if the time period length T is long enough, $\hat{p}_\tau$ must converge to τ. This information is redundant with testing uniformity of the PIT, but it can be used to assess the calibration of specific quantiles, for example those used to compute prediction intervals that are relevant for decision making with probabilistic forecasts.

Sharpness

Sharpness refers to the concentration of the predictive distribution, i.e the spread of the predictive distribution. It is a feature of the model only and does not assess the ability of the model to follow the actual values we wish to predict. Therefore, its assessment must be subject to calibration. Prediction interval widths are good diagnostics of the sharpness of a probabilistic model. In this study, the 50% and the 90% prediction interval widths will be used as a measure of sharpness. In the following, we refer to sharpness as the assessment of the accuracy of the model though it implicitly suggests that the model (or climatology) is calibrated. Nevertheless, we are aware that it is not the case everywhere so that a proper scoring rule like the Continuous Ranked Probability Score is always used as a complementary diagnostic of the accuracy as it adresses both calibration and sharpness.

Proper scoring rules

The Continuous Ranked Probability Score (CRPS) is a widely used scoring rule in meteorological probabilistic forecasts (Candille and Talagrand, 2005; Candille et al., 2007). It aims to evaluate both calibration and sharpness simultaneously. The CRPS for a single predictive distribution F and realization y_t is defined by:

$$CRPS(F, y_t) = \int_{-\infty}^{\infty} (F(y) - \mathbf{1}_{\{y \leq y_t\}})^2 dy. \tag{3.5}$$

For the entire sample of size T we define the CRPS by

$$CRPS = \frac{1}{T} \sum_{t=1}^{T} CRPS(F_t, Y_t).$$

3.3.2 Optimization of the model

To keep only the best model at each grid point of the domain, we use the following methodology to choose the optimal number of PCs used to compute the index of the conditional probability density function. We first test uniformity of the S-PIT with a 99% confidence level using the Knuppel test (Knuppel, 2015). If the hypothesis of adequate calibration (uniformity of the S-PIT) cannot be rejected (the model is considered calibrated) for any of the 6 models, we keep the model that minimizes the

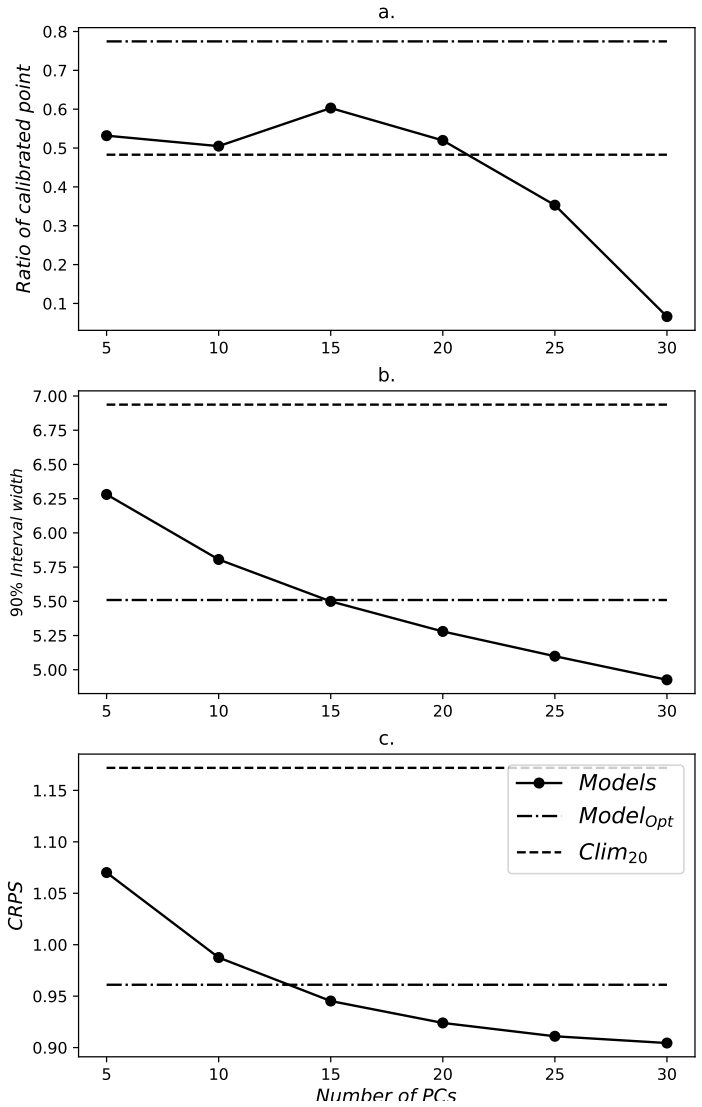

Figure 3.1: Performance of the models (full curves), Climatology (dashed lines) and of the optimized model (dashed dotted lines). (a) number of calibrated point over the entire domain following a test at 99% confidence level ; (b) 90% interval width averaged over the domain ; (c) CRPS averaged over the domain.

CRPS. If the null hypothesis is rejected (the model is considered not calibrated) for all 6 models, we keep the model that maximizes the p-value of the Knuppel test, with the risk to have a non-calibrated model. Figure 3.1 shows the number of calibrated points over the domain as measured by the Knuppel test at 99% confidence level (Fig 3.1a), the sharpness measured using the 90% interval width averaged over the domain (Fig 3.1b), and the CRPS value averaged over the domain (Fig 3.1c), for the 6 models as a function of the number of PCs used to compute the index.

Unfortunately, on average, adding PCs sharpens the model, but also reduces

calibration quality. The averaged CRPS is minimal for a large number of PCs where the test gives a very low number of calibrated points, so that selection of the best model cannot be based on this scoring rule only.

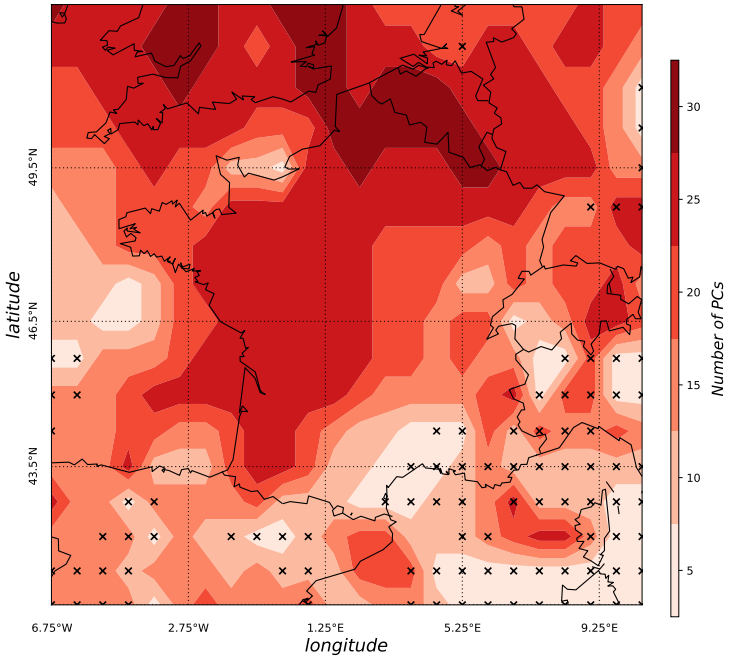

Figure 3.2: Number of PCs chosen for each location following the optimization process. Cross markers show locations where the optimized model is not calibrated at 99% confidence level.

Figure 3.2 shows the result of the choice described above. By adding more PCs, the variability of the large scale circulation is better accounted for, but too many PCs can also lead to overfitting and thus poor calibration of the model. Depending on the region, the optimal number of PCs can be estimated. In the North and Western coast of France, 20 to 30 PCs can be related to surface wind speed without compromising the calibration quality of the model. This results in a sharper model than when using less PCs.

In the Southeast of France, over the Mediterranean coast and the sea, the model is not calibrated. The bad behaviour of the model in this region may be explained by the complex phenomena driving the wind variability, such as the Mistral, which refers to the strong wind blowing over the Mediterranean sea after being channeled in the valley formed by the Alps and the Massif Central (Drobinski et al., 2017), and the Tramontane, which refers to an orographic wind blowing over the same region but channeled in the valley formed by the Pyrenées and the Massif Central (Brossier and Drobinski, 2009) (Fig 1.9b).

Figure 3.3 shows the p-values resulting from the Knuppel test of the S-PIT of the optimized model (Fig 3.3a) and the climatology (Fig 3.3b). Cross markers indicate

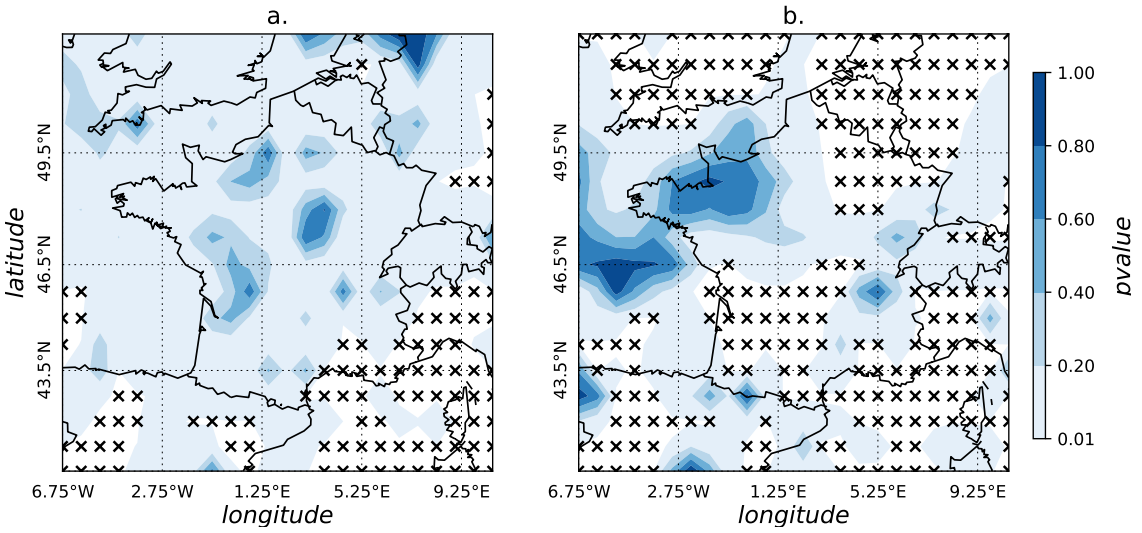

Figure 3.3: p-values of the Knuppel test performed on the S-PIT of (a) the optimized model (b) Climatology. Cross markers show location where the given p-value is under the significance level $\alpha = 0.01$

locations where the p-value is under the significance level $\alpha = 0.01$. The p-value for the climatology ranges between 0 and 1.0, while it ranges between 0 and 0.5 for the model. The null hypothesis of adequate calibration cannot be rejected in the North part of the domain for the model (Fig 3.3a), while for the climatology this hypothesis is rejected over much larger areas (Fig 3.3b). This can be surprising as the climatology is built using 20 years of data. Nevertheless, it has been shown that annual wind trends can be significant over 1 to 2 decades in France (Jourdier, 2015).

The CRPS value for both the climatology and the optimized model are larger offshore than onshore (Fig 3.4a,b). Signature of orographic winds in the South of France can be well identified. The same results are observed when looking at the prediction interval width *(Not shown)*. This is the consequence of wind speeds, which can be much stronger offshore than onshore resulting in a wider predictive distribution. The CRPS values seem to be strongly correlated with the prediction interval widths, but do not highlight calibration patterns shown in Fig 3.3. On the validation period, in terms of sharpness (Fig 3.5) and CRPS scoring rule (Fig 3.4c), the optimized model performs better than the climatology on almost the entire domain, except in the South of France where it is badly calibrated anyway.

On average, the optimized model is 29% and 26% sharper than the climatology when looking respectively at the 50% and 90% prediction interval width. By averaging the interval width separately for each season, we can highlight a strong seasonal variability of the intervals given by the climatology, which is not so noticeable for the model (Table 3.1). Thus, the model shows even better performance compared to the climatology in winter and fall (about 40% sharper than the climatology on average over the domain) which are the seasons when the risk of high LOLE (Loss

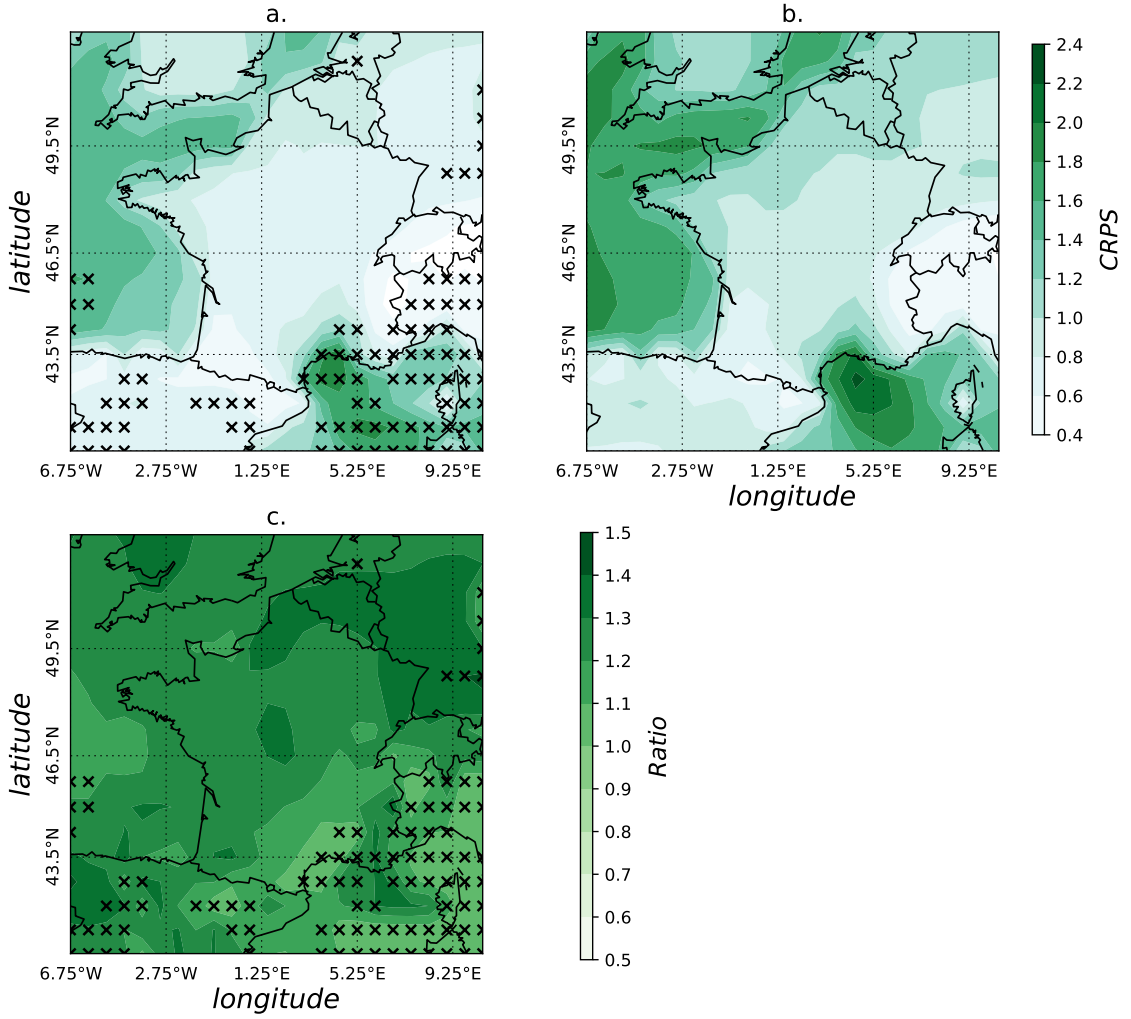

Figure 3.4: CRPS value averaged over the validation period computed for (a) the optimized model (b) Climatology, (c) ratio of maps (b) over (a). The cross marks show the regions where the optimized model is not calibrated.

Of Load Expectation (see chapter 1 in section 1.3.2) may be larger because of low temperature. The model can be as much as 50 to 60% sharper than the climatology in the Northern (where a large part of the installed capacity in France is located) and Western regions in winter and fall *(Not shown)*. Differences between land and sea are present for all seasons, and the Mediterranean region is always more problematic.

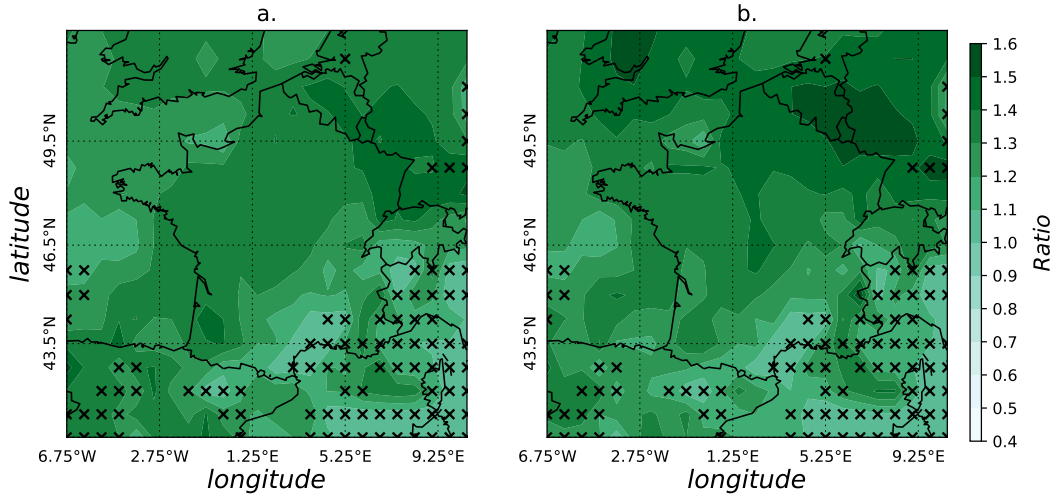

Figure 3.5: Ratio between the prediction interval width of Climatology and of the optimized model (a) 90% IW ; (b) 50% IW

	Winter		Spring		Summer		Fall	
	Model	Clim	Model	Clim	Model	Clim	Model	Clim
CRPS	1.04	1,33	0,92	1,07	0,86	1,00	1.02	1,29
CRPS Ratio	1.27		1.16		1.16		1.26	
I90	5.86	7,92	5.38	6,39	5,06	5,78	5.75	7,67
I90 Ratio	1.35		1.19		1.14		1.34	
I50	2.41	3.39	2.22	2.65	2.08	2,39	2.37	3,30
I50 Ratio	1.41		1.19		1.15		1.39	

Table 3.1: CRPS, 90% & 50% prediction interval width values averaged over the domain for the optimized model and Climatology, averaged separately over the seasons, and the ratio of the values for Climatology over the optimized model.

3.4 Probabilistic wind speed forecasting at the monthly and seasonal horizon

3.4.1 Methodology

To make monthly / seasonal forecasts with our model, we must take into account the uncertainty of the Z500 forecast, and thus also of the index. For each member of the ensemble, we first calculate the values of the principal components by projecting the corresponding Z500 field onto the EOFs identified during the stage of model calibration. Next, for each member of the ensemble forecast, and for each location where surface wind speed forecast is needed, we compute the corresponding index value using equation (3.1), where the coefficients β_i were identified during the stage of model calibration. This gives us an ensemble of index values $I_1, \ldots, I_n$. From this

ensemble we construct the predictive distribution of index values, denoted by Λ. This can be done in two different ways. The first method (raw forecast) consists in taking simply the empirical distribution of $I_1, \ldots, I_n$, that is, $\Lambda = \frac{1}{n}\sum_{k=1}^{n} \delta_{I_k}$, where δ_x is the point mass at point x. The second method uses statistical post-processing of the ensemble forecast to construct a distribution Λ with better calibration / sharpness properties than the raw forecast. In this paper, we use the Ensemble Model Output Statistics (EMOS) method, described below, for forecast post-processing.

Once the predictive distribution for the index has been constructed, the density of the predictive distribution for the surface wind speed given the forecast $p(y|F)$ is obtained by integrating the density of the conditional distribution of the wind speed given the index with respect to the predictive distribution of the index:

$$p(y|F) = \int_{-\infty}^{\infty} p(y|I = x)\Lambda(dx), \tag{3.6}$$

This should produce a less sharp model with a higher chance to be calibrated than if only the mean of the forecast ensemble is used.

Ensemble Model Output Statistics - EMOS

To recalibrate and sharpen a forecast ensemble different statistical postprocessing methods exist such as the Bayesian Model Averaging (BMA) (Raftery et al., 2005; Sloughter et al., 2013; Moller et al., 2013) or the Ensemble Model Output Statistics (EMOS) (Gneiting et al., 2005; Thorarinsdottir and Gneiting, 2010; Schuhen et al., 2012). EMOS aims at recalibrating the distribution of ensemble forecasts, but also at sharpening it. This method is inspired by Gneiting et al. (2005) apart from the optimization algorithm. This method is based on the assumption that Λ has a normal distribution $N(m_I, \sigma_I)$, where m_I is a weighted linear combination of the index values of the ensemble,

$$m_I = b_0 + \sum_{m=1}^{n} b_m I_m, \tag{3.7}$$

and σ_I is parameterized by

$$\sigma_I = c + d\,\mathrm{Var}(I), \tag{3.8}$$

where $\mathrm{Var}(I)$ is the empirical variance of the ensemble.

The parameters of the EMOS method $b_0, \ldots, b_m$, c and d are estimated as follows separately for each grid point. We define a training period of 3 years to estimate the parameters that would be used for the remaining year. We create 3 series of 3 years each, corresponding to different forecast horizons. The first series contains foreacasts with horizon up to 1 month, the second one contains forecasts with horizons from 1 to 2 months, and the third one contains forecasts with horizons from 2 to 3 months. In other words, we use the same EMOS parameters for the forecasts with horizons between 2 and 3 months, but different parameters are used for short range and long-range forecasts.

In the first step of the estimation procedure, on the training period, we perform a linear regression of the index I computed from the actual ERA-I reanalysis on the index values $I_1, \ldots, I_n$ computed from the ECMWF seasonal forecasts. This gives us a first estimate of $b_0, \ldots, b_m$. In this first step we set $c = 0$ and $d = 1$. Then, in the second step, we improve the first-step estimates by minimizing the Continuous Ranked Probability Score (CRPS) of the forecasts, averaged over the training period, seen as function of the parameters $b_0, \ldots, b_m$, c and d using the Powell algorithm (Powell, 1964).

In the end, we obtain 3 sets of parameters b_0, ..., b_m, c and d, corresponding to 3 forecast ranges, that minimize the CRPS score. The minimization of the CRPS optimizes the calibration and the sharpness. We apply the obtained parameters on the remaining year of forecasts to estimate the gaussian distribution $N(m_I, \sigma_I)$ of the index and then integrate over this distribution as in eq (3.6). The procedure is repeated 4 times by training on three different years and testing on the remaining year.

3.4.2 Results

Knuppel test is performed for each lead time independently using the 48 forecast values. With such a small dataset the power of the test is reduced, but as mentioned in the description of the data, a longer time period cannot be used due to a change in the forecasting system of ECMWF at the end of 2011. Figure 3.6a shows the proportion of calibrated gridpoints at 99% confidence level as a function of the lead time. The climatology, our model with EMOS postprocessing and our model with raw index forecast, all show a high level of calibration at any horizon. On the contrary (and even with only 48 data points), 10m wind speed forecasts from ECMWF seasonal ensemble display a bad calibration for horizons less than 10 days, because the ensemble distribution is not dispersed. Even after 10 days, the distribution of the ensemble is poorly calibrated over 10 to 60% of the domain. Moreover, it is less sharp than other forecasts. Figure 3.6b shows the 90% prediction interval widths averaged over the domain and over all sets of forecasts as a function of the lead time. The interval width of the raw forecasts tends to climatological prediction interval width after 15 days and is sharper before. EMOS forecasts are on average sharper than climatology at any lead time.

Figure 3.7 shows for the three lead times considered (from top to bottom, 15-days, 1 month, and 3 months respectively) the ratio (climatology over EMOS forecast) of CRPS value (left) and of the 90% prediction interval width (right) averaged over the domain for each forecast. From March to September, CRPS of climatological forecasts are comparable to EMOS forecasts. On the other hand, during winter and fall, they perform better in terms of this proper scoring rule. For longer horizons (1-month and 3-months), CRPS values of the climatology and EMOS forecasts are comparable. For any horizon, and along the entire year (except April) EMOS forecasts are sharper than climatological forecasts, even if there is a loss of accuracy with

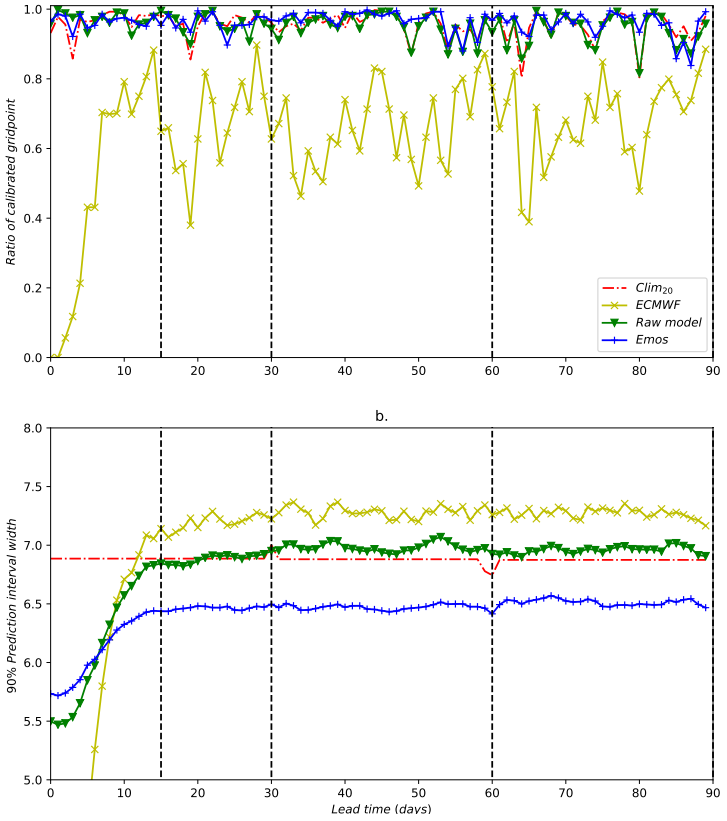

Figure 3.6: a. Ratio of calibrated gridpoints over the domain as a function of the forecast lead time. Knuppel test is performed at significance level $\alpha = 0.01$ on the S-PIT built from 48 forecasts. b. 90% prediction interval width averaged over the domain and all forecast sets as a function of the forecast lead time.

increasing lead time, especially after the first month of forecast. Same results are found for 50% prediction interval width *(Not shown)*. Following a Mann-Whitney test (Mann and Whitney, 1947) performed on the samples of Figure 3.7, the hypothesis of equal mean of CRPS cannot be rejected at the 99% confidence level for lead times 1-month and 3-months. The same test rejects this hypothesis for 90% prediction interval widths for any horizon.

Maps of CRPS and prediction interval width highlight better scores of the EMOS forecasts in the North of France, especially in fall and winter *(Not shown)*. For specific forecasts, EMOS forecasts seem to be better calibrated than climatology at 3-months horizon as well as sharper in this specific area where a large part of the French wind energy installed capacity is located. In the following, we focus on this region, and show results for the specific forecasts starting on the 1^{st} of October, for which we indeed have better scores than climatology. Several other forecasts display similar results, especially from fall 2012 to winter 2013 (e.g. starting months October, December, January and February) (Note that in late december 2012 a sudden stratospheric warming could have had an impact on the seasonal

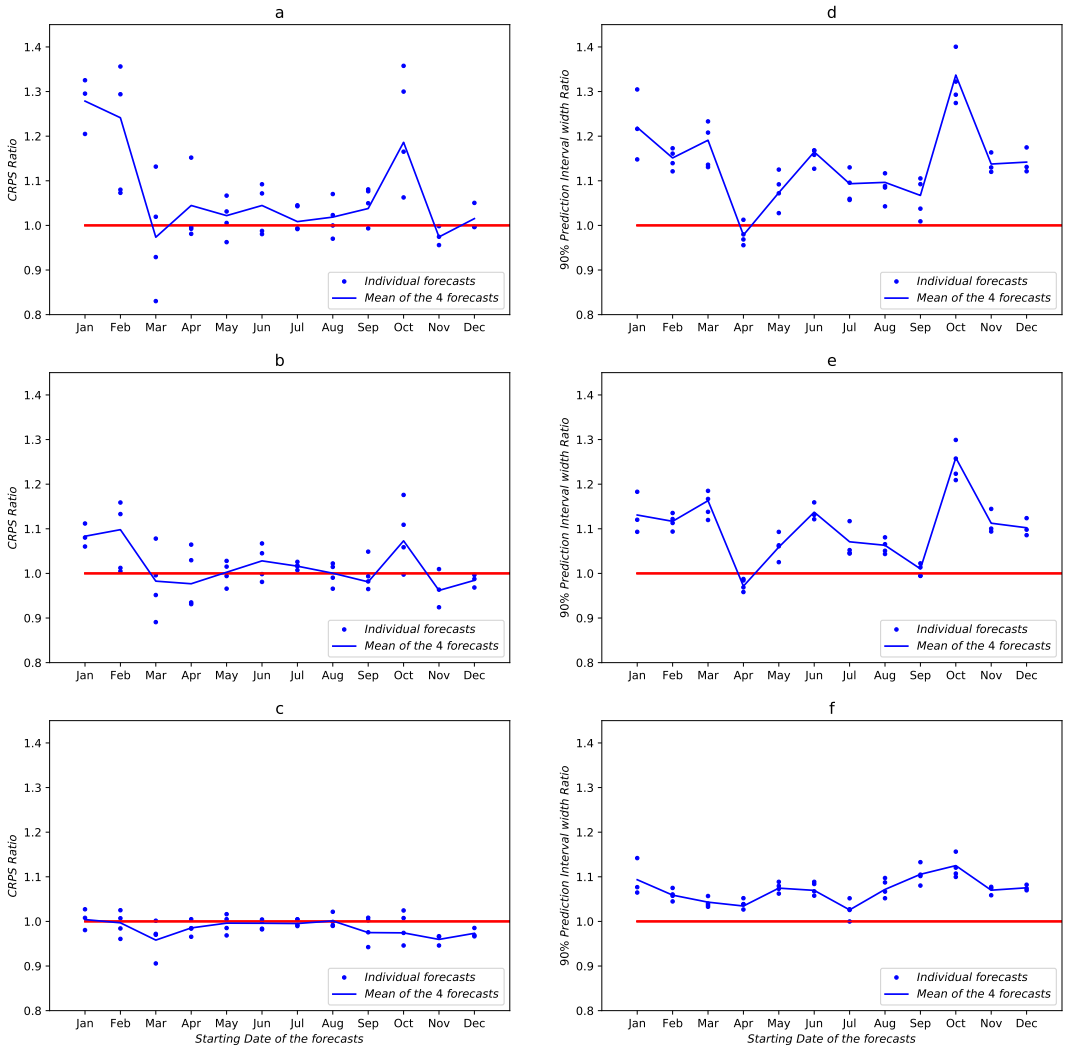

Figure 3.7: Left column displays the ratio of the CRPS value for the climatology over that for the EMOS forecasts averaged over the domain and over 15-days (a), 1-month (b), and 3-months (c) for each forecast as a function of the starting date of the forecast. Right column displays the same for the 90% prediction interval width. Each point corresponds to one forecast and the blue line corresponds to the average value for the 4 forecasts starting the first day of the indicated month.

predictability of large scale circulation patterns in Europe (Coy and Pawson, 2015; Scaife et al., 2016)). Forecasts from fall 2013 and winter 2014 also display good skill in this region.

Figure 3.8 shows the ratio of CRPS scores (a) and 90% prediction interval widths (b) averaged over the 3-months of forecasts and over the 4 forecasts starting on the 1^{st} of October. Over this domain, CRPS of EMOS forecast is better or comparable to the one computed for climatology. Sharpness of EMOS forecast is 10 to 25%

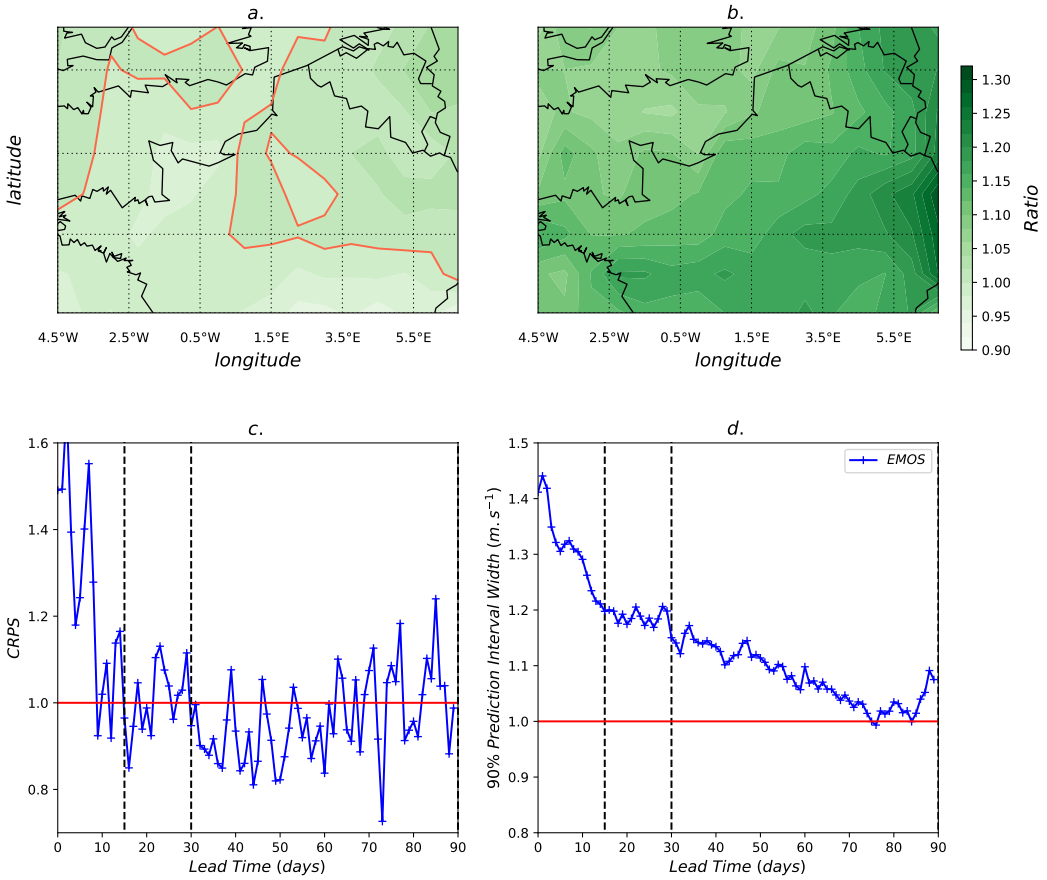

Figure 3.8: Results averaged over forecasts starting the 1^{st} of October of each year on a smaller domain spanning the North of France: (a) Ratio of CRPS of climatology over EMOS forecast averaged over the 3-months of forecast, contour lines indicate level 1.0 of the ratio ; (b) Same as (a) for the 90% prediction interval width; (c) CRPS ratio averaged over the domain as a function of the lead time ; (d) Same as (c) for the 90% prediction interval width.

larger than that of the climatology, especially onshore. Figure 3.8 (c and d) shows the correponding scores averaged over the domain as a function of the lead time. CRPS value (or Ratio) is highly variable, even when averaged over this domain, because it depends on wind speed values. No large differences between climatology and EMOS can be found in the time serie, except in the first 10 days of forecasts when the model displays better score than climatology. Sharpness of EMOS forecast decreases with the lead time to finally tend to climatological value after about 75 days.

Reliability diagram is another tool to assess the statistical reliability of forecasts. Such diagram displays the forecasted probability of an event as a function of the observed occurrence of this given event (see for instance Pinson et al. (2010);

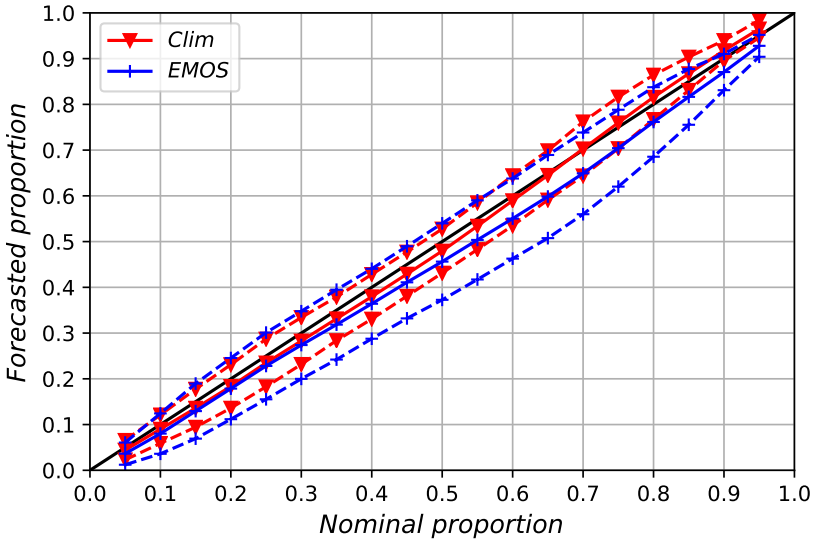

Figure 3.9: Results for the 4 forecasts starting the 1^{st} of October : Reliability diagram drawn from the quantiles built over the domain in figure 3.8 and over the 3-months of forecasts. Dashed lines show the dispersion (2σ) of the forecasted quantiles over the domain and forecasts sets.

Weisheimer and Palmer (2014)). Here, we consider the events given by each observed percentile ($[0.05, 0.10, ..., 0.95]$) of the wind speed. Reliability diagram (Figure 3.9) shows that forecasted quantiles used to build the intervals are slightly overconfident, but quite accurately retrieved by the EMOS forecast as well as by the climatology on this domain.

3.5 Conclusion

As in chapter 2, we propose to link the surface wind speed distribution with the large-scale atmospheric circulation patterns, represented by the Z500 geopotential height field. The model proposed is nevertheless different as it is non-parametric and as it issues a distribution of the wind speed distribution on a daily basis. The study thus lies in the context of probabilistic forecasting. The distribution implied by the model is compared to the climatology, which is the reference long-term forecast used in energy management.

In the first part of the study, we address the first objective of the thesis which is to show that the large scale circulation of the atmosphere explains a major part of the interannual variability of the surface wind speed in France. In particular, we show that the proposed model is able to follow long term trends of the surface wind speed in France (Figure 3.3). We also show that the proposed probabilistic model is on average, over France, 29% to 26% sharper than the climatology when considering respectively 50% and 90% prediction interval width. Considering the

CRPS, the model also overperforms climatology over France. More specifically, we find that the model performs even better regarding climatology during cold seasons and in the North of France. These results confirm results of chapter 2 that the large-scale circulation patterns contain useful information for predicting the surface wind speed.

In the second part of the chapter, we address the second objective of the thesis which is to show that the information on the large scale atmospheric circulation contained in seasonal ensemble forecasts provides useful information on the surface wind speed, on monthly to seasonal timescales. We combine the probabilistic model with the seasonal ensemble forecasts of the Z500 fields of ECMWF, to test its predictive power. To improve the calibration and sharpness of the ECMWF forecasts, we use the EMOS statistical post-processing technique. We find that the surface wind speed forecasts obtained with our method are sharper than climatology on average even for 3-month forecast horizon. In the North of France, especially during winter and fall, the forecast is better (or as well) calibrated as climatology and can be as much as 25% sharper. Those results are nevertheless difficult to generalize to all forecasts, and to the entire domain, as they are dependent on the predictability of the PCs.

The use of such forecasts in the frame of seasonal risk assessment for network safety for instance may not be totally relevant. Nonetheless, as wind energy penetration is high in the North of France, as during cold seasons wind energy production is higher than in spring and summer, and as these seasons can be particularly risky for the network balance, because of potential high consumption due to cold temperatures, we conclude that this forecasting methodology is very promising and might be useful to improve the risk management systems, used, in particular, by the network operators.

Chapter 4

Measuring the Risk of supply and demand imbalance at the Seasonal scale

Contents

4.1 Introduction

This chapter adresses the third objective of the thesis which is to show that the large scale atmospheric patterns not only influence the local surface wind speed, but can also explain the seasonal risk of imbalance between production and consumption at the national scale.

Wind energy resource and production forecasts at the seasonal scale are important for maintenance planning, and even more so for network management. Accurate forecasting of lower or higher than normal wind production for the next season would allow Transmission System Operators (TSOs) to include the interannual wind variability in the seasonal risk assessment and thus to have a better knowledge on the future risk. Currently, the seasonal risk in France is addressed by comparing climatological scenarii of consumption with available production capacity given by producers. Renewable intermittent production is also usually assessed using climatological scenarii (Figure 1.7, (RTE, 2016a)).

In 2009-2010, United Kingdom (UK) experienced a very severe winter characterised by uncommonly cold temperatures and a long period of low capacity factor of wind power generation. It is a good example of the meteorological factors that could lead to an imbalance of consumption and production. This event has been well documented (Prior and Kendon, 2011; Brayshaw et al., 2012; Leahy and Foley, 2012; Cradden and McDermott, 2018). Luckily, this winter has not led to a blackout, and actually, TSOs did not report any problem of imbalance, as the event coincided with winter holidays and a period of economic recession (Leahy and Foley, 2012). Therefore, we need to keep in mind that an extreme meteorological situation does not always lead to the appearance of the risk, because other factors are drivers of this complex issue. The papers cited, that document the UK extreme winter of 2009-2010, give very interesting insights on the typical meteorological large scale situations leading to such extreme events.

The purpose of this chapter is to take advantage of the ability of NWP models to predict the probability of extreme meteorological situations at the scale of the season, in order to quantify the risk of imbalance at the seasonal scale. We propose a method to jointly reconstruct the wind energy production and the temperature driven consumption in France, in winter and fall. It allows to quantify the risk, and extreme risk of imbalance in comparison with the climatological state. The method is based on the Principal Components (PCs) of the 500hPa geopotential height (Z500) which describe the large scale atmospheric circulation variability. The analysis of the PCs of the large scale circulation field corresponding to a large potential imbalance allows to highlight the role of large scale patterns in the occurrence of a given risk at the seasonal scale.

In Section 2, we describe the data used to compute production and consumption as well as the method to reconstruct the joint probability of consumption and production, and we give the definition of two types of risk measures which are addressed in the study. In Section 3, we assess the performance of the models in reconstructing

the two types of risk measures defined. Section 4 aims at analysing the explanatory value of the large scale circulation patterns, and gives insights on the typical meteorological situations associated with the seasonal risks. In Section 5, results are discussed and summarized.

A manuscript is in preparation on this work, for a future submission.

4.2 Data & Methodology

4.2.1 Data

Daily surface wind speed and daily surface temperature are retrieved from ERA-Interim data on the French domain (Figure 1.9) between 01/01/1979 to 31/12/2015. We keep only winter and fall seasons (here we define winter and fall respectively as the three months of January, February, March and of October, November, December). We retrieve from Réseau de Transport d'Électricité (RTE) website[1], the hourly national consumption, together with the national hourly wind energy production in 2015.

From this data, we compute the daily mean and the peak at 7pm of the national consumption, and the daily mean wind energy production in France in 2015. We are interested in the peak of consumption at 7pm because it is the time when the risk is the highest. At this time of the day, photovoltaic production (PV) in winter and fall is null, and the only intermittent energy able to respond to the demand is wind energy. Using national mean daily temperature from ERA-Interim, we compute the temperature driven mean consumption for winter and fall using the following relation :

$$C_n^{era} = \begin{cases} 2.4 \times (15 - T_n), & \text{if } T < 15°C. \\ 0, & \text{otherwise.} \end{cases} \tag{4.1}$$

Here C_n^{era} is the national mean consumption in GW, and T_n the national mean temperature in $°C$. This simple relation is inspired from the relation used by RTE to compute the 'weather-adjusted demand' (RTE, 2016a). In fact, RTE's model is much more sofisticated. For instance, it uses a smoothed temperature gradient that takes into account slow response due to building inertia, and fast response due to consumers behaviour. It also include the impact of cloud cover on lighting and heating behaviours. We then perform a linear regression between the national maximum consumption given by RTE data (Consumption at 7pm) and the national temperature-driven consumption C_n^{era} computed with ERA-Interim data to obtain the computed maximum consumption :

$$\hat{C}_n^{7pm} = \beta_c C_n^{era} + I_{Cn}. \tag{4.2}$$

[1] https://opendata.rte-france.com/

The intercept I_{Cn} corresponds to the base maximum consumption (around 50GW) in France, and the slope β_c takes values of 1.09 and 0.84 respectively for winter and fall. It results in the time series presented in figure 4.1 c & d, respectively for winter and fall. Maximum daily consumption in RTE data follows a clear weekly cycle with higher consumption during working days than during weekends. This variability is not retrieved in the computed maximum consumption as it only represents the temperature-driven consumption. One could take into account the weekly cycle of the consumption, for instance by performing two different linear regressions, but we choose not to address this problem here. We finally apply the same relation (i.e. equation (4.1) and linear regression coefficients) to all years in ERA-Interim between 1979 and 2015. It results in a long time series of 37 years following atmospheric variability and consistent with the current consumption in France.

To compute the national wind energy production we place several turbines (Vestas V90-2.0 MW, with cut-in speed equal to 4 $m.s^{-1}$ (U_{in}), nominal power reached at 13 $m.s^{-1}$ (U_{nom}), and cut-out speed equal to 25 $m.s^{-1}$ (U_{out})) of nominal power 2MW at each point of the grid of France (Figure 1.9b). The number of turbines at one gridpoint corresponds to the regional installed capacity given in (RTE, 2016b) divided by 2MW. We then adapt the power curve to 10m wind speed by finding a of figure 2.7 (Chapter 2) so that computed national wind energy production in 2015 equals national wind energy production from RTE data in 2015 ((RTE, 2016b) - 21.1TWh). It results in a power curve adapted to surface wind speed with characteristics given by $\frac{U_{in}}{a}$, $\frac{U_{nom}}{a}$ and $\frac{U_{out}}{a}$, with a equal to 1.4. We finally perform a linear regression between the computed daily production and the daily production given by RTE in year 2015 :

$$\hat{P}_n = \beta_p P_n^{era} + I_{Pn}. \tag{4.3}$$

Here P_n^{era} is the computed production from ERA-I surface wind speed, $\hat{P}_n$ is the final production obtained by linear regression, β_p is the linear coefficient, and I_{Pn} is the intercept. This results in the time series presented in figure 4.1 a & b for winter and fall 2015. We finally apply this process on the entire time series of ERA-Interim between 1979 to 2015. We thus obtain 37 years of wind energy production consistent with the current wind power capacity in France.

4.2.2 Modelling the joint PDF of Consumption and Production

Model definition

The challenge is to model the joint PDF of the wind energy production Pr and the temperature-driven maximum consumption Co, knowing a certain amount of PCs $(X_1, ..., X_n)$ representing the large-scale circulation of the atmosphere:

$$P(Pr, Co|X_1, ..., X_n) = \frac{P(Pr, Co, X_1, ..., X_n)}{P(X_1, ..., X_n)} \tag{4.4}$$

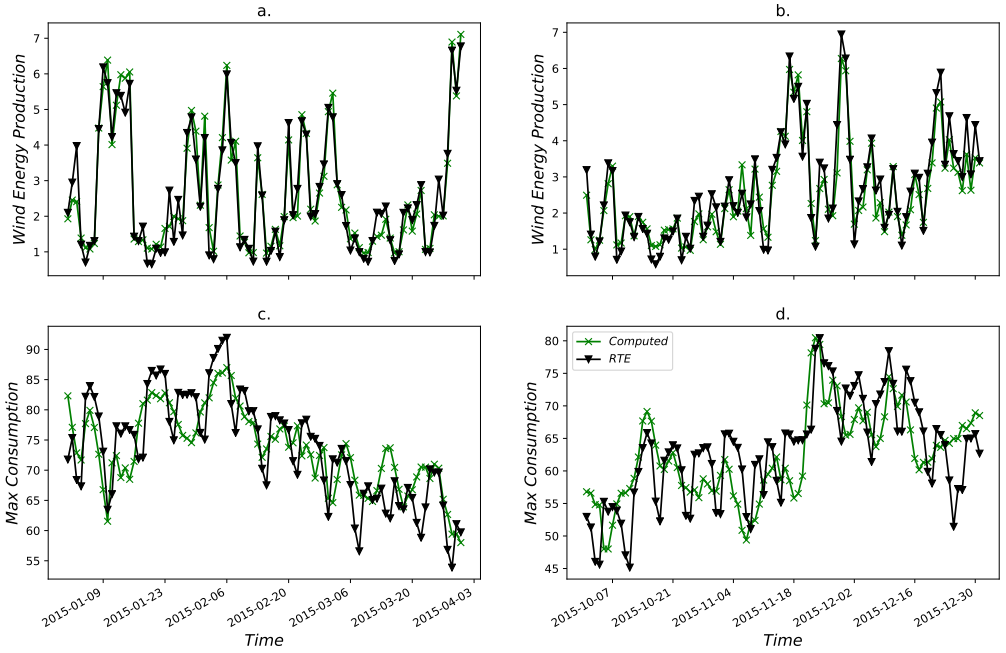

Figure 4.1: French daily wind energy production in winter (a) and fall (b) 2015 coming from RTE data and computed from ERA-I surface wind speed ; and French daily maximum consumption in winter (c) and fall (d) 2015 coming from RTE data and computed from ERA-I surface temperature.

Again the high dimensionality of such PDF is problematic. We thus define 2 indexes I_{Pr} and I_{Co} aimed at explaining respectively Pr and Co. As in the preceding chapter, these 2 indexes result from the polynomial regression of a number n of PCs with Pr and Co given by equation (4.5).

$$I_t = \beta_0 + \sum_{i=1}^{N} \beta_i X_t^{(i)} + \sum_{i=1}^{N} \beta_{ii} (X_t^{(i)})^2 + \sum_{i=1}^{N-1} \sum_{j>i}^{N} \beta_{ij} X_t^{(i)} X_t^{(j)}, \tag{4.5}$$

The joint PDF can be written as follows:

$$P(Pr, Co | I_{Pr}, I_{Co}) = \frac{P(Pr, Co, I_{Pr}, I_{Co})}{P(I_{Pr}, I_{Co})} \tag{4.6}$$

Following equation (4.6) the PDF needs to be estimated in 4 dimensions, which requires a lot of data and thus induce estimation errors. This model gives comparable results to the one described below in reconstructing the risk measure (see below). As it is longer to fit and harder to handle, we choose to use the estimation described in the following.

To simplify the model, we make the assumption that (i) conditionally on the indexes I_{Pr} and I_{Co}, production and consumption are independent and (ii) the production depends only on I_{Pr} while the consumption depends only on I_{Co}. This

amounts to writing

$$P(Pr, Co|I_{Pr}, I_{Co}) = P(Pr|I_{Pr}).P(Co|I_{Co}) \tag{4.7}$$

To check the assumption of conditional independence, we compare the conditional and unconditional correlation between Pr and Co. The unconditional correlation coefficients for winter and fall are given, respectively, by -0.22 and -0.11. The conditional correlation coefficient is defined as the correlation between $\tilde{Pr}$ and $\tilde{Co}$, the residuals of linear regression of Pr and Co on their respective indexes, defined by

$$\tilde{Pr} = Pr - \rho(Pr, I_{Pr})I_{Pr}, \quad \text{and} \quad \tilde{Co} = Co - \rho(Co, I_{Co})I_{Co}$$

with

$$\rho(Pr, I_{Pr}) = \frac{Cov(Pr, I_{Pr})}{Var(I_{Pr})} \quad \text{and} \quad \rho(Co, I_{Co}) = \frac{Cov(Co, I_{Co})}{Var(I_{Co})}$$

We find the conditional correlation values of -0.04 for winters and -0.09 for falls with 25 PCs to fit the indexes (see below). These correlation values are found to be significant at the 95% confidence level, so that only part of the dependence between Pr and Co is taken into account by the model.

The seasonal joint distribution $P(Pr, Co)$ of equation (4.7) is computed as the seasonal mean of the daily estimation given by $P_t(Pr|I_{Pr} = i_{Pr}).P_t(Co|I_{Co} = i_{Co})$, t being a given day. The model thus follows variations of the indexes. We choose in this study to use only the seasonal joint distribution, but one could imagine to reconstruct joint distributions for each month or week of the season. However, this raises the question of the uncertainties induced by the estimation of the real joint distribution with smaller samples, thus the verification of the results that could be obtained. Note that our model may also be used to measure the risk for a given day, but it does not take into account entirely the temporal dependence structure and therefore cannot be used to predict the persistence of a given meteorological event (e.g., the duration of a cold wave).

Cross validation

We define a period of 33 years between 1979 and 2011 to apply our model to ERA-I computed data and to assess its accuracy for reconstructing risks of imbalance in a cross validation mode. The years from 2012 to 2015 are kept for forecast purpose, though it is not presented in the chapter. Conditional PDF of Pr and Co knowing their respective index is estimated by Kernel Density Estimation (KDE) over 32 years and the joint PDF is reconstructed for the remaining year. We also estimate by Kernel Density Estimation (KDE) the real joint PDF for the given year over real samples of Pr and Co. Doing this 33 times, we obtain 33 reconstructed and real joint PDF for winter and fall. A seasonal joint PDF of the climatology is estimated by KDE on the entire sample of 33 years, after checking that no significant variations can be found after removing one of the 33 years (stable climatology).

4.2.3 Risk measures

Risk of deviation of Pr and Co from their climatological mean

We end up for each season of the 33 years with 3 distinct joint PDFs of Pr and Co :

- The seasonal climatology of the joint PDF of Co and Pr estimated by KDE over the 33 years from which climatological risks (or base risks) can be derived.
- The real seasonal joint PDF of Co and Pr estimated by KDE from which real risks can be derived
- The reconstructed seasonal joint PDF of Co and Pr given by the model defined in section 4.2.2 from which reconstructed risks can be derived.

As explained previously, only the seasonal joint distribution is used here to measure a seasonal risk, but the model may provide useful information at smaller temporal resolution, such as the month or the week.

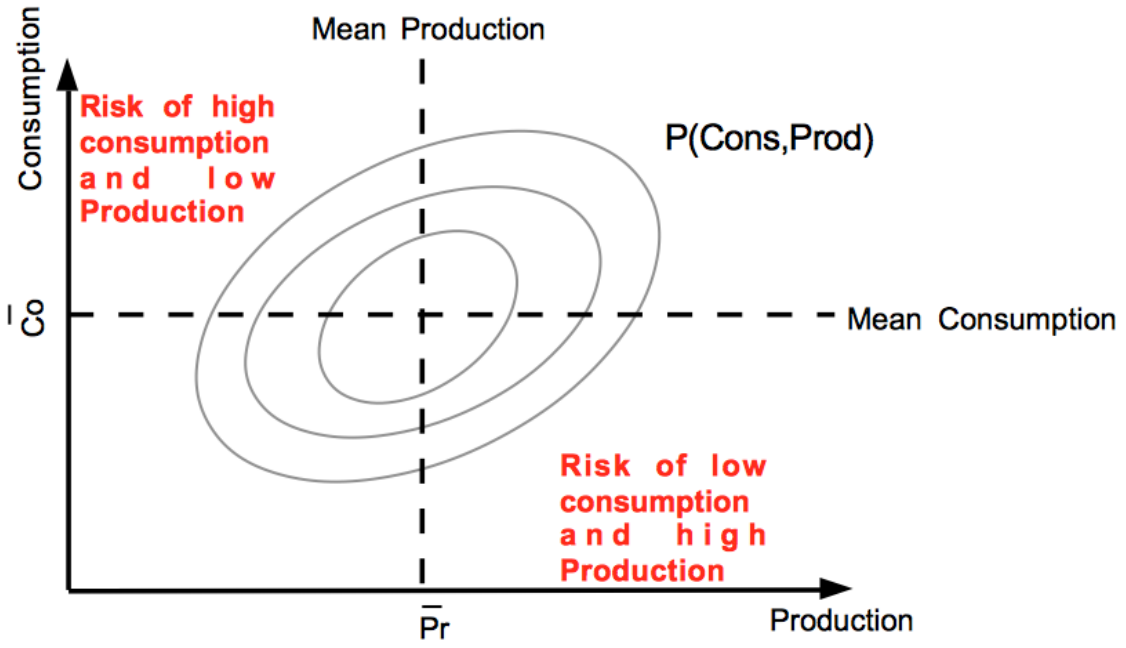

Figure 4.2: Schematic view of the areas of risk of supply and demand imbalance given the joint PDF of consumption and production.

Figure 4.2 shows a schematic joint PDF that could be one of the three PDFs described above. Four quadrants are defined by the vertical and horizontal lines corresponding respectively to the climatological mean of the production $\bar{Pr}$ and the climatological mean of the consumption $\bar{Co}$. Two of the quadrants highlight risky areas of imbalance between production and consumption :

- In the top-left of the distribution, where $Co > \bar{Co}$ and $Pr < \bar{Pr}$ corresponds to a risk of high consumption and low production.
- In the bottom-right of the distribution, where $Co < \bar{Co}$ and $Pr > \bar{Pr}$ corresponds to a risk of low consumption and high production.

Integrating the joint PDF over these risky areas allows to measure the risk in terms of probability. Both risk measures can thus be expressed as :

$$R_{hclp} = P(Pr < \bar{Pr}, Co > \bar{Co}) \tag{4.8}$$

and

$$R_{lchp} = P(Pr > \bar{Pr}, Co < \bar{Co}) \tag{4.9}$$

$P(Pr, Co)$ being the climatological, the real or the reconstructed joint PDF of Pr and Co.

The integration of the climatological PDF gives a measure of the base risk which is already well handled by TSOs. Integrating over real and reconstructed PDFs gives respectively the real and reconstructed risk measures for a given year and season. Comparing the climatological risk measure with real and reconstructed risk measures allows to highlight higher or lower risk than normal, and comparing real and reconstructed risk measures relative to the measure of the base risk (climatology) allows to assess the accuracy and ability of the model to highlight deviation from the climatology. In the following, we refer to the real and reconstructed risk measures normalised by the measure of the base risk as the risk measures 'normalised by climatology'.

Measuring the risk of extreme situations

Risk indicators R_{hclp} and R_{lchp} are defined as the probability of being superior/inferior to the historical mean consumption and production. One can wonder if this measure is relevant to highlight extreme situations of imbalance. Indeed, the probability of deviating from the mean consumption and production may be high, without having high probability of encountering extreme values of consumption and production.

We thus define another measure of the risk with regard to this notion of extreme situation. The balance between consumption and production can be measured by the quantity $D_{CoPr} = Co - Pr$. In finance, the risk associated to a loss X is often measured using the Value at Risk (VaR) measure defined as follows:

$$VaR_\tau = F^{-1}(\tau), \tag{4.10}$$

where F is the cumulative distribution function of X, and τ is the confidence level which is typically taken as 95% or 99%. VaR_τ is the percentile corresponding to the confidence level τ. In the following we use the 95% confidence level. The expected

shortfall is another measure of the risk which takes into account the entire tail of the distribution. It is defined by :

$$Esh = E[X|X > VaR_\tau] \tag{4.11}$$

It is actually the expectation of X conditional on being superior to VaR_τ.

In the following, we only use VaR_τ as an indicator of the risk, because the tail of the distribution of D_{CoPr} does not extend very far. We use the quantile regression (Koenker and Hallock, 2001) to estimate the 95^{th} percentile of D_{CoPr} to measure the extreme risk of high consumption and low production. It is referred in the following as VaR_{95}. The measure of the extreme risk of low consumption and high production is taken as the 5^{th} percentile of D_{CoPr} and is referred in the following as VaR_{05}. Note that it corresponds also to the 95^{th} percentile of $D_{PrCo} = Pr - Co$ in absolute value.

Quantile regression is a minimisation problem in which we minimise the loss function ρ_τ, also known as the quantile score (Bentzien and Friederichs, 2014). Let $D_y = (y_i - \hat{q}_\tau)$ be the difference between the random event y and the quantile estimate $\hat{q}_\tau$. The loss function ρ_τ is defined as :

$$\rho_\tau(D_y) = \begin{cases} \tau D_y, & \text{if } D_y > 0. \\ (1-\tau)D_y, & \text{otherwise.} \end{cases} \tag{4.12}$$

The minimisation problem can be written:

$$\min_{\epsilon \in \mathbb{R}} \sum_i \rho_\tau(y_i - \epsilon(x_i, \theta)) \tag{4.13}$$

where y_i are the realisations of D_{CoPr}, x_i is the vector of explanatory variables which contains the indexes I_{Co} and I_{Pr} defined previously, θ is a free parameter and $\epsilon(x_i, \theta)$ represents a linear function that can be written as :

$$\epsilon(x_i, \theta) = y_i - \theta^T x_i - \theta_0 \tag{4.14}$$

4.3 Estimation of the risk measures

4.3.1 Modelling the risk of deviation from climatological means

In this subsection we give the results of the modelling of the joint PDF of Co and Pr, and of the reconstruction of the risk measures R_{hclp} and R_{lchp} (as defined above). They correspond to measures of the risk of deviation of Co and Pr from their climatological mean value.

Sensitivity of the model to the number of PCs used to fit the indexes

We first build 6 models by increasing the number of PCs to fit both indexes from 5 to 30 with increments of 5. We compute the mean absolute error (MAE) between the real and reconstructed risk measures normalised by climatology. Figure 4.3 displays the result of the sensitivity analysis. The minimal error is found for 20 PCs for the risk measure R_{lchp} and 25 for the risk measure R_{hclp} for both seasons. The difference in MAE between 20 and 25 PCs for the risk measure R_{lchp} is nevertheless very low. Interestingly, the optimal number of PCs corresponds to the maximum of partial correlation explained by the indexes which is around 26 and 27 PCs *(Not shown)*. In the following, 25 PCs are used to compute the two indexes for any risk measure and season.

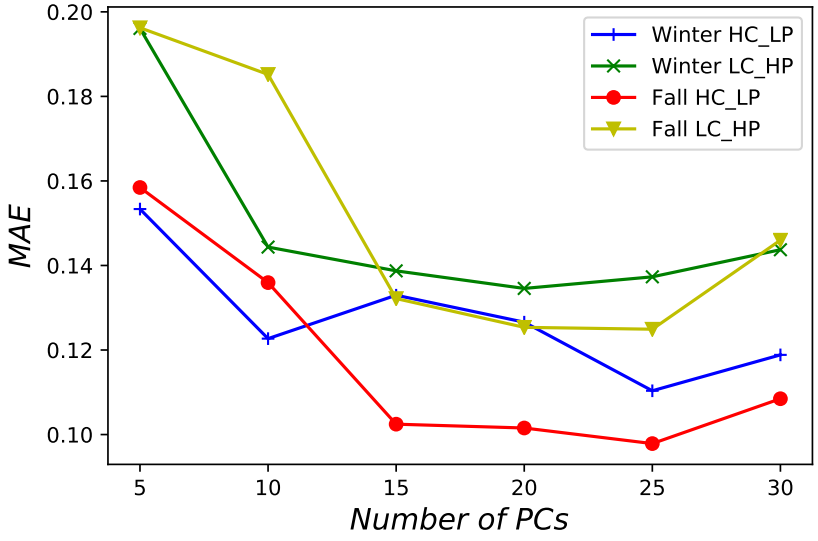

Figure 4.3: MAE between the real and reconstructed risk measures normalized by climatology as a function of the number of PCs used to fit the indexes I_{Pr} and I_{Co}.

Significance levels for the risk measures

We define the significance levels of the risk measure normalised by climatology. Recall that the risk measure is defined as the integral of the joint PDF of Pr and Co over a quadrant defined by the climatological means of Pr and Co. By comparing a seasonal risk measure to climatological risk measure, we can quantify higher or lower risk than normal. Nevertheless, the estimated risk may be considered lower or higher than normal even if the seasonal sample does not significantly differ from the climatological sample. This is the issue addressed in this paragraph.

We perform a 2 dimensional Kolmogorov-Smirnov test (Fasano and Franceschini, 1986) to test whether the real seasonal samples (used to build the real joint PDF and compute the real risk) and the sample gathering all winter (or fall) realisations

(seasonal climatology) are drawn from the same distribution. We also compute the 2 risk measures normalised by climatology defined previously for the estimated real distributions. Plotting the p-value obtained as a function of the real risk measure normalised by climatology results in figure 4.4.

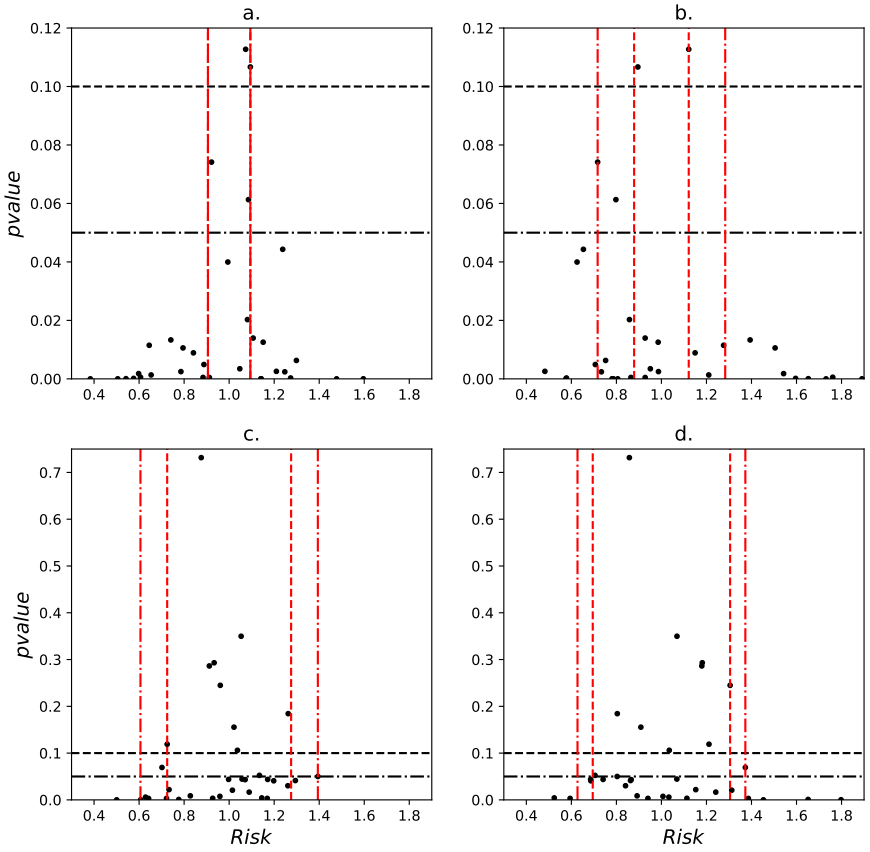

Figure 4.4: p-value resulting from the 2 dimensional Kolmogorov-Smirnov test performed between the climatological sample and the seasonal samples as a function of the real computed risk measure normalised by climatology. Black dash-dotted lines and black dashed lines respectively represent the 5% and 10% significance levels for which the hypothesis of 2 samples coming from the same distribution cannot be rejected ; Red dotted lines and Red dashed lines represent the thresholds defined ; (a) for winter and R_{hclp}, (b) for winter and R_{lchp}, (c) for fall and R_{hclp}, (d) for fall and R_{lchp}.

We define the 2 significance levels of 5 and 10%, which correspond respectively to dash-dotted and dashed black lines in figure 4.4. Small p-values show that the 2 samples may not come from the same distribution, while high p-values show that the hypothesis that the seasonal sample and the climatology have the same distribution cannot be rejected. Red dotted and dashed lines correspond to the thresholds for which we consider that the risk measure highlights a significant risk higher or lower

than normal. They are defined by the highest value of deviation from 1 (as 1 corresponds to the base risk measure) when the p-value is above significance levels of 5 and 10%.

From figure 4.4 we can already draw 2 conclusions. First, winter seasons more often deviate from the wintertime climatology (figure 4.4 a & b) than fall seasons from fall climatology (figure 4.4 c & d). Second, that the risk measure can be as much as 40% (30%) higher or lower than climatological risk measure and still not significant at 5% (10%) confidence level. This is the case for fall seasons and for both risk measures (Table 4.1). In winter significance levels are smaller : around 10% at 10% level. For the R_{hclp} in winter, the significant levels at 5% and 10% are equal (Table 4.1).

Seasons	Risk	Thresholds	
		5%	10%
Winter	R_{hclp}	0.09	0.09
	R_{lchp}	0.28	0.12
Fall	R_{hclp}	0.39	0.28
	R_{lchp}	0.37	0.31

Table 4.1: Thresholds of risk measure significance defined by the p-value at 10% and 5% resulting from the 2 dimensional KS test performed between climatology and real samples

Modelling results

Figure 4.5 shows the time series of the real and reconstructed risk measures normalised by climatology. A value above (below) 1.0 highlights a higher (lower) risk than normal. Dashed and dashed dotted red lines are respectively thresholds corresponding to significance levels of 10% and 5% defined previously.

For winters and R_{hclp} (Figure 4.5a.), the model predicts 13 significantly more risky winters than normal. Amongst these 13 winters, 4 are in fact not significant (based on the real distribution). The model misses only 3 significant risks in 1979, 1981 and 1984. For winters and R_{lchp} (Figure 4.5b.), considering 5% significance level the model does not miss any of the risky winters even if it often underestimates the risk, especially in years 2007 and 2008. Considering 10% significance level, the model is less accurate and misses 2 risky winters in 1998 and 1999, and predicts 1 risky winter in 1981 whereas the real PDF does not deviate from climatology. In the fall season, R_{hclp} cannot be considered significant at 5% level except for the year 1994 when the risk is lower than normal (Figure 4.5c.). The model allows to highlight this event. The risk R_{lchp} higher than normal is significant at level 5% for 5 years. Two of them are missed by the model in 2002 and 2009 (Figure 4.5d.).

The MAE computed between the real and the reconstructed risk measures relative to the climatology goes from 0.11 to 0.15 (Table 4.2). The correlation is always higher than 0.80 and is even 0.90 for R_{lchp} in winter. The correlation for the risk

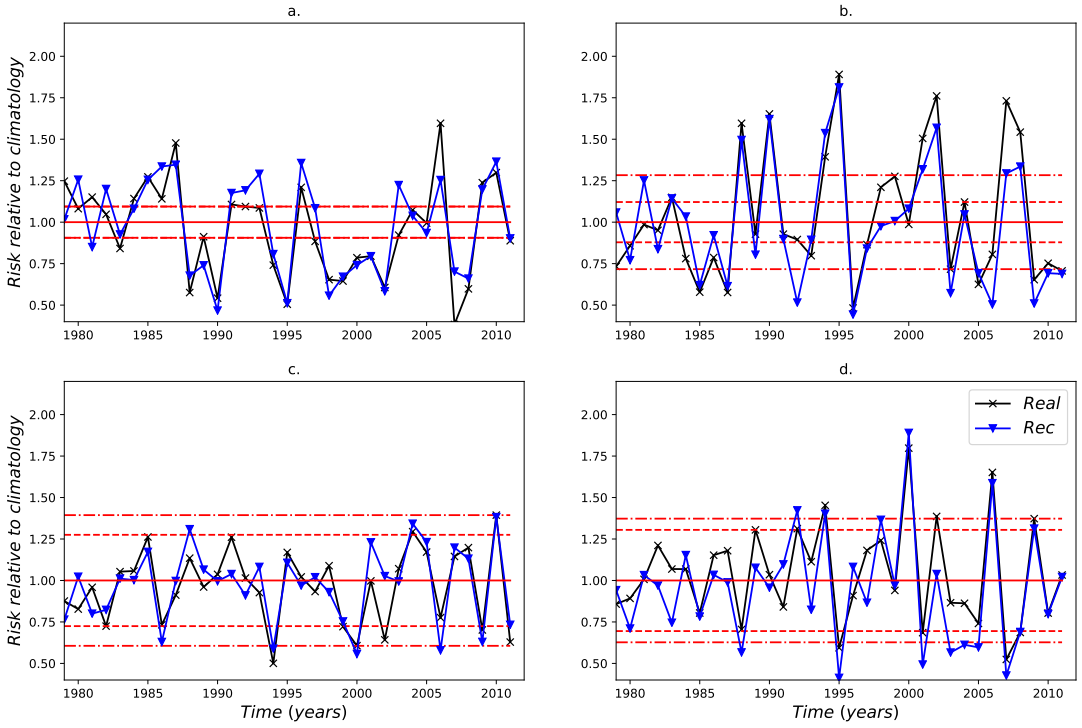

Figure 4.5: Time series of the real and reconstructed risk measures relative to climatology (a) for winter and R_{hclp}, (b) for winter and R_{lchp}, (c) for fall and R_{hclp}, (d) for fall and R_{lchp}. A value above (below) 1.0 highlights a higher (smaller) risk than normal. Dashed and dashed dotted red lines are respectively significance levels at 5% and 10%.

Season	Risk	Accuracy	
		MAE	Correlation
Winter	R_{hclp}	0.12	0.86
	R_{lchp}	0.14	0.90
Fall	R_{hclp}	0.11	0.82
	R_{lchp}	0.15	0.89

Table 4.2: Mean absolute error and correlation between the real and the reconstructed risk measures.

R_{hclp} is worse than for R_{lchp} and it seems to come from the first 4 years of the period where the real and reconstructed are anticorrelated (Figure 4.5).

Tables 4.3 and 4.4 gather the number of well reconstructed deviations from climatology (i.e higher and lower risks than normal), respectively when considering 10% and 5% significance level. Let us consider first the thresholds corresponding to 10% significance level (Table 4.3). In winter, significant deviations from climatology appear more than 80% of the time. Among these deviations, a little less than 50% concern higher risks than normal. As in winter, the opposite risks R_{hclp} and R_{lchp}

Season	Risk	Significance			
		Rreal $Nsig_{10\%}$	$N+_{10\%}$ ok	$N-_{10\%}$ ok	Ratio
Winter	R_{hclp}	26 (12^+ , 14^-)	9	12	0.81
	R_{lchp}	27 (12^+ , 15^-)	9	11	0.74
Fall	R_{hclp}	9 (2^+ , 7^-)	2	3	0.56
	R_{lchp}	11 (7^+ , 4^-)	5	4	0.82

Table 4.3: Number of more and less risky seasons than normal when considering significance at 10% for the real and the reconstructed risk measure relative to climatology. First column gives the total number of significant real risks at 10%; Numbers in parenthesis give the number of higher (+) and lower (-) risks than normal. The second and the third column respectively give the number of higher risk and lower risk than normal that are well reconstructed by the model. Last column gives the proportion of well reconstructed deviation from climatology.

Season	Risk	Significance			
		Rreal $Nsig_{5\%}$	$N+_{5\%}$ ok	$N-_{5\%}$ ok	Ratio
Winter	R_{hclp}	26 (12^+ , 14^-)	9	12	0.81
	R_{lchp}	15 (8^+ , 7^-)	8	7	1.0
Fall	R_{hclp}	2 (1^+ , 1^-)	0	1	0.5
	R_{lchp}	7 (5^+ , 2^-)	3	2	0.71

Table 4.4: Same as table 4.3 for the significance level of 5%

do not appear at the same time and we can count 24 significantly risky winters over the 33 years. 18 of these risks are highlighted by the model, and the model allows to highlight 74 to 81% of the deviations from climatology depending on the risk considered. In fall, much less deviations from climatology appear (about 60% of the years). Among these deviations, less than a half correspond to higher risk than normal. The model only misses 2 of them. Considering now thresholds of 5% significance levels (Table 4.4), in winter, the model highlights significant deviations from climatology 81% to 100% of the time. In fall, the ratio is still worse than for the winter as only 50% to 70% of the deviations are highlighted by the model, but the fall season is less often risky.

In winter 2010, the model shows a good ability to highlight a higher R_{hclp} than normal. Recall that it corresponds to the winter when UK experienced severe situation with cold temperature and low capacity factor. Figure 4.6 shows the real (contour lines in panel a.) and reconstructed (contour lines in panel b.) joint PDF for this winter. Full coloured contours show the winter climatological joint PDF and red vertical and horizontal lines define the 4 quadrants as in figure 4.2. Deviation from climatology is indeed clear for the real and reconstructed PDFs. The maximum probability is well located by the reconstructed PDF and is situated in the quadrant corresponding to R_{hclp}. The overall shape of the distribution is also very satisfying, even if the reconstructed PDF seems to have difficulty to represent the extremes and

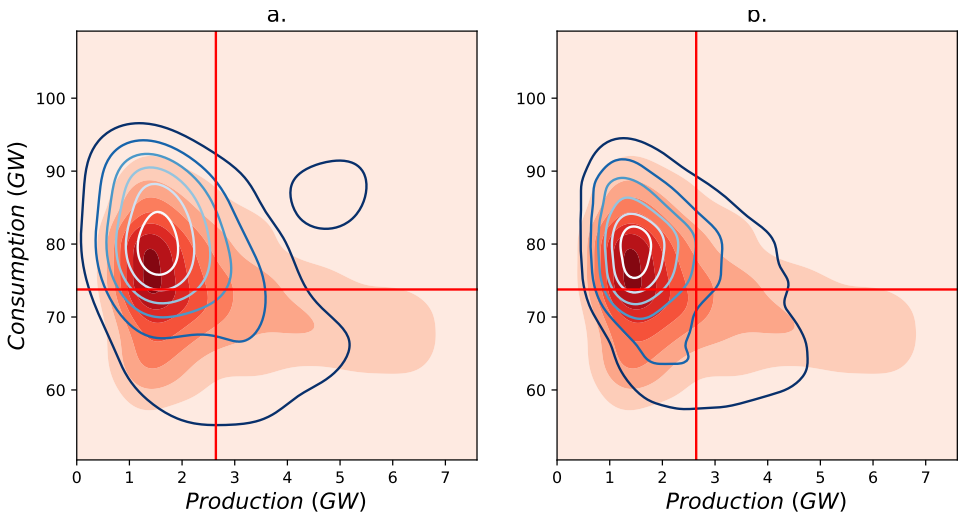

Figure 4.6: Blue contour lines show the real (a) and reconstructed (b) joint PDF for winter 2010. Full colours show the winter climatological joint PDF. Red vertical and horizontal lines correspond respectively to the mean production and mean consumption given by climatology.

part of the correlation.

Figure 4.7 shows the time series of production (in blue) and consumption (in red) of winter 2010. It indeed highlights a long period (between the 1st of January until mid-February) of higher consumption than normal (dashed red line) and lower production than normal (dashed blue line). During this period, production displays peaks that could help to satisfy the demand on some occasions, but they are indeed very brief. Around the 20th of February, consumption decreases while production sharply increases. This event only lasts 5 days and is very likely to correspond to a front passing over France bringing strong winds as well as warmer air. Conversely, stable anticyclonic conditions in winter often result in colder temperatures and less wind. This winter seems to have been characterised by stable anticyclonic conditions interspersed by briefly passing fronts. Maps of Z500 allow to confirm this pattern (*Not shown*).

Using the model to reconstruct the risk at the monthly frequency would have allowed to highlight a higher risk in February than in March for instance, and at the weekly time step, we would be able typically, to look at the event of the 20^{th} of February.

4.3.2 Modelling the risk of extreme situations

In this subsection, we present the results of the modelling of the extreme risk measures defined by the the Value at Risk of the loss function D_{CoPr}. Quantile regression is performed to estimate the Value at Risk (Section 4.2.3).

For one season, we measure the extreme risks as the maximum of the VaR_{95} and

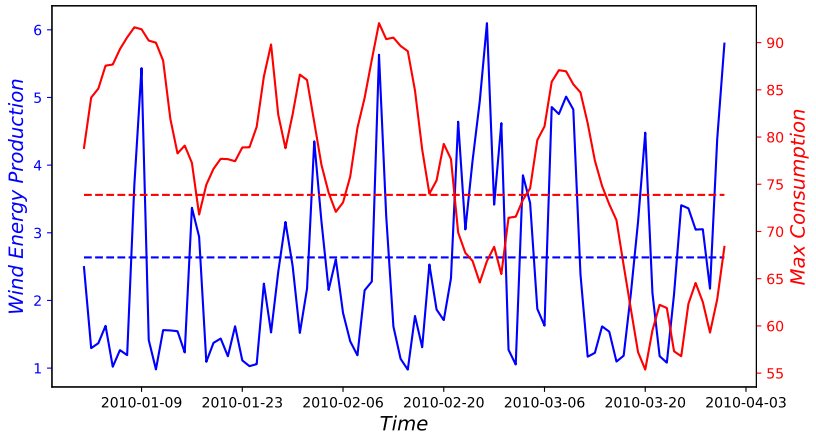

Figure 4.7: Time series of the wind energy production (in blue) and the temperature driven consumption (in red) during winter 2010. Dashed lines show the winter mean climatological value of the wind energy production (in blue) and of the consumption (in red).

the minimum of the VaR_{05}. The number of events and the persistence of an event is also of interest. Therefore, we compute the number of days when the VaR_{95} (VaR_{05}) predicted is superior (inferior) to the climatological VaR_{95} (VaR_{05}), as well as the length of the longest corresponding period. It should nevertheless be noticed that the time dependence of D_{CoPr} is not fully described by the model proposed here, even if the indexes I_{Pr} and I_{Co} may help to model part of the temporal correlation, there may be still uncertainty on the persistence of an event.

	Winter	Fall
$N_{hits}\ \tau_{95}$	0.947	0.947
$N_{hits}\ \tau_{05}$	0.054	0.052

Table 4.5: Reliability of VaR_{05} and VaR_{95} for winter and fall seasons

First, the reliability of the predicted percentiles needs to be evaluated. Table 4.5 gathers the proportion of 'hits' i.e, the number of times the realisation D_{CoPr} is indeed above the predicted VaR_{95} and below the VaR_{05}. The value for perfectly reliable percentile should tend to $\tau = 0.95$ and $\tau = 0.05$, respectively. Table 4.5 shows that the predicted percentiles are reliable, and are very slightly overconfident.

Figure 4.8 shows for each season, the predicted VaR_{95} minus the climatological VaR_{95}, as well as the total number of days and the maximum number of consecutive days when the predicted VaR_{95} is superior to the climatological VaR_{95}. The difference between the climatological and the maximum predicted VaR_{95} can be as much as 20GW for both winter and fall. In other words, on the day when the maximum risk is reached, there is a 5% chance to be 20GW above the VaR_{95} given by climatology, so that if a TSO is prepared for the climatological risk only, there may

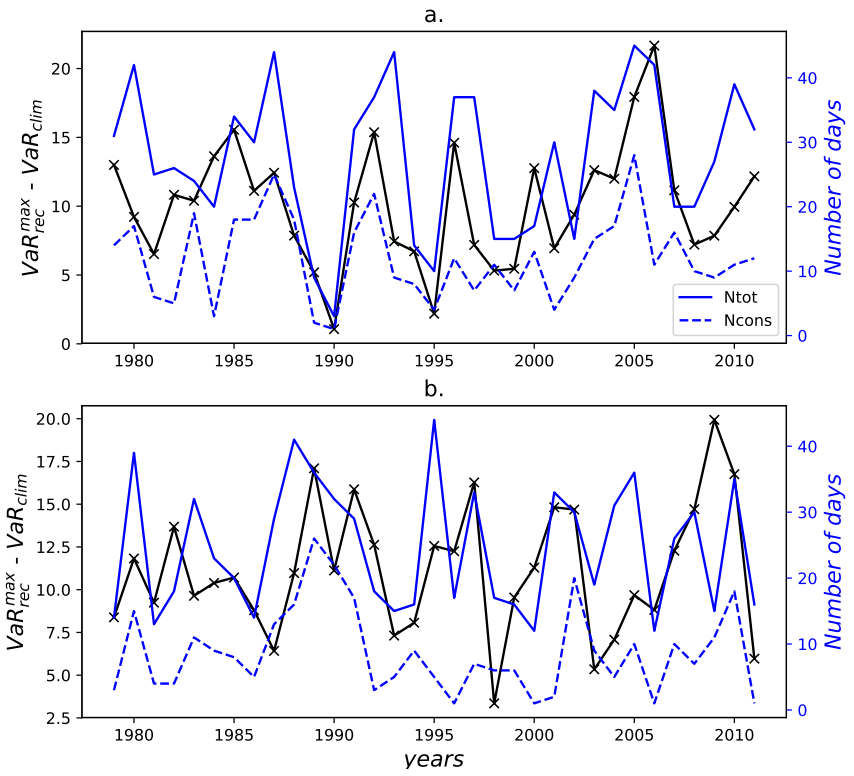

Figure 4.8: Difference between the maximum VaR_{95} and the climatological VaR_{95} (86GW) (black line), total number of days (blue line) and maximum number of consecutive days (dashed blue line) when the predicted VaR_{95} is superior to the climatological VaR_{95} for winter (a.) and fall (b.) seasons

be a lack of 20GW of electricity on the network. The predicted VaR_{95} is superior to the climatological VaR_{95} at most half of the time during a given season, and some very persistent risky situations are highlighted, especially for winter seasons. It can be noticed that the highest predicted maximum VaR_{95} during the winter of 2006 corresponds to the most risky winter given by the previous measure of the risk R_{hclp}. Conversely, the winter of 2005 is not considered risky by previous measure, while it seems to be a risky winter in terms of maximum VaR_{95} and persistence of extreme situations. More generally, the maximum predicted VaR_{95} for winter season is well correlated to the previous risk R_{hclp}, whereas in fall, it is not. A similar result holds for the opposite risk.

Figure 4.9 shows for each season, the climatological VaR_{05} minus the VaR_{05}, as well as the total number of days and the maximum number of consecutive days when the predicted VaR_{05} is inferior to the climatological VaR_{05}. In winter, the difference between climatological and the minimum predicted VaR_{05} reaches 13 GW in 1995, but never exceeds 10GW otherwise. The number of days when the predicted VaR_{05} is inferior to the climatological VaR_{05} reaches 50 days during the same year. However, the persistence of the extreme events in winter does not often exceed 15

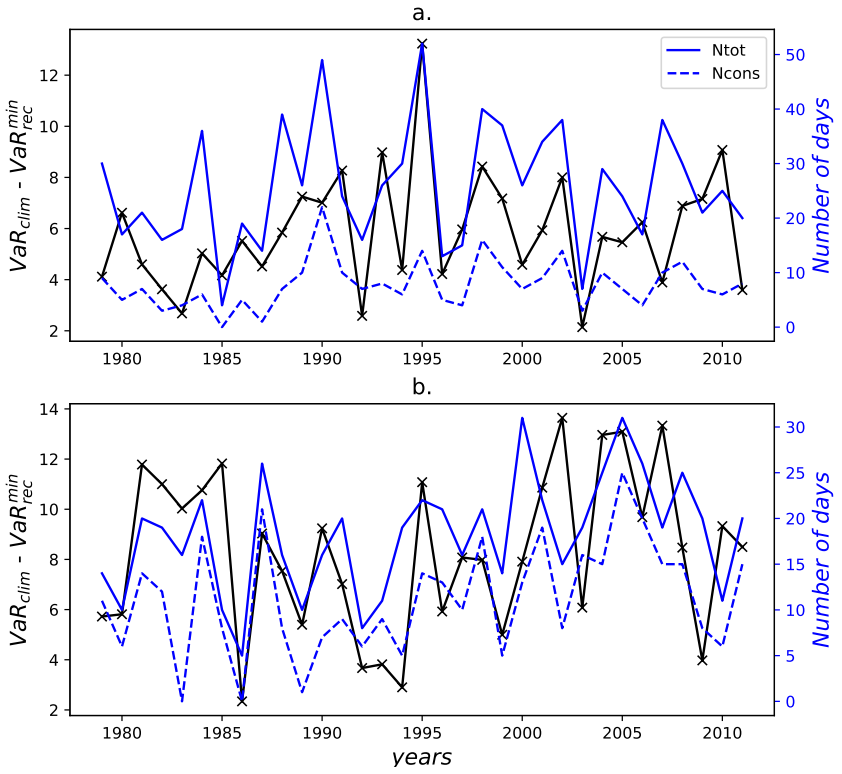

Figure 4.9: Same as Figure 4.8, for the inverse risk, i.e VaR_{05}

days. In fall, the difference between climatological and predicted minimum VaR_{05} is of the same order as in winter. The total number of days when the predicted VaR_{05} is inferior to climatological VaR_{05} does not exceed 30 days, but the extreme events are on average more persistent than in winter.

4.4 Explanatory value of the first PCs

In this section, we analyse the explanatory value of the first PCs used to compute the indexes I_{Pr} and I_{Co}. Indeed, more or less risky seasons should be related to different atmospheric conditions and thus different states of the PCs. Such analysis should provide information on the specific atmospheric conditions that lead to high (or low) risk and extreme risk measures.

Figure 4.10 shows the distribution of the three first PCs used to compute the indexes, namely the seasonal pattern (a & b), NAO (c & d) and SCA (e & f). Black distributions are computed using the entire dataset, while blue (red) distributions are computed over the seasons which are less (more) risky than normal. Left and right panels show results for the risk measures R_{hclp} and R_{lchp} respectively. First, left panels seem to be the mirror of right panels, so that the state of a PC resulting in higher (lower) risk R_{hclp} can be also related to a lower (higher) risk R_{lchp}. Thus, let us

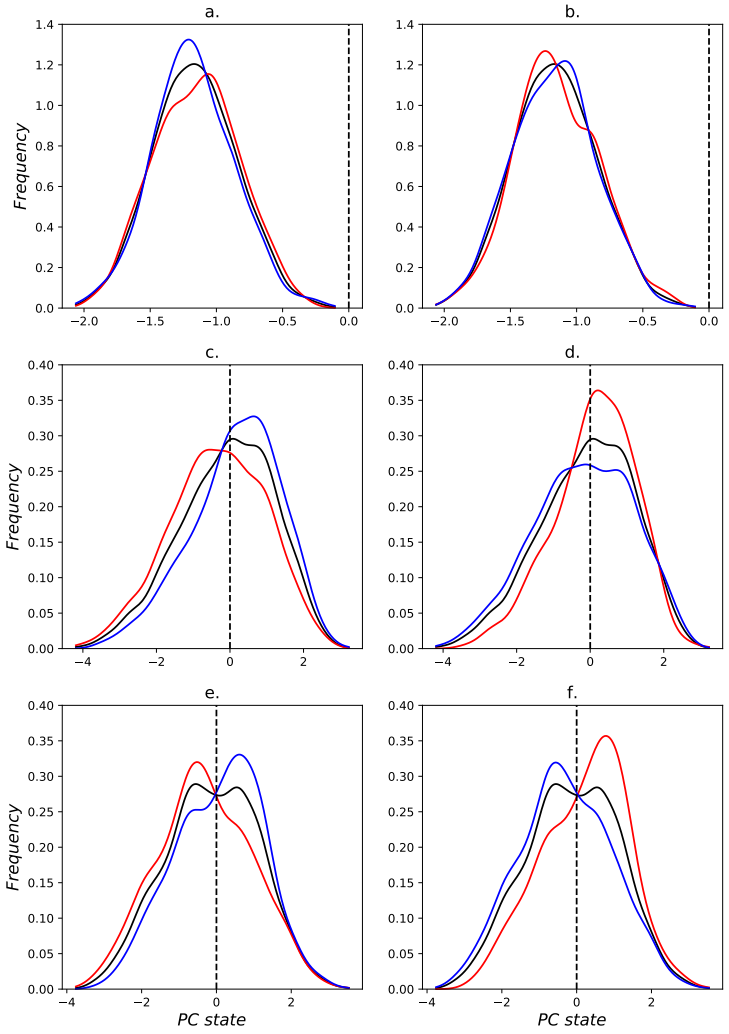

Figure 4.10: Winter distributions of the 3 first Principal Components used to fit the indexes : the seasonal pattern (a & b), NAO (c & d) and SCA (e & f). In each panel 3 distributions are plotted, the distribution of all winters in black ; the distribution of more risky winters than normal (in red) ; and the distribution of less risky winters than normal (in blue). Left and right panels correspond to the risk measures R_{hclp} and R_{lchp} respectively.

consider the risk R_{hclp} (left panels) only. For the winter season, clear differences can be seen between the red and blue distributions highlighting the role of the large-scale circulation in driving the French weather variability at the seasonal scale.

The seasonal pattern for higher risk measure than normal (figure 4.10 a, red distribution) is less negative than normal. It corresponds to a less marked Southward shift of the pressure gradient that influences the position of the jet stream which will be positioned more to the North than normal. The NAO pattern for higher risk than normal (figure 4.10 c, red distribution) is more negative than normal which

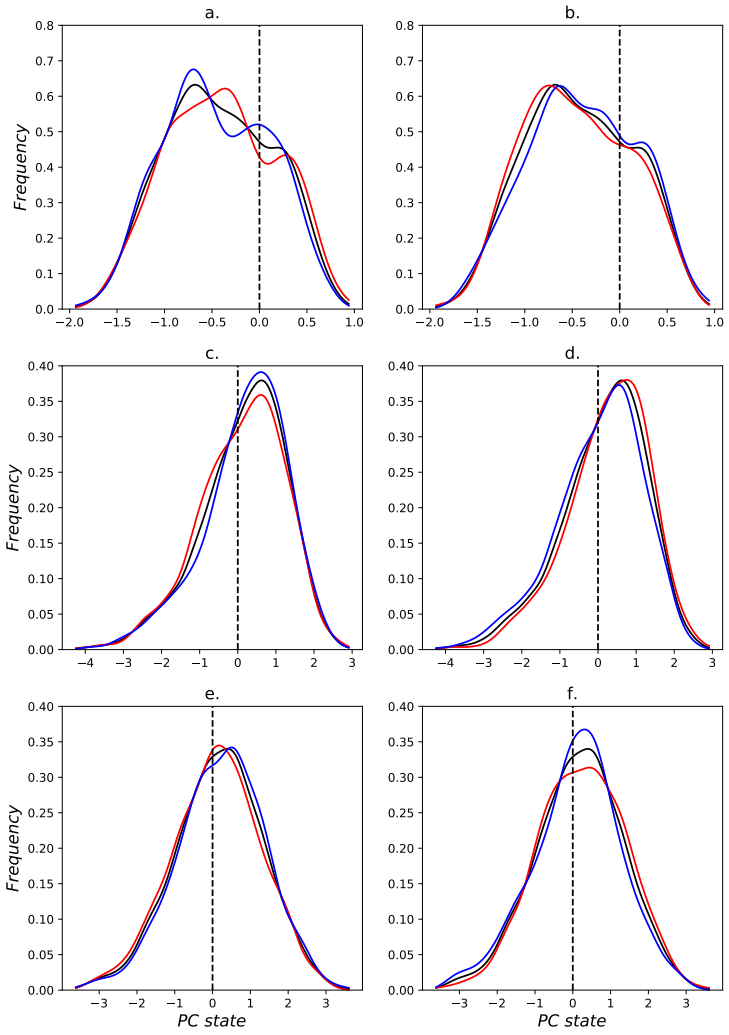

Figure 4.11: Same as Figure 4.10 but for fall seasons.

highlights a less marked pressure gradient between Northern Atlantic low and Azores high. It results in a less active storm track, thus less fronts and storms bringing high wind speeds and warmer air. The SCA pattern for higher risk than normal (figure 4.10e, red distribution) is also more negative than normal. It is interesting to see that the overall distribution displays two modes which can be clearly associated with the two risk types. Bueh and Nakamura (2007) show that during negative phases of SCA pattern, the storm track activity is enhanced, but it is also shifted Northward. This is in agreement with Jourdier (2015) who shows that the NAO pattern is spatially modulated by the SCA pattern. It is also in agreement with less wind energy production than normal in France, especially in the North of France where a large part of the installed capacity is situated.

In fall (Figure 4.11), there is much less signal highlighted by the distributions. First, more risky seasons than normal are not clearly marked by one state of the

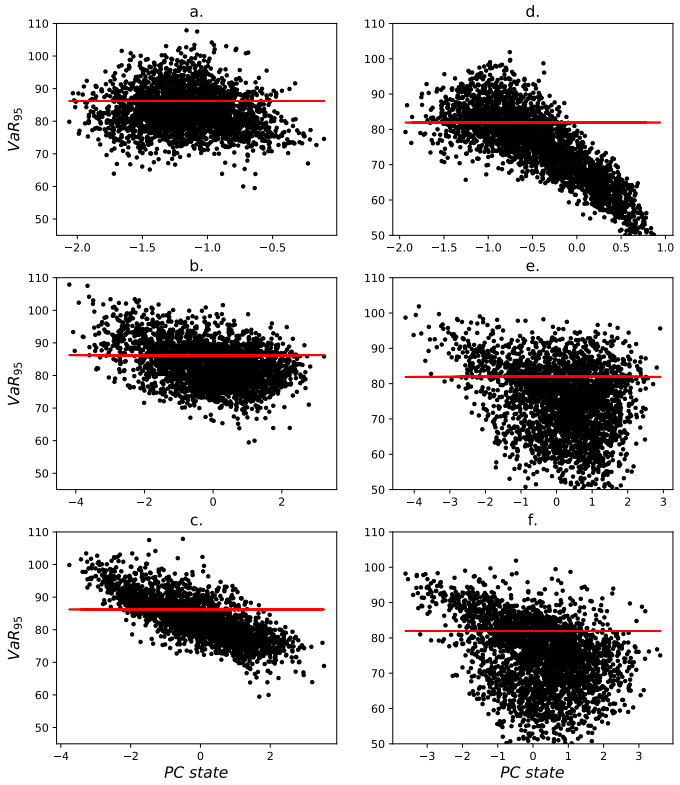

Figure 4.12: Extreme risk measure (VaR_{95}) as a function of the PCs state: For winter (left panels) and fall (right panels) season ; from top to bottom, Seasonal pattern (a & d), NAO pattern (b & e) and SCA pattern (c & f).

PCs, which could explain the worse behaviour of the model in fall compared to winter. Second, the states of the PCs corresponding to higher or lower risk than normal do not deviate from the overall distribution which could partly explain that thresholds defining significance for fall are higher than for winter.

Figure 4.12 shows the reconstructed VaR_{95} as a function of the 3 first PCs state, for winter (right) and fall (left) seasons. It thus highlights how the extreme risk measure is related to the state of these PCs. For winter season, extreme risks do not seem to be related to the seasonal pattern (Figure 4.12a), but display strong linear relation with NAO pattern and even stronger with SCA pattern. This is in agreement with the relations found for the other risk measure R_{hclp} (Figure 4.10, a., b. and c.), and can explain why a good correlation is found between the two risk measures for winter season. Conversely, for fall seasons, extreme risks can mainly be related to the seasonal pattern which highlights that the extreme risks for fall may be linked to an early winter season. NAO and SCA patterns display a relation with the extreme risk measure only when they are in a negative state, and when the risk measure is high.

4.5 Discussion and concluding remarks

This chapter adresses the last main objective of the thesis which is to show that the large scale atmospheric circulation can be used directly to assess and quantify the risk of imbalance between production and consumption at the seasonal scale. We defined two risk measures of the imbalance between production (Pr) and consumption (Co) at the seasonal scale. The first risk measure is based on the integration of the joint probability of Co and Pr in areas where Co and Pr deviate from their historical mean. This risk measure is aimed at highlighting the risk of significant deviation from the climatology with a high probability of encountering imbalance situations. It is nevertheless not aimed at addressing the issue of extreme risk, for which a second measure is proposed. The Value at Risk (VaR) at the confidence level 95% measures the risk of encountering extreme values of the loss function $Co - Pr$.

A model based on the knowledge of the large-scale atmospheric circulation is proposed to reconstruct the joint probability of consumption and production. The first risk measure computed from the model shows a very satisfying correlation with the real computed risk measure. Significance levels for the computed risk measures have been defined by testing the two-dimensional samples with the Kolmogorov-Smirnov test as proposed by Fasano and Franceschini (1986). The good results obtained for winter seasons show that the model is able to follow the interannual variations of Co and Pr. We can be quite confident with a large part of the risky winters highlighted by the model. Looking at the overall reconstructed distribution for a given season strengthens this feeling, as the real and reconstructed joint PDF are very similar. Further work could be dedicated to the assessment of the model performance in quantifying the risk at higher temporal resolution (e.g monthly, weekly frequency).

The second risk measure is estimated by quantile regression. The reconstructed percentiles (at 5% and 95% confidence levels) are shown to be reliable. The analysis of the maximum VaR, as well as the number of appearances of higher values of VaR than climatological VaR, and the persistence of these events show that the predicted imbalance due to high Co and low Pr at 95% confidence level can be as much as 20GW higher than when the climatological measure is considered. For the inverse risk, this value drops to around 10GW. The persistence of these extreme situations can reach more than 25 days for several seasons, and the number of days when it appears during a season is very variable and goes from less to 5 days to more than 50 days.

The explanatory value of the first PCs is analysed for both risk measures. The analysis highlights that NAO and SCA patterns have very high explanatory value for both the first and the second risk measure in winter. For the fall seasons, the relation between the PCs and the first risk measure is not clear, and the extreme risk measure is mainly driven by the seasonal pattern.

The study presents here only modelling results, but future work will be dedicated to forecasts of the risk measures at the scale of the season, as the large scale circula-

tion patterns indeed explain the appearance of the risk of imbalance in France. We must also keep in mind that the models are designed to predict risks associated with wind energy production and temperature driven consumption. The seasonal risk for energy systems related to meteorological uncertainties is also driven by hydrological reservoirs, thus long-term precipitation affecting the hydropower, incoming solar radiation at the surface, directly related to cloudiness affecting the photovoltaic power (PV). Other non-meteorological factors affecting the balance between consumption and production include the availability of conventional power plants, long term storage capacity such as pumping power plants, and Power to Gas, as well as more social factors such as the hour of the day, the day of the week, holidays, and even long term trends in electricity demand coming from economic recession for instance.

Chapter 5

From Numerical Weather Prediction outputs to accurate local surface wind speed : statistical modelling.

Contents

5.1 Introduction

The perfect model approach (Elia et al., 2002) followed along the manuscript, also denoted 'Big Brother Experiment' approach by Omrani et al. (2011, 2013) for instance, aimed at isolating errors coming from the methods proposed. This approach is strengthened by the previous work of Jourdier (2015) who shows that ERA-I is the best reanalysis product regarding surface wind speed in France, compared to MERRA and NCEP/NCAR reanalysis. However, the wind speed from ERA-I reanalysis, used as a reference in our studies, does not perfectly represent the surface wind speed at a specific location of a wind farm for instance. Indeed, when comparing output from a numerical model to a local measurement, there will always be several sources of error: representativity error (contrast between the value over a grid-box and the value at a specific point), numerical error (even if we were describing only processes governed by well-established physical laws, discretization is unavoidable), and error tied to the physics described (because processes, especially parameterized ones, are not well modelled).

To obtain more realistic representation of the wind energy resource and production, downscaling techniques can be used to reduce those errors. One strategy to reduce representativity errors and to better represent small-scale processes, in particular those tied to topography and surface roughness, consists in downscaling with numerical models that describe the atmospheric flow on finer scales (e.g Wagenbrenner et al. (2016)). One disadvantage of this approach is the numerical cost, and one limitation is the need for finer observations to initialize the state of the atmosphere, if details of the flow other than those directly implied by the topography and surface condition are sought for. Other techniques, often referred as Model Output Statistics (MOS), have been developed in weather forecasting for several decades to estimate the weather related variability of a physical quantity based on Numerical Weather Prediction (NWP) model outputs (Glahn and Lowry, 1972).

Wind energy domain is nowadays a very active branch in downscaling techniques because of the need for accurate forecasts at specific location of a wind farm. For describing winds close to the surface, 10m wind speed is often a convenient variable as it has been for decades a reference observed variable and also now a reference NWP model output. In the case of wind energy, the wind speed then needs to be extrapolated at the hub height to have access to wind power, leading to an increase of the error on the predicted power (Kubik et al., 2011; Howard and Clark, 2007; Mohandes et al., 2011). Wind speed at the hub height (typically 100m) is a variable of interest as it allows to avoid vertical extrapolation errors (Cassola and Burlando, 2012), but it is rarely available in observations. Different outputs of NWP models can be used as explanatory variables of the near surface wind speed. It seems that there is no strong consensus on the predictors to use, mainly because relations between predictors and predictand should differ from one location to the other. However, different studies have shown the importance of a certain set of variables to predict surface wind speed. Amongst them, markers of large-scale systems (geopotential height,

pressure fields) and boundary layer stability drivers (surface temperature, boundary layer height, wind and temperature gradient) can be cited (Salameh et al., 2009), Devis et al. (2013), Davy et al. (2010). In terms of methodology, several models have already been studied, including Linear regression, Support Vector Models (SVM) or Artificial Neural Network (ANN) (Jung and Broadwater, 2014; Soman et al., 2010).

The aim of this chapter is, in particular, to explore how different statistical models perform in downscaling the observed wind speed at 10m and 100m height at the SIRTA observatory in the south of Paris, using informations of ECMWF analyses outputs. We choose multiple linear regression because it is a widely used technique, and Random Forests which have not been, to our knowledge, deeply studied in the framework of downscaling surface wind speed. We show that linear downscaling models are sensitive to the explanatory variables selected. On the contrary, Random Forest models handle the variety of explanatory variables on itself. We show that improving linear models accuracy is possible by understanding the environment of the observation site and by adapting relationship to the specificity of the terrain. Best linear model and Random Forests performance are comparable. But while fitting Random Forests does not require an a-priori study of the wind speed variability and a step of variable selection, linear regression models need upstream study of explanatory variables and site specificity to achieve better results.

The paper is organized in 4 parts. The next section describes together the data and the statistical models to be used. In section 3, the training dataset is explored, and used to calibrate the statistical models. In the last section, we discuss the results, conclude and give perspectives to this work.

This work has been published as a chapter in the book *Renewable Energy: Forecasting and Risk Management, Springer, Editor P. Tankov et al.* The full citation can be found in the bibliography of the manuscript (Alonzo et al., 2018).

5.2 Data and Methodology

5.2.1 Data

Observed Wind speed

In this chapter, we use observations of the wind speed at the SIRTA observation platform (Haeffelin et al., 2005). Surface wind speed at 10m height from anemometer recording is available at the 5-minutes interval. The wind speed at 100m height from Lidar recording is available at 10-minutes interval. Both data span for 5 years from 2011 to 2015. We filter observations by a sinusoidal function over a 6-hour window centered at 00h, 06h, 12h and 18h to obtain a 6-hourly observed wind speed to be compared to the NWP model outputs available at this time frequency. We find that the resulting time series are not sensitive to the filter function. We also try different filtering windows, concluding that 6-hours is the best to compare to the NWP model outputs. Due to some missing data, two final time series of 5049 filtered observations are computed (compared to 7304 if all data were available).

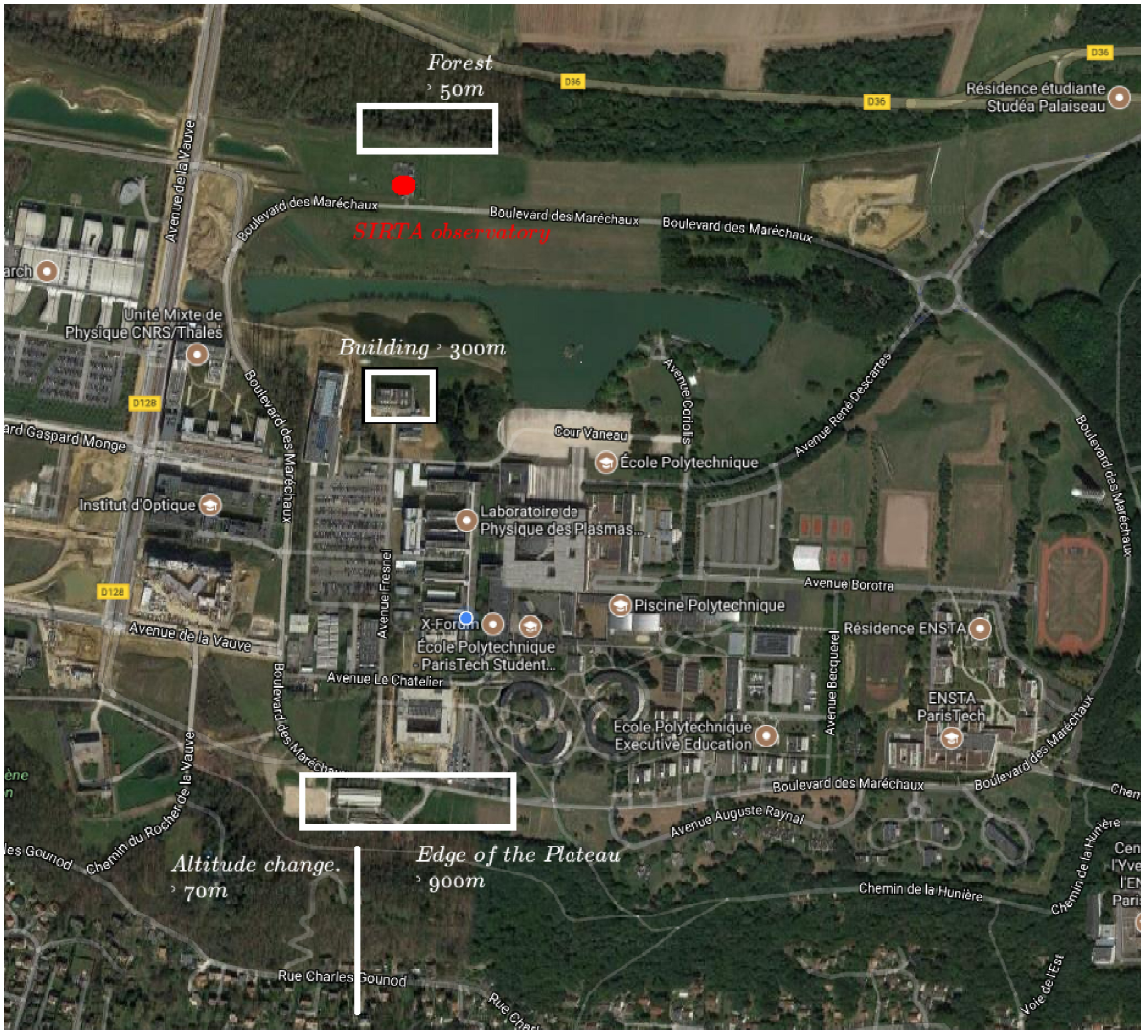

Figure 5.1: Map of the SIRTA observation platform and its surroundings.

SIRTA observatory is based 20km in the south of Paris on the Saclay plateau ($48.7°N$ and $2.2°E$). Figure 5.1 shows the SIRTA observation platform location, marked by the red point on the map, and its close environment. Regarding the relief near SIRTA, observe that a forest is located at about 50m North to the measurement devices. South, buildings can be found at about 300m from the SIRTA observatory. In the East-West axis, no close obstacle are encountered. Further South, the edge of the Saclay plateau shows a vertical drop of about 70m, from 160m on top to 90m at the bottom.

NWP model outputs - ECMWF Analyses

Variables are retrieved from ECMWF analyses at 4 points around the SIRTA platform. The spatial resolution of ECMWF analyses is of about 16km (0.125° in latitude and longitude). Topography is thus smoothed compared to the real one.

As the surface wind speed is very influenced by the terrain, the modeled surface wind speed is not necessarily close to the observed wind speed. The data spans from 01/01/2011 to 31/12/2015 at 6-hourly interval. It is sampled at each date where a filtered sampled observation is available.

The near surface wind speed at a given location can be linked to different phenomena. The large-scale circulation brings the flow to the given location explaining the slowly varying wind speed. The wind speed in altitude, the geopotential height, the vorticity, the flow divergence, sometimes the temperature can be markers of large systems like lows, fronts, storms, or high pressure systems explaining a large part of the low frequency variations of the surface wind speed (Table 5.2). At a finer scale, what is happening in the boundary layer is very important to explain the intra-day variations of the wind speed. The state and stability of the boundary layer can be derived from surface variables describing the exchanges inside the layer. Exchanges are driven mostly by temperature vertical gradient and wind shear that develop turbulent flow (Table 5.3). Thermodynamical variables like surface, skin, and dew point temperatures and surface heat fluxes can also inform on the stability of the boundary layer, as well as its height and dissipation on its state (Table 5.1). In the end, 20 output variables are retrieved from ECMWF analyses at the 4 points around the SIRTA observatory and at different pressure levels. Note that we restrict the study to local variables (at the location of measurements or in the column above). It might also be possible to take advantage from larger scale information (Zamo et al., 2016; Davy et al., 2010). The choice of taking 4 points around the SIRTA platform has the advantage of being simple and straightforward. Providing instead the explanatory variables by their interpolated value at SIRTA and the two components of their gradient does not lead to significantly different results.

Altitude (m)	Variable	Unit	Name
10m/100m	Norm of the Wind speed	$m.s^{-1}$	F
10m/100m	Zonal Wind speed	$m.s^{-1}$	U
10m/100m	Meridional Wind speed	$m.s^{-1}$	V
2m	Temperature	K	T
2m	Dew point Temperature	K	Dp
Surface	Skin temperature	K	skt
Surface	mean sea level pressure	Pa	msl
Surface	Surface pressure	Pa	sp
-	Boundary layer height	m	blh
-	Boundary layer dissipation	$J.m^{-2}$	bld
Surface	Surface latent heat flux	$J.m^{-2}$	slhf
Surface	Surface sensible heat flux	$J.m^{-2}$	sshf

Table 5.1: Surface Variables

Pressure level (hPa)	Variable	Unit	Name
1000hPa/925hPa/850hPa/700hPa/500hPa	Zonal Wind speed	$m.s^{-1}$	U
1000hPa/925hPa/850hPa/700hPa/500hPa	Meridional Wind speed	$m.s^{-1}$	V
1000hPa/925hPa/850hPa/700hPa/500hPa	Geopotential height	$m^2.s^{-2}$	Z
1000hPa/925hPa/850hPa/700hPa/500hPa	Divergence	s^{-1}	Di
1000hPa/925hPa/850hPa/700hPa/500hPa	Vorticity	s^{-1}	Vo
1000hPa/925hPa/850hPa/700hPa/500hPa	Temperature	K	T

Table 5.2: Altitude Variables

Pressure level (hPa)	Variable	Unit	Name
10m to 925hPa	Wind shear	$m.s^{-1}$	ΔF
10m to 925hPa	Temperature gradient	K	ΔT

Table 5.3: Computed Variables

5.2.2 Methodology

Our aim is to model the real observed wind speed from outputs of NWP model described above. More specifically, we use ECMWF analyses i.e the best estimate of the atmospheric state at a given time using a model and observations (Kalnay, 2003). In what follows, the observed wind speed is the target and the analysed variables are potential explanatory variables. Because of the complexity of meteorological phenomena, statistical modelling provides an appropriate framework for corrections of representativity errors and the modelling of site dependent variability. In this context, two main directions may be as usual investigated, *parametric* and *nonparametric* models.

Parametric models assume that the underlying relation between the target variable and the explanatory variables has, relatively to a certain noise, a particular analytical shape depending on some parameters, which need to be estimated through the data. Among this family of models, the linear model with a Gaussian noise is widely used, mostly thanks to its simplicity (Friedman et al., 2001). Associated to an adequate variable selection, it may be very effective.

Nonparametric models do not suppose in advance a specific relation between the variables: instead, they try to learn this complex link directly from the data itself. As such, they are very flexible, but their performance usually strongly depends on regularization parameters. The family of nonparametric models is quite large: among others, one may cite the nearest neighbors rule, the kernel rule, neural networks, support vector machines, regression trees, random forests... Regression trees, which have the advantage of being easily interpretable, show to be particularly effective when associated to a procedure allowing to reduce their variance as for the Random Forest Algorithm.

Let us describe the linear model and random forests in our context with more details. The linear model assumes a relation between the target Y_t, observed wind speed at time t, and explanatory variables $X_t^1, \ldots, X_t^d$, available from the ECMWF,

at this time t. For lightening the notation, we omit the index t in the next equation. The linear model is given by

$$Y = \beta_0 + \sum_{j=1}^{d} \beta_j X_j + \varepsilon,$$

where the β_j's are coefficients to be estimated using least-square criterion minimization method, and $\varepsilon \sim \mathcal{N}(0, \sigma^2)$ represents the noise. Among the meteorological variables $X_1, \ldots, X_d$, some of them provide more important information linked to the target than others, and some of them may be correlated. In this case, the stepwise variable selection method is useful to keep only the most important uncorrelated variables (Friedman et al., 2001). Denoting by $\beta_0, \ldots, \beta_d$ the final coefficients obtained this way (some of them are zero), the estimated wind $\hat{Y}$ is then given by

$$\hat{Y} = \beta_0 + \sum_{j=1}^{d} \beta_j X_j. \tag{5.1}$$

An alternative approach to perform variable selection and regularization is to use the Lasso method (see for instance Tibshirani (1994)), relying on minimization of the least square criterion penalized by the ℓ^1 norm of the coefficients $\beta_1, \ldots, \beta_d$. More specifically, for this model, the predicted wind speed at time t is a linear combination of all the previous variables as in equation (5.1), the coefficients $\hat{\beta}_1, \ldots, \hat{\beta}_d$ being estimated using the least square procedure, under the constraint $\sum_{j=1}^{d} |\beta_j| \leq \kappa$ for some constant $\kappa > 0$.

Regression trees are binary trees built by choosing at each step the cut minimizing the intra-node variance, over all explanatory variables $X_1, \ldots, X_d$ and all possible thresholds (denoted by S_j hereafter). More specifically, the intra-node variance, usually called deviance, is defined by

$$D(X_j, S_j) = \sum_{X_j < S_j} (Y_s - \overline{Y}^{-})^2 + \sum_{X_j \geq S_j} (Y_s - \overline{Y}^{+})^2,$$

where $\overline{Y}^{-}$ (respectively $\overline{Y}^{+}$) denotes the average of the observed wind speed in the area $\{X_j < S_j\}$ (respectively $\{X_j \geq S_j\}$). Then, the selected j_0 variable and associated threshold is given by $(X_{j_0}, S_{j_0}) = argmin_{j,S_j} D(X_j, S_j)$. The prediction is provided by the value associated to the leaf in which the observation falls.

To reduce variance and avoid over-fitting, it may be interesting to generate several bootstrap samples, fitting then a tree on every sample and averaging the predictions, which leads to the so-called Bagging procedure (Breiman, 1996). More precisely, for B bootstrap samples, the predicted wind is given by

$$\hat{Y} = \frac{1}{B} \sum_{b=1}^{B} \hat{Y}^b, \tag{5.2}$$

where $\hat{Y}^b$ denotes the wind speed predicted by the regression tree associated with the b-th bootstrap sample. To produce more diversity in the trees to be averaged, an additional random step may be introduced in the previous procedure, leading to Random Forests, where the best cut is chosen among a smaller subset of randomly chosen variables. The predicted value is the mean of the predictions of the trees, as in equation (5.2).

5.3 The relationship between analysed and observed winds

5.3.1 10m/100m wind speed variability comparison

In this section we compare the observed wind speed at 10m and 100m with the 10m and 100m wind speed output of the ECMWF analyses at the closest grid point, respectively. No significant difference can be found when using other grid points, or the mean of the four surounding locations.

Figure 5.2 shows the Probability Density Function (PDF) of the wind speed coming from ECMWF analyses and observations, and also for illustration an example of a time series of corresponding wind speeds. It appears that the 10m wind speed from ECMWF analyses displays a systematic bias by overestimating the 10m observed wind speed (Figure 5.2, a and b). The wind at 100m is comparatively well modeled in terms of variations in the time series, but also in terms of distribution (Figure 5.2, c and d). It seems that the errors mainly come from the overestimation of peaked wind speeds and the underestimation of low wind speeds (Figure 5.2, c and d). As 10m wind speed is very influenced by even low topography and surrounding obstacles, which are smoothed or not represented in ECMWF analyses, some of its variations are not well described, and even textcolorbluea bias is displayed. The effect of the topography and terrain specificity have less impact on the 100m wind speed, so that it is much better represented in ECMWF analyses.

The ability of the model to represent the observed wind speed is quantified in Table 5.4 by the deviation, the Root Mean Square Error (RMSE), and the Pearson correlation which formula are given by equations (5.3),(5.4), and (5.5) respectively.

$$\text{Deviation for the } i^{th} \text{ observation} = (y_i - x_i) \tag{5.3}$$

$$\text{RMSE} = \sqrt{\frac{\sum_{i=1}^{n}(x_i - y_i)^2}{n}} \tag{5.4}$$

$$\text{Correlation} = \frac{\sum_{i=1}^{n}(x_i - \bar{x})(y_i - \bar{y})}{\sqrt{\sum_{i=1}^{n}(x_i - \bar{x})^2}\sqrt{\sum_{i=1}^{n}(y_i - \bar{y})^2}}, \tag{5.5}$$

where x_i is the wind speed from the NWP model and y_i the observed wind speed ;

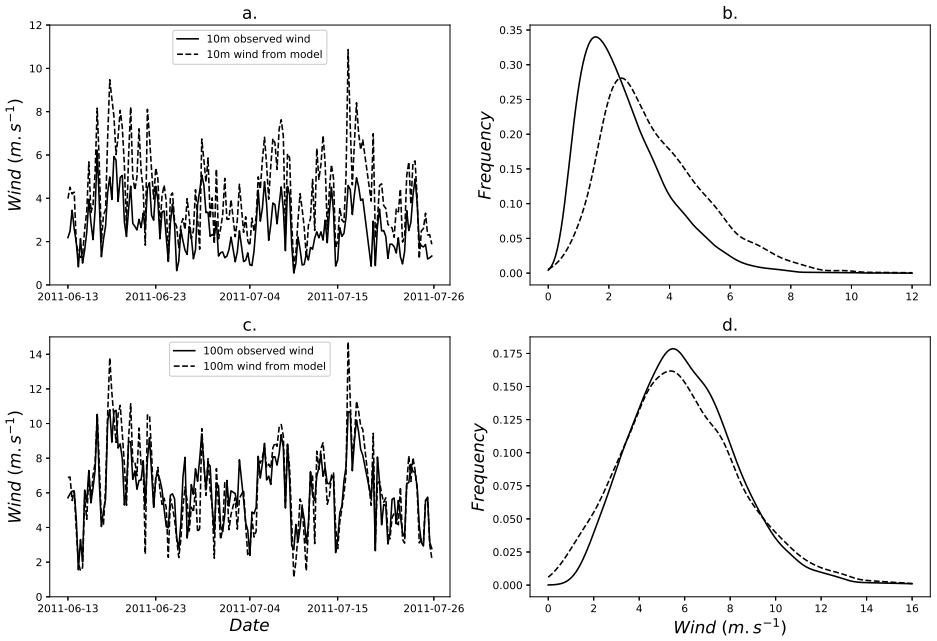

Figure 5.2: 10m (top) and 100m (bottom) wind speed time series in summer 2011 (panels a and c, respectively) and the respective probability density function estimated over the 5 years sample wind speed (panels b and d).

n is the number of samples (x_i, y_i) and $\bar{x} = \frac{1}{n}\sum_{i=1}^{n} x_i$ (the sample mean) and analogously for $\bar{y}$.

Periods	Deviation	(in $m.s^{-1}$)	RMSE	(in $m.s^{-1}$)	Correlation	
	F10	F100	F10	F100	F10	F100
2011-2015	-1.00	0.14	1.41	1.01	0.82	0.93
2011	-1.19	0.04	1.59	1.06	0.80	0.91
2012	-0.94	0.23	1.31	1.03	0.85	0.92
2013	-1.13	0.06	1.52	0.93	0.82	0.94
2014	-0.88	0.26	1.30	1.00	0.80	0.93
2015	-0.87	0.14	1.30	0.97	0.82	0.94
Winter	-0.97	0.04	1.41	0.97	0.83	0.94
Spring	-1.11	0.27	1.56	1.02	0.71	0.90
Summer	-0.92	0.33	1.31	1.04	0.80	0.91
Fall	-1.04	-0.10	1.36	1.00	0.87	0.93

Table 5.4: Mean Deviation, RMSE, and Correlation performed by ECMWF analyses for modelling the 10m and 100m wind speed.

No clear improvement coming from changes in the model or data assimilation

system used for ECMWF analyses over the years from 2011 to 2015 can be detected in Table 5.4. The correlation stays quite constant over the years for both 10m and 100m wind speeds. The Deviation and RMSE seem to decrease for the 10m wind speed but it cannot be confirmed because of the good score performed in 2012. The variations of performance may only come from changes in the predictability of the weather over Europe (Folland et al., 2012). Seasonal variations of the performance of ECMWF analyses can be seen, especially on the correlation between the observed and modeled wind speed. At both 10m and 100m, the analysed wind speed is better correlated with the observations in winter and fall than in spring and summer. In all cases, the scores shown are better for the 100m wind speed than for the 10m wind speed.

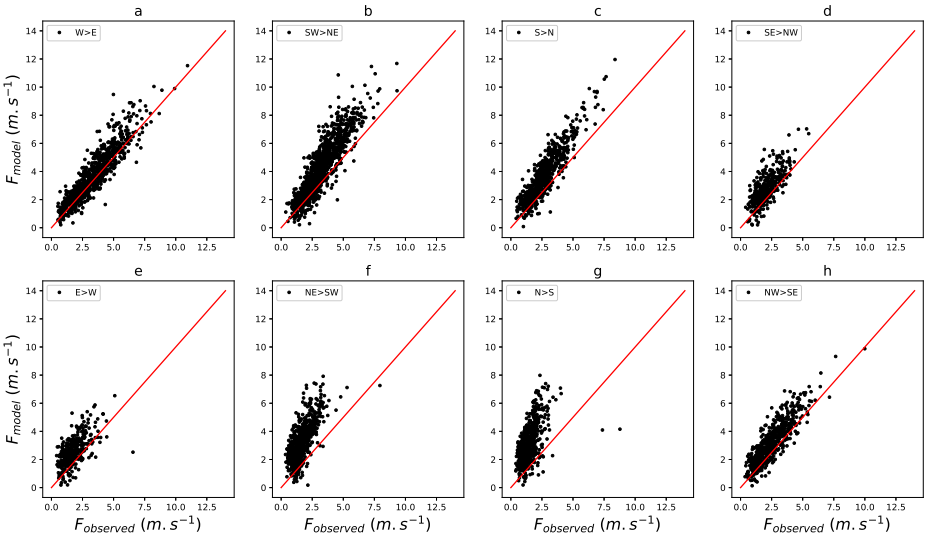

Figure 5.3: 10m wind speed from ECMWF analyses as function of the 10m observed wind speed given cardinal directions. Panels correspond to a direction modeled by ECMWF analyses ; the wind blows from a. West, b. Southwest, c. South, d. Southeast, e. East, f. Northeast, g. North, h. Northwest.

Variations of the performance of the ECMWF analyses in representing the observed wind speed are evidenced by Figure 5.3. The figure shows the 10m wind speed from ECMWF analyses as a function of the 10m observed wind speed for different directions of the analysed wind. It is obvious that the errors made by the numerical model differ regarding the direction of the wind. For instance, when the wind comes from the West (figure 5.3, a), the wind speed is well represented by the model, but for a wind coming from the North/Northeast (Figure 5.3, f and g), the model highly overestimates the 10m wind speed. It can be easily linked to the specificity of the terrain. Indeed, when a Northerly wind is recorded, it has been blocked by the forest North of the anemometer. The same happened for Southerlies with the building situated further and which influence is thus not as substantial as the forest. Figure 5.4 displays the same as Figure 5.3 but for the 100m wind speed. It seems that there

is no more dependence of the performance of the ECMWF analyses regarding the direction of the 100m wind speed ; it appears to be not significantly impacted by the surrounding forests and buildings.

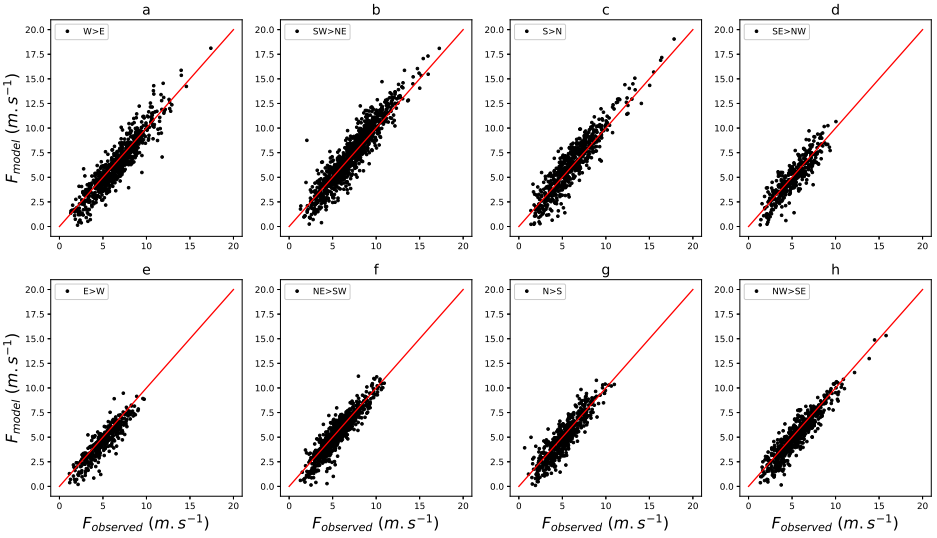

Figure 5.4: Same as Figure 5.3 but for 100m wind speed.

5.3.2 Reconstruction of the 10m/100m observed wind speed using NWP outputs

In the sequel, a k-fold cross validation is performed over 10 different periods taken within the 5-years of analyses and observation. Each time, statistical downscaling models are trained on a given period of about 4500 data points and applied over the remaining period of about 500 data points to reconstruct the 10m and 100m wind speed, so that it results in 10 reconstructions that span the 5 years of data. Table 5.5 enumerates the statistical downscaling models assessed in this study. Models differ by their types (Linear Regression and Random Forests), the explanatory variable selection, and whether a model is conditionally fitted regarding the direction of the wind speed or not. We evaluate the different statistical models in terms of RMSE and Correlation with the observed wind speed on the reconstruction period.

10m wind speed reconstruction

Figure 5.5 shows results for the reconstruction of the 10m wind speed. Each box contains the 10th reconstructed k-fold periods. First, by using only wind speed with a linear model LR_F, RMSE is reduced by about 40%, but the correlation stays constant. Adding other variables to linear model (i.e. LR_A, LR_{SW} and LR_{La}) allows to reduce the RMSE by 60%, and to significantly improve correlation from 0.80 to 0.91 between reconstructed wind speed and observed one. Using stepwise

Model type	Explanatory variables	Direction dependence	Name
Linear	F10	No	LR_F
Linear	All	No	LR_A
Linear	Stepwise	No	LR_{SW}
Linear	Lasso	No	LR_{La}
Linear	F10	Yes	LR_F^{dir}
Linear	All	Yes	LR_A^{dir}
Linear	Stepwise	Yes	LR_{SW}^{dir}
Random Forest	All	No	RF_A
Random Forest	All	Yes	RF_A^{dir}

Table 5.5: Statistical models used to downscale 10m and 100m wind speed.

selection of variables, the Lasso penalization or all variables does not change results in this case, showing that only a part of the information is useful. Using variable selection as stepwise or ℓ_1 penalization (Lasso) avoids over-fitting. Random Forests models perform slightly better than linear models without defining one given model per cardinal wind directions. Variables selected stepwise are very diverse (wind speed, large scale variables, boundary layer state drivers), while Lasso technique mainly selects wind speed and wind components, thus using redundant information. Analyzing the main variables used by Random Forests shows that this methods seems to put much weight on wind components first, highlighting the dependence of the error on the 10m wind speed regarding its direction.

By fitting a linear model in each direction (noted with '*dir*') we manually introduce a relevant information, especially for 10m wind speed (Figure 5.3). The model is however more exposed to under-fitting as the sample size of the training data in one direction can be low. Nevertheless, LR_{SW}^{dir} performs better than all other models. Indeed, stepwise choice is made for each direction so that the model is deeply adapted to each direction. This method results in a significant improvement of the RMSE and correlation scores. As expected regarding Figure 5.3 (g), the best improvement is retrieved for Northerly wind speed and is of more than $0.1m.s^{-1}$ compared to LR_{SW}. No improvement is found for easterlies, surely because the number of data is too small. Fitting a Random Forest in each direction does not improve results, maybe because the direction is already well handled by this model by using the zonal and meridional components of the wind. So one big advantage of Random Forests over linear regression is that it does not require to explore previously deeply the data for extracting appropriate and relevant features as inputs to the model. Figure 5.6 shows time series of 10m observed wind speed, NWP model wind speed output over summer period of 2011 (panel a) and the probability density function corresponding to the entire period, 2011 to 2015 (panel b). Panels c and e show respectively time series of the reconstructed 10m wind speed by LR_{SW}^{dir} (red line) and LR_{SW} (blue line), and by RF_A^{dir} (magenta line) and RF_A (cyan line). Panels d and f show the corresponding probability density functions. All statistical models allow for a good

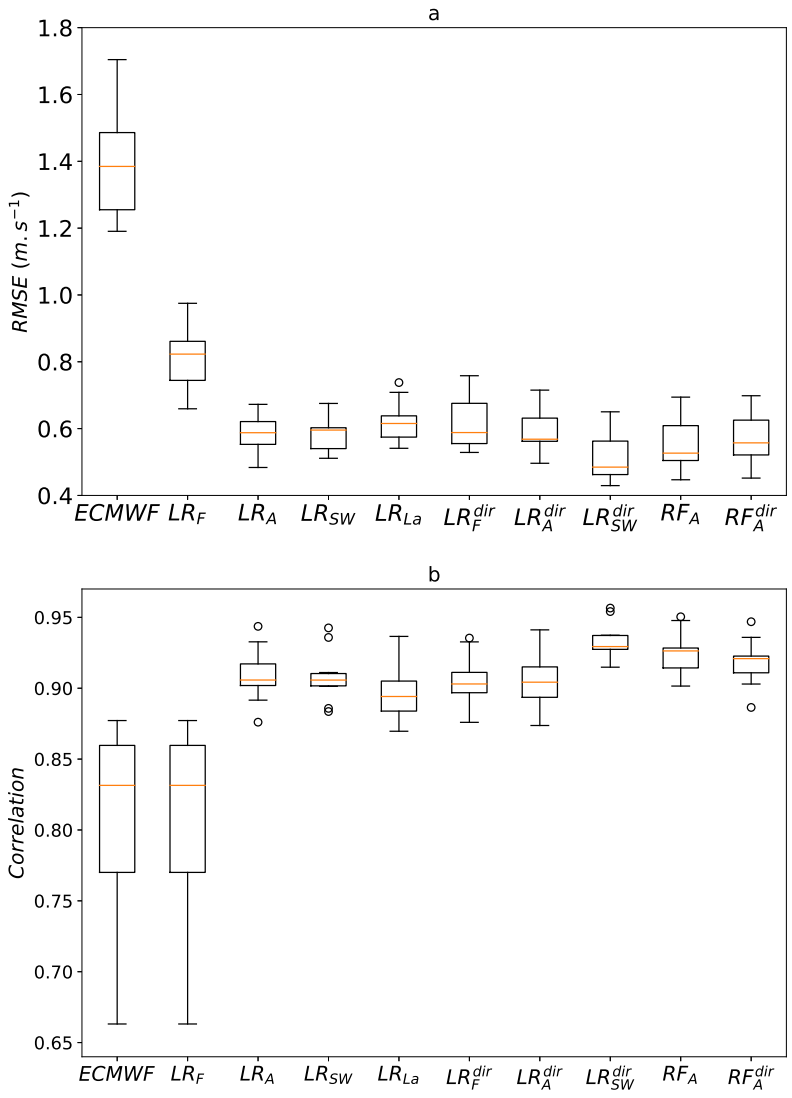

Figure 5.5: RMSE and Correlation results when reconstructing 10m wind speed with models described in Table 5.5. The first boxes stand for the ECMWF analyses 10m wind speed.

bias correction. All models underestimate the lower percentiles of the distribution and give a distribution very peaked around the mean observed wind speed. Upper percentiles are however well reconstructed. This is encouraging because this part of the distribution is important in terms of energy production. We can nevertheless expect an overestimation of the wind energy production with those models because of the underestimation of lower percentiles.

100m wind speed reconstruction

Figure 5.7 shows results of the reconstruction of 100m wind speed with statistical

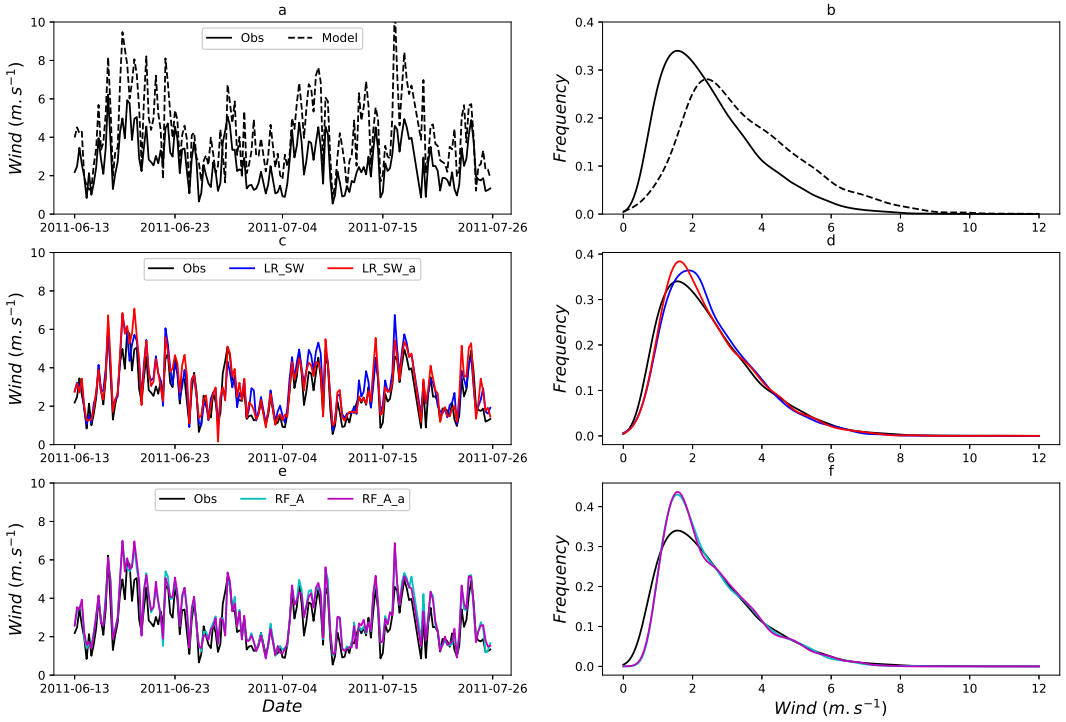

Figure 5.6: Time series (left) and PDF (right) of the observed 10m wind speed (straight black line), and 10m wind speed from ECMWF (dotted black line) (a and b), Linear models (LR_{SW} (blue) and LR_{SW}^{dir} (red)) (c and d), Random Forest models (RF_A (cyan) and RF_A^{dir} (magenta)) (e and f).

models described in Table 5.5. LR_F allows a reduction of the RMSE of about 15% corresponding to 0.14 $m.s^{-1}$ and the best model LR_{SW}^{dir} reduces the RMSE by 23% corresponding to 0.23 $m.s^{-1}$. The correlation is improved from 0.92 to 0.94. Adding the direction dependence to linear model with only 100m wind speed (i.e. LR_F^{dir}) does not improve results regarding LR_F. Indeed, the error on the 100m wind speed does not depend on the direction. Using all explanatory variables (i.e. LR_A^{dir}) leads to a strong over-fitting. Surprisingly, the linear model using stepwise selection of explanatory variables in each direction (i.e. LR_{SW}^{dir}) recovers an important information as it performs significantly better than the other. Again, its adaptability may be the cause of its good performance. In the case of 100m wind speed, the best improvement is found for easterly wind speeds. The information on the direction in Random Forests does not improve the results like for 10m wind speed reconstruction. The more important variables for Random forests and stepwise choice are mainly the 100m wind speed and components, but also the wind shear in the boundary layer. Lasso technique selects mainly 100m wind speed.

Figure 5.8 shows time series of 100m observed wind speed, NWP model wind speed output over summer period of 2011 (panel a) and the probability density function corresponding to the entire period from 2011 to 2015 (panel b). panel c

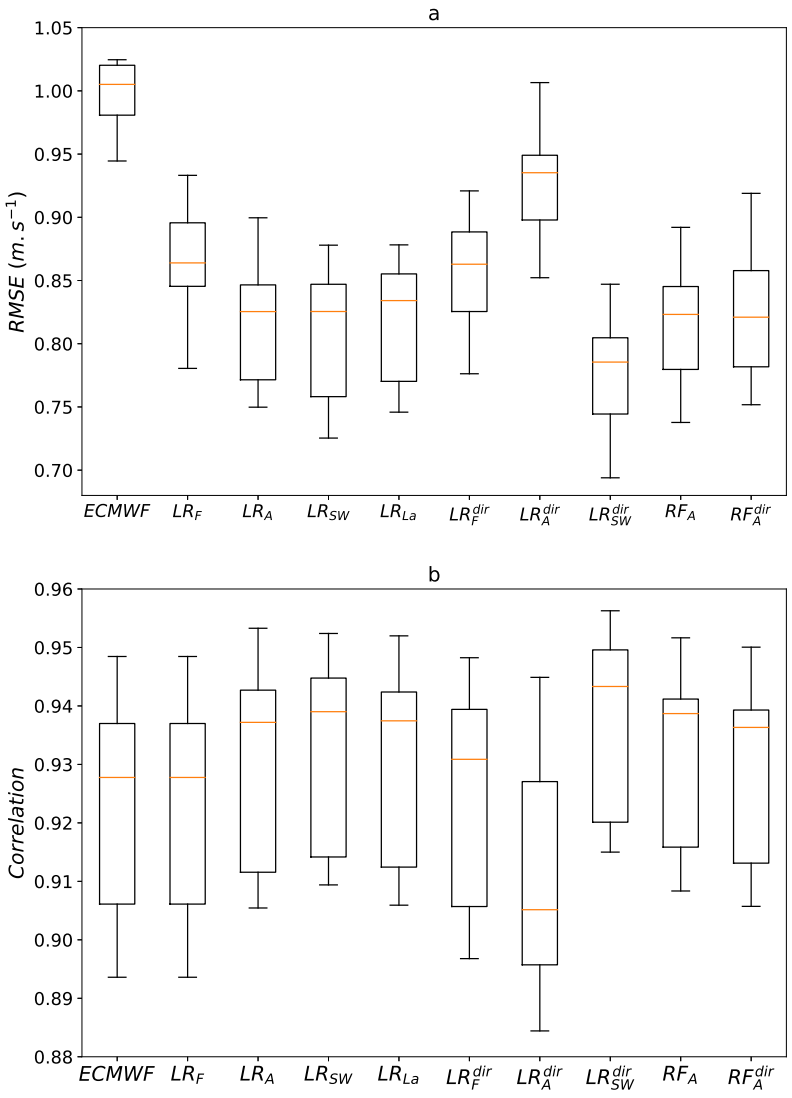

Figure 5.7: Same as Figure 5.5, for 100m wind speed.

and e show respectively time series of the reconstructed 100m wind speed by LR_{SW}^{dir} (red line) and LR_{SW} (blue line), and by RF_A^{dir} (magenta line) and RF_A (cyan line). Panels d and f show the corresponding probability density functions. Some peaked wind speeds are less overestimated after statistical downscaling. As for the 10m wind speed, statistical models underestimate the lower quantiles of the distribution and give a distribution peaked around the mean observed wind speed.

To conclude, we built different statistical models to improve the representation of the 10m and 100m wind speed of the ECMWF analyses. It has been shown that the 100m wind speed in ECMWF analyses is already well represented as it displays no systematic bias and a good correlation. Nevertheless the RMSE computed for

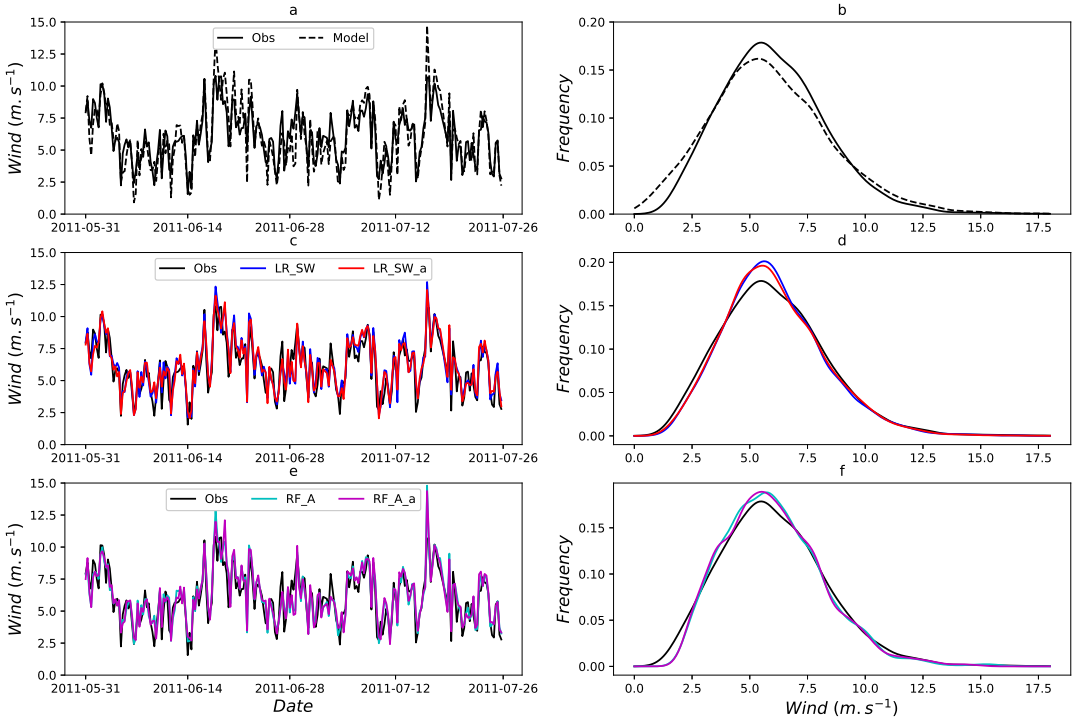

Figure 5.8: Same as Figure 5.6, for 100m wind speed.

the period 2011 to 2015 is still of 1.0 $m.s^{-1}$. Statistical models reduce the RMSE on the 10m wind speed between 40% and 65%, and between 15% and 23% for the 100m wind speed. They improve at the same time the correlation between the observed wind speed and the reconstructed one. For linear models, the variables selection is of great importance to avoid over-fitting, and an exploration step allows to improves results significantly. Random Forests give quite comparable results as the best linear models, without needing variable selection and a preliminary exploration of the data.

5.4 Summary and concluding remarks

In this chapter, we address a different issue which concerns the realism of the surface wind speed modelled by NWP model of ECMWF. This study is to be seen as a perspective to leave the scope of the perfect model approach used along the manuscript. Nonetheless, we investigate this problem using the analysis of the ECMWF (not the reanalysis) so that further work would be needed to take on the problem.

We have used statistical models to evaluate 10m and 100m wind speed at a given location from output of a NWP model. Comparison of the observed wind speed and ECMWF wind speed output at 10m and 100m within the 5 years of data show that ECMWF analyses well represent 100m wind speed. The computed RMSE is of 1.0 $m.s^{-1}$ (the mean wind speed being of 5.8 $m.s^{-1}$) and no systematic bias is

displayed. On the contrary, 10m wind speed output from ECMWF analyses displays a systematic overestimation of the observed wind speed. The computed RMSE is of 1.4 $m.s^{-1}$ (the mean wind speed being of 2.4 $m.s^{-1}$).

By applying linear regression between a certain amount of selected variables and observed wind speed, we reduce the RMSE for the 10m and 100m reconstructed wind speed up to 65% and 23%, respectively. Those good results have been achieved by fitting a linear model in 8 directions and by automatic selection of valuable variables in those directions. Building such a model thus requires a special treatment and a good knowledge of the specific site so that it cannot be systematically applied to another site. Very interestingly, using Random Forests to reconstruct 10m and 100m wind speed gives comparable results as the best linear models (about 57% and 20%, respectively), while their performance is not sensitive to any preparation of the data. Computing time is a bit longer than simple linear models, but it is quite similar when a linear model is fitted in each direction.

In this study, we choose to use only local informations coming from NWP outputs. Additive valuable informations may be retrieved from larger-scale NWP outputs such as large-scale horizontal gradients of the pressure. However, the discussion on the added value of any other NWP outputs is site dependent, and is already part of research matters. For instance, it has been proved that large scale circulation patterns give valuable information at timescales up to months in some regions of France (Alonzo et al., 2017).

Conclusion

Overview and discussion of the main results

This work brings important insights on the possibility to predict wind energy resource and production in France at the seasonal scale, with better performance than the climatology, which is the current reference. Interannual variations of the wind energy resource and production can be attributed to large-scale atmospheric circulation variability (Krakauer and Cohan, 2017; Torralba et al., 2017; Clark et al., 2017), which has recently been proved to be relatively well forecasted by NWP models (Scaife et al., 2014; Dunstone et al., 2016; Smith et al., 2016). We describe the statistical relationship between the large-scale atmospheric circulation and the surface wind speed in France, and show that it explains an important part of the interannual variability of the wind energy resource and production at the seasonal scale, as well as of the risk of imbalance between consumption and production. To our knowledge, the modelling of such relationship between large scale atmospheric patterns and surface wind speed has not previously been explored.

The thesis is structured into 4 studies. Three of them are within the framework of seasonal forecasts of the wind energy resource and production, and the associated risk of imbalance. These three studies follow a perfect model approach, taking ERA-I reanalysis wind speed as a reference. By contrast, the last study deals with the realism of the surface wind speed modelled by the Numerical Weather Prediction model of the European Centre of Medium-range Weather Forecasts, thus giving a perspective to leave the scope of the perfect model approach.

In the first two studies, two types of modelling are proposed :

- The first is parametric and assumes that the local distribution of the daily wind speed is well approximated by a Weibull distribution. The model reconstructs the parameters of the Weibull distribution from the knowledge of the large scale state of the atmosphere.

- The second is referred to as a non-parametric model and is anchored in the context of probabilistic forecasting. The relationship between large-scale circulation patterns and surface wind speed is estimated directly from daily data by conditional kernel density estimation.

The two models exhibit spatial and seasonal variations of performance relative to the climatology. They both show their best performance in the North of France, in winter and fall. It can be attributed to the more important impact of the large-scale circulation patterns on the surface wind speed, in this region and during those seasons. It seems to be a fairly robust result, as it can be supported by physical interpretation, and by other studies for different regions in Europe (Lau, 1988; Rogers, 1997; Trigo et al., 2002).

The first parametric model displays better results than climatology in reconstructing the monthly and seasonal distribution of the surface wind speed, but also in estimating the capacity factor when the parameters are chosen to represent well the tail of the distribution. The main limitation of this type of model comes from its parametric character. Indeed, imposing the Weibull distribution is an important source of error. Applying such model to seasonal forecasts shows that the information on the large-scale circulation carried by the ensemble mean is lost after at most 1 month and a sharp increase of the error appears after 15 days.

The second non-parametric model is shown to be better calibrated than the climatology, mainly because the climatology does not take into account long term trends of the surface wind speed. It is also shown to be more accurate compared to climatology. The accuracy of the probabilistic model applied to the raw ensemble seasonal forecasts tends to the climatological accuracy after at most one month. However, using post-processing method (EMOS) to recalibrate and sharpen the ensemble leads to further improvements. In a significant number of cases, the model can be calibrated and sharper than the climatology even at the seasonal horizon, in a large region North of France and mainly for forecasts starting in fall and early winter.

This work not only addressees the forecast of the wind energy resource and production, but also proposes a model aimed at forecasting the risk of imbalance between production and consumption in France. This issue is becoming more and more important as penetration of intermittent sources of production grows. In addition, in France the consumption is highly driven by temperature changes. The

risk associated with meteorological factors is thus very important. In chapter 4, we define two different risk indicators :

- The first one measures the probability that consumption and production deviate from their climatological mean. We build a model able to reconstruct the joint PDF of the national consumption daily peak and national wind energy production in winter and fall. The integration of the two-dimensional PDF over quadrants defined by climatological means of consumption and production allows to compute the probability of imbalance for a given season. The model is able to accurately predict more than 75% of the deviations from the climatology in winter. The reconstructed joint PDFs are often very similar to the real estimated joint PDFs even though they are built on the hypothesis of conditional independence between consumption and production.

- The second one measures the extreme values (95^{th} percentile) of the difference between consumption and production and is estimated by quantile regression. The predicted risk indicator of extreme situations of imbalance is reliable and not necessarily related to the first risk indicator. It is shown that extreme risks can be as much as 25% above climatological percentile and that the persistence of such events can reach almost 30 days.

The analysis of the explanatory value of the first principal components, namely the seasonal pattern, NAO and SCA patterns show that in winter, risks and extreme risks of imbalance can be clearly attributed to NAO and SCA patterns, and to a more or less marked seasonal transition. In fall, the seasonal pattern seems to play an important role in the appearance of extreme risks.

Refinement of the surface wind speed represented by NWP models would allow to get out of the perfect model approach by better representing surface wind speed at location of specific wind farms for instance. The last chapter is dedicated to the downscaling of the wind speed at a specific observation site in France. It is shown that ECMWF analysis (used as the initial state of the model) better represents the wind speed at 100m than 10m height which displays a systematic bias, mainly due to the strong influence of close environment at this altitude. Using both linear regressions and random forests allows to significantly reduce the error of the numerically modelled 10m and 100m surface wind speed, respectively by about 60% at 10m and 20% at 100m. Random forest gives the same results as linear regression without an a-priori knowledge of the specificity of the terrain, and of the explanatory value of the predictors. Ongoing work highlights that it is also more robust for generalization to a larger spatial scale.

Limitations & perspectives

By modelling the link between the large scale atmospheric circulation and surface wind speed, this work gives promising results on the predictability of wind energy resource, production and the associated risk at the seasonal scale. The results can nevertheless be criticized at some points, and more positively raise very interesting perspectives.

Atmospheric variability and seasonal predictability

First, the basis of this work is to use the large scale atmospheric circulation patterns deduced from the Principal Component Analysis (PCA) of the Z500 geopotential height field, to explain the surface wind speed at the scale of the season. The choice of Z500 variable is common in meteorology to represent large scale atmospheric circulation, and the addition of Mean Sea Level Pressure (MSLP) did not show any improvement, maybe because it carries redundant information compared to Z500 (Chapter 2). However, other variables could be tested, and in particular the Sea Surface Temperature (SST). Indeed, SST is related to the ocean circulation variability in interaction with the atmosphere. This variable should carry supplementary information on the large scale atmospheric circulation, and should also highlight more persistent patterns than a variable only tied to the atmospheric circulation such as Z500.

PCA can also be performed separately for each season. Indeed, some modes of variability may have no influence on a given season, while other modes can be very important. It would also be interesting to perform the PCA over the entire Northern hemisphere in order to take into account some of the Pacific oscillations that could also influence the European climate. One could imagine a "smart" selection of PCs depending on the ability of NWP seasonal ensemble forecasts to accurately predict their state and variability at the seasonal scale. The use of recalibrated multi-ensembles could also improve the accuracy of the seasonal forecasts, as shown by Scaife et al. (2014).

Representation of wind energy resource and production

In the last chapter, we show that downscaling wind speed from NWP model grid to an observation site allows to reduce significantly the error and improve the correlation between observed and modelled surface wind speed. Downscaling surface wind speed at locations where wind farms are installed would allow for a better spatial representation of the wind energy resource and production in France. The new reanalysis product from ECMWF (ERA-5) could be well suited for such refinement of the proposed models as it gives access to much higher spatial resolution than ERA-Interim, and spans a longer period. Moreover, ERA-5 gives access to 100m

wind speed which has been shown to be quite well represented by ECMWF NWP model, in chapter 5, and corresponds to the hub height of a wind turbine.

From the French to the European grid system

Last but not least, the electricity grid does not only extend at the French scale, but should be seen at a European level. The inadequacy of the transmission grid is a major limitation of the penetration of wind power, nowadays and more importantly in the future (Hammons, 2008; Becker et al., 2014). The exchange of electricity between the European countries is going to be more and more important as the intermittent means of production continue to increase. Therefore, the seasonal risk of imbalance between production and consumption in France is related to the production of its neighbours. For instance, France can import solar/wind energy from Spain, wind energy from Portugal, Germany, Denmark... The large scale oscillation patterns, such as NAO, have different influence in Southern and Northern Europe, so that we can expect difference in wind energy production from Northern countries like Denmark, Norway and Southern countries like Portugal. Such spatial difference of the influence of NAO is also found for other intermittent means of production like solar and hydropower (François, 2016). A first look at German onshore wind energy production does not show a possible complementarity as both productions are highly correlated. Nevertheless, offshore wind production in the North of Germany has not yet been modelled and this work is to be continued. The difference with French production may indeed be highlighted in this region. More generally, the adaptation of the method to compute production would be needed for offshore wind farms. The consumption in different countries does not have the same dependence in temperature as in France, and may be driven more importantly by different electricity uses. This should also be taken into account by the model eventually.

List of Figures

List of Tables

Bibliography

Alessandrini, S., Monache, L. D., Sperati, S., and Nissen, J. (2015). A novel application of an analog ensemble for short-term wind power forecasting. *Renewable Energy*, 76:768–781. 10

Alonzo, B., Plougonven, R., Mougeot, M., Fischer, A., Dupré, A., and Drobinski, P. (2018). *From numerical Weather Prediction outputs to accurate local surface Wind speed: statistical modelling and forecasts.* Springer. 93

Alonzo, B., Ringkjob, H. K., Jourdier, B., Drobinski, P., Plougonven, R., and Tankov, P. (2017). Modelling the variability of the wind energy resource on monthly and seasonal timescales. *Renewable energy*, 113:1434–1446. 27, 107

Anderson, T. (1962). On the distribution of two sample Cramer Von Mises criterion. *The Annals of Mathematical Statistics*, 33:1148–1159. 31

Azad, H. B., Mekhilef, S., and Ganapathy, V. G. (2014). Long-term wind speed forecasting and general pattern recognition using neural networks. *IEEE Transaction on Sustainable Energy*, 5:546–553. 11, 12

Barbounis, T. G., Theocharis, J. B., Alexiadis, M. C., and Dokopoulos, P. S. (2006). Long-term wind speed and power forecasting using local recurrent neural network models. *IEEE Transaction on Energy Conversion*, 21:273–284. 9

Becker, S., Rodriguez, R., Andresen, G., Schramm, S., and Greiner, M. (2014). Transmission grid extensions during the build-up of a fully renewable pan-European electricity supply. *Energy*, 64:404–418. 113

Bentzien, S. and Friederichs, P. (2014). Decomposition and graphical portrayal of the quantile score. *Q. J. R. Meteorol. Soc.*, 140:1924–1934. 75

Bilgili, M., Sahin, B., and Yasar, A. (2007). Application of artificial neural networks for the wind speed prediction of target station using reference stations data. *Renewable Energy*, 32:2350–2360. 11

Bossavy, A., Girard, R., and Kariniotakis, G. (2013). Forecasting ramps of wind power production with numerical weather prediction ensembles. *Wind Energy, Wiley*, 16:51–63. 9

Brayshaw, D. J., Dent, C., and Zachary, S. (2012). Wind generation's contribution to supporting peak electricity demand - meteorological insights. *Proceedings of the Institution of Mechanical Engineers, Part O: Journal of Risk and Reliability*, 226:44–50. 68

Breiman, L. (1996). Bagging predictors. In *Machine Learning*, pages 123–140. 97

Brossier, C. L. and Drobinski, P. (2009). Numerical high-resolution air-sea coupling over the Gulf of Lions during two Tramontane/Mistral events. *Journal of Geophysical Reseasrch*, 114. 55

Bueh, C. and Nakamura, H. (2007). Scandinavian pattern and its climatic impact. *Q. J. R. Meteorol. Soc.*, 133:2117–2131. 86

Burtin, A. and Silva, V. (2015). Technical and economic analysis of the european electricity system with 60% RES. 10, 11

Candille, G., Cote, C., Houtekamer, P., and Pellerin, G. (2007). Verification of an ensemble prediction system against observations. *Monthly Weather Review*, 135:2688–2699. 53

Candille, G. and Talagrand, O. (2005). Evaluation of probabilistic prediction systems for a scalar variable. *Q. J. R. Meteorol. Soc.*, 131:2131–2150. 53

Carney, M. and Cunningham, P. (2006). Evaluating density forecasting models. *Trinity College Dublin, Department of Computer Science*. 52

Carpinone, A., Giorgio, M., Langella, R., and Testa, A. (2015). Markov chain modeling for very-short-term wind power forecasting. *Electric Power Systems Research*, 122:152–158. 9

Casanueva, A., Rodriguez-Puebla, C., Frias, M. D., and Gonzalez-Reviriego, N. (2014). Variability of extreme precipitation over Europe and its relationships with teleconnection patterns. *Hydrol. Earth Syst. Sci.*, 18:709–725. 13

Cassola, F. and Burlando, M. (2012). "wind speed and wind energy forecast through Kalman filtering of Numerical Weather Prediction model output". *Applied Energy*, 99:154–166. 92

Cassou, C. (2008). Intraseasonal interaction between Madden-Julian Oscillation and the North Atlantic Oscillation. *Nature*, 455:523–597. 7, 13

Cassou, C., Terray, L., Hurrel, J. W., and Deser, C. (2004). North atlantic winter climate regimes: Spatial asymmetry, stationarity with time, and oceanic forcing. *Journal of Climate*, 17:1055–1068. 21

Christensen, J. H., Boberg, F., Christensen, O. B., and Lucas-Picher, P. (2008). On the need for bias correction of regional climate change projections of temperature and precipitation. *Geophysical Research Letters*, 35. 41

Clark, R. T., Bett, P. E., Thornton, H. E., and Scaife, A. A. (2017). Skilful seasonal predictions for the European energy industry. *Environ. Res. Lett.*, 12:1–9. 14, 109

Cohen, A. (1965). Maximum Likelihood Estimation in the Weibull distribution based on complete and censored samples. *Technometrics*, 7:579–588. 30

Coy, L. and Pawson, S. (2015). The major Stratospheric Sudden Warming of January 2013: Analyses and forecasts in the GEOS-5 data assimilation system. *Monthly Weather Review*, 143:491–510. 62

Cradden, L. C. and McDermott, F. (2018). A weather regime characterisation of Irish wind generation and electricity demand in winters 2009-11. *Environmental Research Letters*, 13(5):054022. 68

Cui, M., Ke, D., Gan, D., and Sun, Y. (2015). Statistical scenarios forecasting method for wind power ramp events using modified neural networks. *J. Mod. Power Syst. Clean Energy*, 3:371–380. 9

Davies, J. R., Rowell, D. P., and Folland, C. K. (1997). North Atlantic and European seasonal predictability using an ensemble of multidecadal atmospheric GCM simulations. *International Journal of Climatology*, 17:1263–1284. 13

Davy, R. J., Woods, M. J., Russell, C. J., and Coppin, P. A. (2010). Statistical downscaling of wind variability from meteorological fields. *Boundary Layer Meteorol*, 175:161–175. 93, 95

Dee, D. P., Uppala, S. M., Simmons, A. J., Berrisford, P., Poli, P., Kobayashi, S., Andrae, U., Balmaseda, M. A., Balsamo, G., Bauer, P., Bechtold, P., Beljaars, A. C. M., van de Berg, L., Bidlot, J., Bormann, N., Delsol, C., Dragani, R., Fuentes, M., Geer, A. J., Haimberger, L., Healy, S. B., Hersbach, H., Hlm, E. V., Isaksena, L., Kllberg, P., Khler, M., Matricardi, M., McNally, A. P., Monge-Sanz, B. M., Morcrette, J.-J., Park, B.-K., Peubey, C., de Rosnay, P., Tavolato, C., Thpaut, J.-N., and Vitart, F. (2011). The ERA-interim reanalysis: configuration and performance of the data assimilation system. *Q.J.R. Meteorol. Soc.*, 137:553–597. 10, 16, 27, 50

Delacroix, M., Hardle, W., and Hristachea, M. (2003). Efficient estimation in conditional single-index regression. *Journal of Multivariate Analysis*, 86:213–226. 51

Devis, A., van Lipzig, N., and Demuzere, M. (2013). A new statistical approach to downscale wind speed distribution at a site in northern Europe. *Journal of geophysical research : Atmospheres*, 118:2272–2283. 93

Dowell, J. and Pinson, P. (2016). Very-short-term wind power probabilistic forecasts by sparse vector autoregression. *IEEE Transactions on Smart Grid*, 7:763–770. 9

Drobinski, P., Alonzo, B., Basdevant, C., Cocquerez, P., Doerenbecher, A., Fourri, N., and Nure, M. (2017). Lagrangian dynamics of the mistral during the Hymex SOP2. *Journal of Geophysical Research: Atmospheres*, 122:1387–1402. 55

Drobinski, P., Coulais, C., and Jourdier, B. (2015). Surface wind-speed statistics modelling: Alternatives to the Weibull distribution and performance evaluation. *Boundary-Layer Meteorol*, 157:97–123. 7, 17, 30, 40, 48

Dubus, L. (2012). Monthly and seasonal forecasts in the French power. *ECMWF Seminar on Seasonal Prediction*, 12:131–142. 14

Dunstone, N., Smith, D., Scaife, A., Hermanson, L., Eade, R., Robinson, N., Andrews, M., and Knight, J. (2016). Skilful predictions of the winter North Atlantic Oscillation one year ahead. *Nature Geoscience*, 9(11):809. 13, 109

Earl, N., Dorling, S., Hewston, R., and von Glasow, R. (2013). 1980-2010 variability in u.k. surface wind climate. *Journal of Climate*, 26(4):1172–1191. 7, 48

Elia, R. D., Laprise, R., and Denis, B. (2002). Forecasting skill limits of nested, limited-area models: a perfect-model approach. *Monthly Weather Review*, 130:2006–2023. 17, 26, 28, 92

ENTSOE (2016). Winter outlook report - 2016. 11, 12

EWEA (2016). Wind in power: 2015 european statistics. 2

Fasano, G. and Franceschini, A. (1986). A multidimensional version of the Kolmogorov-Smirnov test. *Monthly Notices of the Royal Astronomical Society*, 225:155–170. 76, 88

Folland, C. K., Knight, J., Linderholm, H. W., Fereday, D., Ineson, S., and Hurrell, J. W. (2008). The summer North Atlantic Oscillation: Past, present, and future. *Journal of Climate*, 22:1082–1103. 13

Folland, C. K., Scaife, A. A., Lindesay, J., and Stephenson, D. B. (2012). "How potentially predictable is Northern European winter climate a season ahead?". *Int. J. Climatol.*, 32:801–818. 100

Foster, D. P. and Vohra, R. V. (1998). Asymptotic calibration. *Biometrika,* ,, 85:379–390. 52

François, B. (2016). Influence of winter North-Atlantic Oscillation on climate-related energy penetration in Europe. *Renewable Energy*, 99:602–613. 113

Friedman, J., Hastie, T., and Tibshirani, R. (2001). *The elements of statistical learning*, volume 1. Springer series in statistics New York. 96, 97

Giorgi, M. G. D., Ficarella, A., and Tarantino, M. (2011). "assessment of the benefits of Numerical Weather Predictions in wind power forecasting based on statistical methods". *Energy*, 36:3968–3978. 9

Glahn, H. R. and Lowry, D. A. (1972). "The use of Model Output Statistics (MOS) in objective weather forecasting". *Journal of Applied Meteorology*, 11:1203–1211. 92

Gneiting, T., Balabdaoui, F., and Raftery, A. E. (2007). Probabilistic forecasts, calibration and sharpness. *J. R. Statist. Soc. B*, 69:243–268. 52

Gneiting, T., Raftery, A. E., III, A. H. W., and Goldman, T. (2005). Calibrated probabilistic forecasting using Ensemble Model Output Statistics and minimum CRPS estimation. *Monthly Weather Review*, 133:1098–1118. 59

Gomes, P. and Castro, R. (2012). Wind speed and wind speed forecasting using statistical models: Autoregressive Moving Average (ARMA) and Artificial Neural Networks (ANN). *International Journal of Sustainable Energy Development (IJSED)*, 1:41–50. 9

Guo, Z., Zhao, W., H.Lu, and J.Wang (2012). Multi step forecasting for wind speed using a modified EMD based Artificial Neural Network model. *Renewable Energy*, 37:241–249. 11

GWEC (2016). Global wind statistics - 2017. 2

Haeffelin, M., Barthes, L., Bock, O., Boitel, C., Bony, S., Bouniol, D., Chepfer, H., Chiriaco, M., Cuesta, J., Delanoe, J., Drobinski, P., Dufresne, J.-L., Flamant, C., , Grall, M., Hodzic, A., Hourdin, F., Lapouge, F., Lemaitre, Y., Mathieu, A., Morille, Y., Naud, C., Noel, V., OHirok, W., Pelon, J., Pietras, C., Protat, A., Romand, B., Scialom, G., and Vautard, R. (2005). "SIRTA, a ground-based atmospheric observatory for cloud and aerosol research". *Annales Geophysicae*, 23:1–23. 93

Hall, R., Erdélyi, R., Hanna, E., Jones, J. M., and , A. A. S. (2015). Drivers of north atlantic polar front jet stream variability. *International Journal of Climatology*, 35(8):1697–1720. 6

Hamill, T. M. (2000). Interpretation of rank histograms for verifying ensemble forecasts. *Monthly Weather Review*, 129:550–560. 52

Hammons, T. (2008). Integrating renewable energy sources into European grids. *Electrical Power and Energy Systems*, 30:462–475. 113

Hernández, C. V., Telsnig, T., and Pradas, A. V. (2017). Market, technology and regulatory aspects of wind energy. 7

Horvath, K., Bajic, A., and Ivatek-Sahdan, S. (2011). "dynamical Downscaling of Wind Speed in Complex Terrain Prone to Bora-Type Flows". *Journal of applied Meteorology and climatology*, 50:1676–1691. 9

Howard, T. and Clark, P. (2007). "Correction and downscaling of NWP wind speed forecasts". *Meteorol. Appl.*, 14:105–116. 92

Johansson, A. (2006). Prediction skill of the NAO and PNA from daily to seasonal time scales. *Journal of Climate*, 20:1957–1975. 13

Jourdier, B. (2015). *Wind resource in metropolitan France: assessment methods, variability and trends*. PhD thesis, Ecole Polytechnique. 17, 32, 56, 86, 92

Jourdier, B. and Drobinski, P. (2017). Errors in wind resource and energy yield assessments based on the Weibull distribution. *Ann. Geophys.*, 35:691–700. 7, 30, 38, 48

Jung, J. and Broadwater, R. P. (2014). "Current status and future advances for wind speed and power forecasting". *Renewable and Sustainable Energy Reviews*, 31:762–777. 93

Justus, C., Hargreaves, W., and A.Yalcin (1976). Nationwide assessment of potential output from wind-powered generators. *Journal of Applied Meteorology*, 15:673–678. 29

Kalnay, E. (2003). *Atmospheric Modeling, Data Assimilation and Predictability*. Cambridge University Press. 12, 96

Kariniotakis, G. and Mayer, D. (2004). The anemos project : Next generation forecasting of wind power. *Proceedings, International technical Conference DEWEK 2004, 7th German Wind Energy Conference*. 9

Knuppel, M. (2015). Evaluating the calibration of multi-step-ahead density forecasts using raw moments. *Journal of Business & Economic Statistics,*, 33:270–281. 52, 53

Koenker, R. and Hallock, K. F. (2001). Quantile regression. *Journal of Economic Perspectives*, 15:143–156. 75

Krakauer, N. Y. and Cohan, D. S. (2017). Interannual variability and seasonal predictability of wind and solar resources. *Resources*, 6:1–14. 14, 109

Kubik, M. L., Coker, P. J., and Hunt, C. (2011). Using meteorological wind data to estimate turbine generation output: a sensitivity analysis. In *Proceedings of Renewable energy congress*, pages 4074–4081. 7, 92

Lau, N. (1988). Variability of the observed midlatitude storm tracks in relation to low-frequency changes in the circulation pattern. *Journal of Atmospheric Sciences*, 45:2718–2743. 6, 13, 110

Leahy, P. and Foley, A. (2012). "Wind generation output during cold weather-driven electricity demand peaks in Ireland". *Energy*, 39(1):48 – 53. Sustainable Energy and Environmental Protection 2010. 68

Lun, I. and Lam, J. (2000). A study of Weibull parameters using long-term wind observation. *Renewable Energy*, 20:145–153. 29

Luo, J., Masson, S., and Behera, S. (2005). Seasonal climate predictability in a coupled OAGCM using a different approach for ensemble forecasts. *Climate Research*, 18:4474–4497. 7, 13

Mann, H. and Whitney, D. (1947). On a test of whether one of two random variables is stochastically larger than the other. *The Annals of Mathematical Statistics*, 18:50–60. 61

Manwell, J., McGowan, J., , and Rogers, A. (2009). *Wind energy explained. Theory, Design and Application*. Wiley. 29

Marti, I., Kariniotakis, G., Pinson, P., Sanchez, I., Nielsen, T., Madsen, H., Giebel, G., Usaola, J., Palomares, A., Brownsword, R., Tambke, J., Focken, U., Lange, M., Sideratos, G., and Descombes, G. (2006). Evaluation of advanced wind power forecasting models results of the anemos project. *Proceedings of the European Wind Energy Conference, EWEC 2006*. 9

Michelangeli, P., Vrac, M., and Loukos, H. (2009). Probabilistic downscaling approaches: Application to wind cumulative distribution functions. *Geophysical Research Letters*, 36. 41

Michelangeli, P. A., Vautard, R., and Legras, B. (1995). Weather regimes: Recurrence and quasi stationarity. *Journal of Atmospheric Sciences*, 52:1237–1256. 6, 17, 20

Mohandes, M., Rehmanb, S., and Rahmand, S. (2011). "estimation of wind speed profile using adaptive neuro-fuzzy inference system (ANFIS)". *Applied Energy*, 88:4024–4032. 92

Mohrlen, C. and Bessa, R. (2018). Understanding uncertainty: the difficult move from a deterministic to a probabilistic world. In *17th Wind Integration Workshop*. 10

Möhrlen, C., Lerner, J., Messner, J. W., Browell, J., Tuohy, A., Zack, J., Collier, C., and Giebel, G. (2018). Iea wind recommended practices for the implementation

of wind power forecasting solutions part 2 and 3 : designing and executing forecasting benchmarks and evaluation of forecast solutions. In *17th Wind Integration Workshop*. 9

Moller, A., Lenkoski, A., and Thorarinsdottir, T. L. (2013). Multivariate probabilistic forecasting using Bayesian model averaging and copulas. *Q. J. R. Meteorol. Soc.*, 139:982–991. 59

Molteni, F., Stockdale, T., Balmaseda, M., Balsamo, G., Buizza, R., Ferranti, L., Magnusson, L., Mogensen, K., Palmer, T., and Vitart, F. (2011). The new ECMWF seasonal forecast system (System 4). Technical report, ECMWF Technical Memorandum. 28, 41

More, A. and Deo, M. (2003). Forecasting wind with neural networks. *Marine Structures*, 16:35–49. 11

Najac, J., Boe, J., and Terray, L. (2009). A multi model ensemble approach for assessment of climate change impact on surface winds in France. *Climate Dynamics*, 32:615–634. 10

NationalGrid (2016). Winter outlook report 2016/2017. 10

N.G. Mortensen, L. Landberg, I. T. and Petersen, E. (1998). Wind atlas analysis and application program (WAsP), vol.1: Getting started. vol.2: Users guide. Technical report, Riso National Laboratory. 30

Omrani, H., Drobinski, P., and Dubos, T. (2011). Investigation of indiscriminate nudging and predictability in a nested quasi-geostrophic model. *Q. J. R. Meteorol. Soc.*, 138:158–169. 92

Omrani, H., Drobinski, P., and Dubos, T. (2013). Optimal nudging strategies in regional climate modelling: investigation in a Big-Brother experiment over the European and Mediterranean regions. *Clim Dyn*, 41:2451–2470. 92

Owen, J. and Palmer, T. (1987). The impact of El Nino on an ensemble of extended range forecasts. *Monthly Weather Review*, 115:2103–2117. 13

Pinson, P. and Kariniotakis, G. (2009). Conditional prediction intervals of wind power generation. *IEEE Transaction On Power Systems*, 25:1845–1856. 50

Pinson, P., McSharry, P., and Madsen, H. (2009a). Reliability diagrams for non-parametric density forecasts of continuous variables: Accounting for serial correlation. *Q. J. R. Meteorol. Soc.*, 136:77–90. 52

Pinson, P., McSharry, P., and Madsen, H. (2010). Reliability diagrams for non-parametric density forecasts of continuous variables: Accounting for serial correlation. *Quarterly Journal of the Royal Meteorological Society*, 136(646):77–90. 63

Pinson, P., Nielsen, H., Madsen, H., and Kariniotakis, G. (2009b). Skill forecasting from ensemble predictions of wind power. *Applied Energy*, 86(7):1326 – 1334. 10

Pinson, P., Nielsen, H. A., Moller, J. K., Madsen, H., and Kariniotakis, G. N. (2007). Non-parametric probabilistic forecasts of wind power: required properties and evaluation. *Wind Energy*, 10(6):497–516. 10

Plaut, G. and Simonnet, E. (2001). Large-scale circulation classification, weather regimes, and local climate over France, the Alps, and Western Europe. *Climate Research*, 17:303–324. 6, 20

Potter, C. W. and Negnevitsky, M. (2006). Very Short-Term Wind Forecasting for Tasmanian Power Generation. *IEEE Transactions on Power Systems*, 21:965–972. 9

Powell, M. J. D. (1964). An efficient method for finding the minimum of a function of several variables without calculating derivatives. *The Computer Journal*, 7:155–162. 60

Prior, J. and Kendon, M. (2011). The UK winter of 2009/2010 compared with severe winters of the last 100 years. *Weather*, 66:4–10. 68

Pryor, S., Nielsen, M., Barthelme, R., and J.Mann (2004). Can satellite sampling of offshore wind speeds realistically represent wind speed distributions? Part II: Quantifying uncertainties associated with distribution fitting methods. *Journal of Applied Meteorology*, 43:739–750. 30

Pryor, S. C. and Barthelmie, R. J. (2010). Climate change impacts on wind energy: A review. *Renewable and Sustainable Energy Reviews*, 14:430–437. 10

Racine, J. and Li, Q. (2004). Kernel estimation of multivariate conditional distributions. *Annals of Economics and Finance*, 5:211–235. 51

Raftery, A. E., Gneiting, T., Balabdaoui, F., and Polakowski, M. (2005). Using Bayesian Model Averaging to calibrate forecast ensembles. *Monthly Weather Review*, 133:1155–1174. 59

Rasmusson, E. M. and Carpenter, T. H. (1982). Variations in Tropical Sea Surface Temperature and surface wind fields associated with the Southern Oscillation/El Nino. *Monthly Weather Review*, 110(5):354–384. 7

REN21 (2017). Renewables 2017 global status report. 2

Rodwell, M. J., Rowell, D. P., and Folland, C. K. (1999). Oceanic forcing of the wintertime North Atlantic Oscillation and European climate. *Nature*, 398:320–323. 13

Rogers, J. C. (1997). North Atlantic storm track variability and its association to the North Atlantic Oscillation and climate variability of Northern Europe. *Journal of Climate*, 10:1635–1647. 6, 13, 110

Roulston, M., Kaplan, D., Hardenberg, J., and Smith, L. (2003). Using medium-range weather forcasts to improve the value of wind energy production. *Renewable Energy*, 28:585–602. 10

RTE (2015). Panorama de l'électricité renouvelable 2014. 38

RTE (2016a). Annual electricity report - 2016. 2, 68, 69

RTE (2016b). Panorama de l'électricté renouvelable en 2015. 70

Sailor, D. J., Smith, M., and Hart, M. (2008). Climate change implications for wind power resources in the Northwest United States. *Renewable Energy*, 33:2393–2406. 10

Salameh, T., Drobinski, P., Vrac, M., and Naveau, P. (2009). "Statistical downscaling of near-surface wind over complex terrain in Southern France". *Meteorol Atmos Phys*, 103:253–265. 93

Scaife, A. A., Arribas, A., Blockley, E., Brookshaw, A., Clark, R. T., Dunstone, N., Eade, R., Fereday, D., Folland, C. K., Gordon, M., Hermanson, L., Knight, J. R., Lea, D. J., MacLachlan, C., Maidens, A., Martin, M., Peterson, A. K., Smith, D., Vellinga, M., Wallace, E., Waters, J., and Williams, A. (2014). Skillful long-range prediction of European and North American winters. *Geophysical Research Letters*, 41:2514–2519. 6, 13, 109, 112

Scaife, A. A., Karpechko, A. Y., Baldwin, M. P., Brookshaw, A., Butler, A. H., Eade, R., Gordon, M., MacLachlan, C., Martin, N., Dunstone, N., and Smith, D. (2016). Seasonal winter forecasts and the stratosphere. *Atmos. Sci. Let.*, 17:51–56. 62

Schuhen, N., Thorarinsdottir, T. L., and Gneiting, T. (2012). Ensemble Model Output Statistics for wind vectors. *Monthly Weather Review*, 140:3204–3219. 59

Sfetsos, A. (2002). A novel approach for the forecasting of mean hourly wind speed time series. *Renewable Energy*, 27:163–174. 9

Simpson, J. (1994). *"Sea Breeze and Local Winds."*. Cambridge University Press. 5

Sloughter, J. M., Gneiting, T., and Raftery, A. E. (2013). Probabilistic wind speed forecasting using ensembles and Bayesian Model Averaging. *Journal of the American Statistical Association*, 141:2107–2118. 59

Smith, D. M., Scaife, A. A., Eade, R., and Knight, J. R. (2016). Seasonal to decadal prediction of the winter North Atlantic Oscillation: emerging capability and future prospects. *Quarterly Journal of the Royal Meteorological Society*, 142(695):611–617. 13, 109

Smith, R. (1989). "hydrostatic air flow over mountains". *Advances in Geophysics*, 31:1–41. 5

Soman, S. S., Zareipour, H., and O. Malik, P. M. (2010). "a review of wind power and wind speed forecasting methods with different time horizons". *North American Power Symposium (NAPS)*, pages 1–8. 93

Sperandio, M., Ferreira, A., Moraes, M. R., and Goulart, A. (2013). Short-term wind farm power forecasting with Numerical Weather Prediction. *4th International Conference on Power Engineering, Energy and Electrical Drives*. 9

Taillardat, M., Mestre, O., Zamo, M., and Naveau, P. (2016). Calibrated ensemble forecasts using quantile regression forests and ensemble model output statistics. *Monthly Weather Review*, 144(6):2375–2393. 10

Taylor, J., McScharry, P., and Buizza, R. (2009). Wind power density forecasting using ensemble prediction and time series model. *IEEE Transactions on Energy Conversion*, 34:775–782. 10

Taylor, J. W. and Buizza, R. (2002). Neural network load forecasting with weather ensemble predictions. *IEEE Trans. on Power Systems*, 17:626–632. 10

T.Burton, N.Jenkins, Sharpe, D., and Bossanyi, E. (2011). *Wind Energy Handbook*. Wiley. 29

Thorarinsdottir, T. L. (2013). Calibration diagnostics for point process models via the probability integral transform. *Stat*, 2:150–158. 52

Thorarinsdottir, T. L. and Gneiting, T. (2010). Probabilistic forecasts of wind speed: Ensemble Model Output Statistics using heteroskedastic censored regression. *J. R. Statist. Soc. A*, 173:371–388. 59

Tibshirani, R. (1994). Regression shrinkage and selection via the lasso. *Journal of the Royal Statistical Society, Series B*, 58:267–288. 97

Torralba, V., Doblas-Reyes, F. J., Macleod, D., Christel, I., and Davis, M. (2017). Seasonal climate prediction: A new source of information for the management of wind energy resources. *Journal of applied Meteorology and climatology*, 56:1231–1247. 14, 109

Trigo, R., Osborn, T., and Corte-Real, J. (2002). The North Atlantic Oscillation influence on Europe: climate impacts and associated physical mechanisms. *Climate Research*, 20:9–17. 6, 13, 110

Vitart, F. and Robertson, A. W. (2018). The sub-seasonal to seasonal prediction project (S2S) and the prediction of extreme events. *npj Climate and Atmospheric Science*, 1(3):1–7. 14

Vrac, M., Ayar, P. V., and Yiou, P. (2013). Trends and variability of seasonal weather regimes. *International Journal of Climatology*, 34:472–480. 21

Wagenbrenner, N. S., Forthofer, J. M., Lamb, B. K., Shannon, K. S., and Butler, B. W. (2016). "Downscaling surface wind predictions from Numerical Weather Prediction models in complex terrain with WindNinja". *Atmos. Chem. Phys.*, 16:5229–5241. 9, 92

Wan, C., Xu, Z., Pinson, P., Dong, Z. Y., and Wong, K. P. (2014). Probabilistic forecasting of wind power generation using extreme learning machine. *IEEE Transactions on Power Systems*, 29:1033–1044. 10

Wang, J., Qin, S., Zhou, Q., and Jiang, H. (2015). Medium-term wind speeds forecasting utilizing hybrid models for three different sites in Xinjiang China. *Renewable Energy*, 76:91–101. 11, 12

Weisheimer, A. and Palmer, T. N. (2014). On the reliability of seasonal climate forecasts. *Journal of the Royal Society*, 11 (96). 64

Weisheimer, A., Schaller, N., O'Reilly, C., MacLeod, D. A., and Palmer, T. (2017). Atmospheric seasonal forecasts of the twentieth century:multi-decadal variability in predictive skill of the winter North Atlantic Oscillation (NAO) and their potential value for extreme event attribution. *Q. J. R. Meteorol. Soc.*, 143:917–926. 13

Wytock, M. and Kolter, J. Z. (2013). Large-scale Probabilistic Forecasting in Energy Systems using Sparse Gaussian Conditional Random Fields. *Proceedings of the IEEE Conference on Decision and Control (CDC)*, pages 1019–1024. 9

Zamo, M., Bel, L., Mestre, O., and Stein, J. (2016). "Improved gridded wind speed forecasts by statistical postprocessing of numerical models with block regression.". *Weather and Forecasting*, 31:1929–1945. 95

Titre : Prévision saisonnière de la ressource et de la production éoliennes en France, et du risque associé

Mots clés : Énergie éolienne, Prévisions Saisonnières, Prévision Probabiliste, Risque de déséquilibre

Résumé : L'augmentation de la part des énergies renouvelables intermittentes dans le mix énergétique génère des problématiques liées à la prévisibilité de la production d'électricité. Notamment, à l'échelle saisonnière, les gestionnaires du réseau de transport d'électricité sont contraints de projeter la disponibilité des moyens de production ainsi que de prévoir la demande. Cela permet de garantir l'approvisionnement pour le prochain hiver ou été. Néanmoins, les projections actuelles sont principalement basées sur des données historiques (climatologie) de températures (consommation), vents (production éolienne), ou encore de rayonnement solaire (production photovoltaïque). La thèse présente 4 travaux : trois dans le cadre de la prévision saisonnière, et une étude sur le réalisme du vent de surface tel qu'il est modélisé par le modèle de prévision du temps du Centre Européen. Si la prévisions de l'énergie éolienne aux échelles de temps courtes allant de la minute à quelques jours ainsi que la tendance des vents aux échelles climatiques ont été largement étudiées, la prévision de la production éolienne l'échelle de temps intermédiaire allant d'une quinzaine de jours à la saison n'a reçu que peu d'attention. La prévisibilité du temps aux moyennes latitudes à ces horizons lointains est en effet encore une question ouverte. Cependant, plusieurs études ont montré que les modèles numériques de prévision saisonnières étaient capable d'apporter de l'information sur la variabilité de la circulation atmosphérique de grande échelle via la prévision des oscillations de la circulation grande échelle, comme ENSO dans le Pacifique, ou encore la NAO en Atlantique Nord. Il a aussi été démontré que ces oscillations ont un impact fort sur les précipitations, les températures, et les vents de surface. Construire la relation entre ces indicateurs de la circulation atmosphérique grande échelle et le vent de surface en France permet donc de prendre en compte la variabilité interannuelle du vent de surface, ce dont n'est pas capable par définition la climatologie. C'est là l'idée développée dans les 3 études concernant la prévision saisonnière. Afin de prévoir la ressource et la production éolienne à l'échelle saisonnière, deux modèles probabilistes sont développés. L'un paramétrique, basée sur la prévision de la distribution saisonnière du vent de surface, à différents endroits en France ; l'autre non paramétrique, basé sur l'estimation de la de la densité de probabilité du vent de surface journalier conditionnel à l'état de l'atmosphère. La troisième étude propose de reconstruire la probabilité jointe de la consommation et de la production nationale française, permettant ainsi de mesurer le risque de déséquilibre entre l'offre et la demande.

Title : Seasonal forecasting of wind energy resource and production in France, and associated risk

Keywords : Wind energy, Seasonal forecasts, Probabilistic forecasting, Risk of imbalance

Abstract : The increase of the share of intermittent renewable energy in the energy mix raises issues related to the predictability of electricity production. Especially, at the seasonal scale, the transmission system operators (TSOs) are required to make projections of the availability of means of production as well as to predict the consumption in order to guarantee the security of energy supply during the coming winter or summer. However, current projections are mainly based on historical data (climatology) of temperatures (consumption), wind speed (wind energy production), or solar radiation (photovoltaic production). The thesis presents 4 studies: three within the framework of seasonal forecasts, and one study on the realism of the surface wind speed modelled by the Numerical Weather Prediction model of the European Center of Medium-range Weather Forecasts. If the wind energy forecasts at short timescales going from the minute to several days as well as the wind trends at climatic scale have been thoroughly studied, forecasts of wind energy at the intermadiate scale going from a fortnight to the seasonal horizon have recieved little attention. Predictability at midlatitude and at those long term horizons is indeed still an open question. However, several studies have shown that Numerical Weather Prediction models (NWP) are able to bring valuable information on the large scale atmospheric circulation via the forecast of large scale atmospheric oscillations such as ENSO in the Pacific region, or the NAO in the North Atlantic. It has also been demonstrated that these oscillations have a strong influence on precipitations, temperatures, and surface wind speed. Building the relation between such indicators of the large scale atmospheric circulation and the surface wind speed in France allows to take into account the interannual variability of the surface wind speed, which is not the case of climatology by construction. This is the idea developed in the three studies concerning the seasonal forecasts. In order to forecast the wind energy resource at the seasonal scale, two probabilistic models are proposed. A parametric model based on the forecast of the surface wind speed seasonal distribution at different location in France estimated by the theorical Weibull distribution ; and another non-parametric based on the estimation of the daily surface wind speed distribution knowing the state of the atmosphere. The third study propose to reconstruct the joint probability of the French national consumption and production, allowing to measure the risk of imbalance between supply and demand.